This is to certify that the
dissertation entitled

DEVELOPMENT OF A COMPUTER-AIDED OPTIMIZATION TOOL FOR CENTRIFUGAL COMPRESSOR IMPELLERS

presented by

YING MA

has been accepted towards fulfillment
of the requirements for the

Doctoral degree in Mechanical Engineering

Major Professor's Signature

05/14/09

Date

DEVELOPMENT OF A COMPUTER-AIDED OPTIMIZATION TOOL FOR CENTRIFUGAL COMPRESSOR IMPELLERS

By

Ying Ma

A DISSERTATION

Submitted to
Michigan State University
in partial fulfillment of the requirements
for the degree of

DOCTOR OF PHILOSOPHY

MECHANICAL ENGINEERING

2009

ABSTRACT

DEVELOPMENT OF A COMPUTER-AIDED OPTIMIZATION TOOL FOR CENTRIFUGAL COMPRESSOR IMPELLERS

By

Ying Ma

Development of a fast, automatic and effective computer-aided design and optimization tool for centrifugal compressor impellers has attracted great attention and interest both in industry and academia because centrifugal compressors are widely used and more stringer criteria such as shorter design cycle time and higher efficiency has been proposed by consumers.

In my study, a centrifugal compressor impellers optimization procedure is established. A geometry generation tool is developed; a flow solver with streamline curvature method is modified and linked to this geometry generation tool. This geometry generation tool with the flow solver is used to generate the geometry cases and calculate their corresponding performance to form a database. Two types of Artificial Neural Networks (ANNs): Feed-forward Neural Network (FFNN) and Radial Basis Function Network (RBFN) are used to create the performance map of centrifugal compressor impellers based on this database. Genetic Algorithm (GA) used as the optimization method to search the optimal geometry based on given desired conditions.

Furthermore, Principle Component Analysis (PCA) or Independent Component Analysis (ICA) is applied to improve optimization procedure by transforming training database and make the creating of the performance map in a new coordinate system. The aim of applications of PCA or ICA is to decrease the errors caused by approximate performance map. In this dissertation, the accuracies of three different trained ANNs: RBFN, RBFN with PCA, and RBFN with ICA. As well as total

performances of centrifugal compressor impeller optimization procedures using these three different trained ANNs are compared.

An online flow solver is also developed to overcome the drawbacks of modeling tools, in which the flow solver is used directly to evaluate the performances of centrifugal compressor impellers. This optimization procedure is compared with offline flow solver optimization procedure Furthermore; influences of GA operators, parameters and local search algorithm on online and offline flow solver optimization procedure are also investigated.

Finally, an industrial centrifugal compressor impeller designed by Solar Turbine Inc. is optimized by using five different types of optimization procedures and new impeller geometries are evaluated by ANSYS CFX.

Results show that GA has a good performance on this optimization problem and PCA greatly increase the accuracy of created performance maps and following optimization performances. It is indicated the developed optimization tool is capable of finding an impeller geometry, which has the exact desired relative velocity distribution. Online flow solver and offline flow solver with PCA optimization procedures have best performance for achieving desired velocity distribution. However, results of CFX suggest that all online flow solvers, offline flow solver with PCA and RBFN, offline flow solver with FFNN optimization procedures are capable of reaching the desired efficiencies.

ACKNOWLEDGMENTS

I would like to thanks to my advisor Dr. Abraham Engeda for his guidance, support and also for recommending me to be an intern in Solar Turbine Inc., Caterpillar, in which I learned a lot of industrial design and optimization experiences. His knowledge and expertise in turbomachinery help me to build background and prepare for this project.

I would also like to thank to the guidance committee Dr. Chiu, Dr. Mueller and Dr. Somerton for their helpful and constructive suggestions and comments.

I would like to express M. Cave and Dr. Di Liberti all my sincere gratitude for the support and guidance which they gave me, for their knowledge and experience which they shared with me during my academic years.

Next, I am also very thankful for all the students in turbomachine laboratory who help and support me.

Finally, I would like to thank my parents for their loving support and education.

Ying Ma

TABLE OF CONTENTS

LIST OF TABLES

LIST OF FIGURES

NOMENCLATURE

α	Absolute flow angle measured from meridional plane or Slope angle of meanline in meridional plane
β	Blade angle or Relative flow angle measured from normal direction factor for two-order polynomials
γ	Ratio of specific heat or Slope angle
ω	Weight factor
ε	Ratio of mass flow or relative blade blockage
φ	Flow coefficient
η	Efficiency
ρ	Density
σ	Slip factor
ψ	Head coefficient
Θ	Circular angle
π	Circular constant
A	Area
a	Sound speed
b	Blade width
C	Absolute Velocity
C_p	Specific heat under constant pressure
c	Velocity
child	Chromosomes of child individual

D	Diameter or Width at some certain radius
F	Fitness function
f	Penalty function or objective function
G	performance map or model
g	Gravitational acceleration or Constraint function
H	Head
h	Enthalpy
I	Rothalpy
i	Incidence
ite	iteration number
k	Blade blockage coefficient
M	Mach number or Meridional distance
$\%M$	Percentage of section to begin splitter blades
m	Mass or Meridional distance
$\%m$	Normalized meridional distance
$\dot{m}$	Mass flow rate
N	Blade rotating speed or Number of individuals in GA
n	number of control point nodes
Ns	Specific Speed
O	Throat width
$order$	Order of Bezier polynomials
Pr	Reduced Pressure
P	Pressure

p	Coefficients of polynomials
parent	Chromosome of parent individual
Q	Heat added to the system or Volume
$\dot{Q}$	Volume flow
R	Radius or Specific gas constant
rnd	A random number
s	Entropy or Curve length
T	Temperature or Thickness
Tr	Reduced temperature
Tn	Normal thickness
Tq	Torque
U	Blade Velocity
u	Normalized arc length along streamlines or normalized distance of Bezier polynomial
v	Specific Volume or Normalized arc length along quasi-normal lines
W	Work done by the system or Relative Velocity
$\dot{W}$	Work per unit time
$\dot{W}_f$	Fluid friction on the stationary component
$\dot{w}$	Specific work per unit time
w	Specific Volume or Normalized arc length along normal thickness lines
x	Variables or x coordinate
y	y coordinate or Performance

Z	Blade number or Compressibility factor
z	Height

SUBSCRIPT

0	Stagnation, or Entry of IGV
1	Impeller inlet (Inducer Inlet)
2	Impeller outlet
4	Diffuser inlet
5	Diffuser Outlet
actu	Actual
c	Head or Center
Cur	Current
d	diffuser
des	Desired
H	At hub
i	Ideal or impeller, or the ith point
j	Jet or Integer number
kb	Due to blockage of blades
Lean	Lean angle
LE	Leading edge
Max	Maximum
Min	Minimum
ML	Meridional plane
m	In meridional direction

node	At node points
PS	Pressure surface
pre	Pressure side or Pressure surface
Rake	rake angle
r	In axis or radial direction
SS	Suction surface
S	At shroud
s	Isentropic process or slip
spl	Splitter blades
suc	Suction side or Suction surface
TE	Trailing edge
th	Throat
u	In tangential direction

SUPERSCRIPT

‘	Revised
*	Desired

CHAPTER 1

FUNDALMENTALS OF CENTRIFUGAL COMPRESSORS

1.1 Introduction

A turbomachine describes a device that transfers energy between a rotor and a fluid. The turbomachinery are constituted of a large class of machines. Their functions and application area varies a lot. However, each of these includes several certain elements including a rotor and a casing. A rotor is the rotating part and the most important component, through which energy transfers. A casing provides a boundary as guides to direct the flow. The turbomachinery are used for a wide range and are found virtually everywhere in this world. The application field of turbomachinery includes aerospace, automotive, refrigeration and air conditioning, power generation as well as marine. The design of turbomachinery covers a wide range of subjects including fluid mechanics, thermodynamics, aerodynamics, solid mechanics and vibration. Generally, two main categories of turbomachine are identified based on its purpose. Those, which produce energy by expanding fluid to a lower pressure, are classified as turbines. Inversely, those that absorb energy to increase the fluid pressure are classified as compressors or pumps. A pump uses liquids for a working fluid and a compressor uses gases. For a compressor, three different terms (a fan, a blower, and a compressor) may be used depending on the pressure ratio or the pressure rise achieved. Compressors can be classified as axial, mixed flow and centrifugal (or radial) depending on the discharge flow direction. The inlet and outlet flow directions of axial, mixed flow and centrifugal compressors are illustrated in Figure 1-1 respectively.

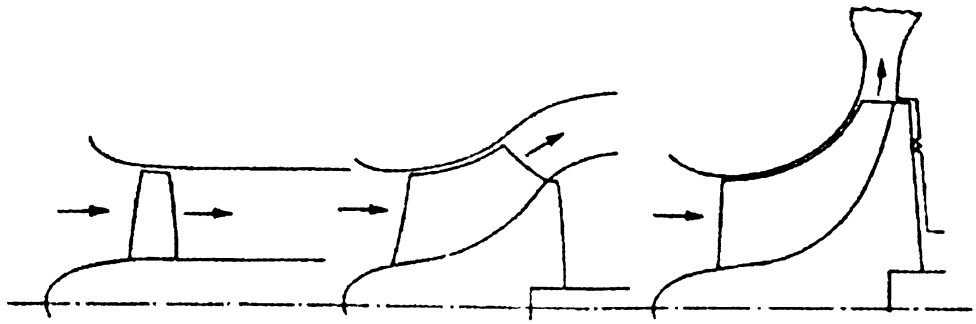

Figure 1-1 Illustration of inlet and outlet flow directions of three types of compressors: axial, mixed flow and centrifugal ones [1]

The fluid flows parallel to the rotation to axial coordinate in axial compressors. Compared to centrifugal compressors, axial compressors have the large mass flow capacity and higher efficiency. Therefore they are widely used in gas turbines, especially jet engines. However, they provide lower pressure rise per state than centrifugal compressors.

The increase of centrifugal compressor efficiency during last decades has resulted in the wider industrial application. The centrifugal compressors offer several advantages: small weight, lower maintenance, higher reliability, simplicity of components and ease of manufacturing.

Mixed flow centrifugal compressors combine impeller blade features from both the axial and radial to produce a diagonal unit. The exit mean radius is greater than one at the inlet, which is similar to centrifugal compressor. However, the flows exit in both axial and radial direction. Therefore, it eliminates the requirement of the diffuser, which is another important component in compressors and introduced in the next section.

1.2 Centrifugal Compressors

A centrifugal compressor, sometimes referred as a radial compressor shown in Figure 1-2, is generally made up from four basic components: an inlet casing, a rotating impeller, a stationary diffuser of the vaneless or vaned type and a volute (a collector).

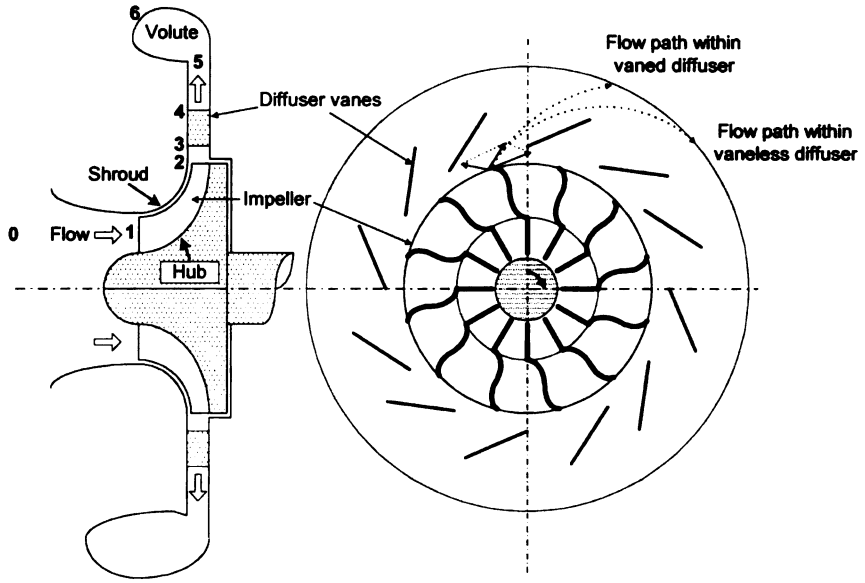

Figure 1-2 Components of centrifugal compressors[2]

1.2.1 Inlet Casing

The main purpose of inlet casing is to provide the pre-rotation by using inlet guiding vanes, which allows circumventing the incidence and extending the flow range. There are three different pre-rotations, shown in Figure 1-3. The positive pre-rotation leads to a reduction in mass flow and a slightly less enthalpy rise. On the opposite, the negative pre-rotation leads to a higher mass flow and an increased pressure ratio. The comprehensive effects of pre-rotation will be discussed in the chapter 2.

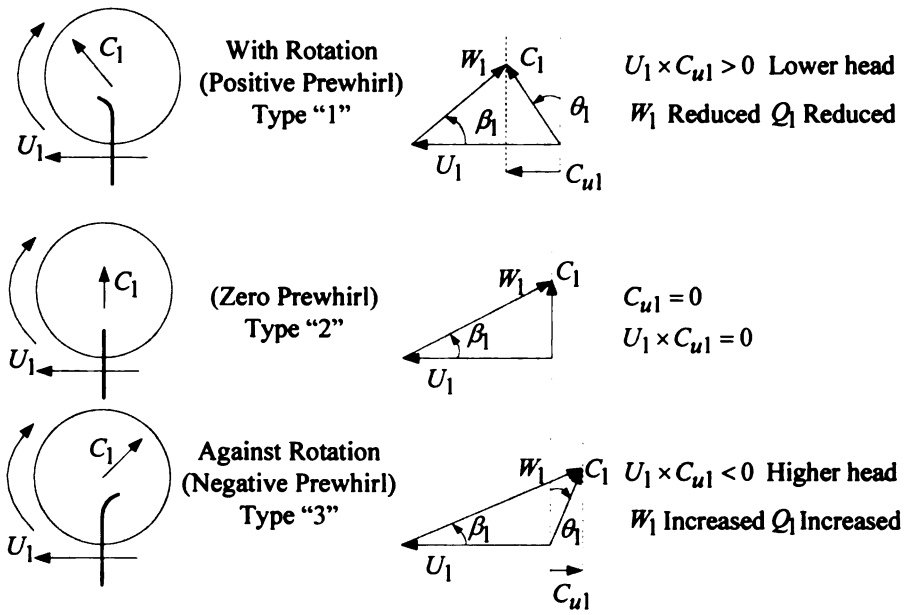

Figure 1-3 Three types of pre-rotation caused by inlet guiding vanes[2]

1.2.2 Impeller

The purpose of an impeller (rotor) includes: deflecting the flow in axial and radial direction, increasing the static pressure as well as the kinetic energy of the flow.[3] The impeller is the most important and complex element in geometry in the centrifugal compressor. The nomenclature of an impeller is as shown in Figure 1-4.

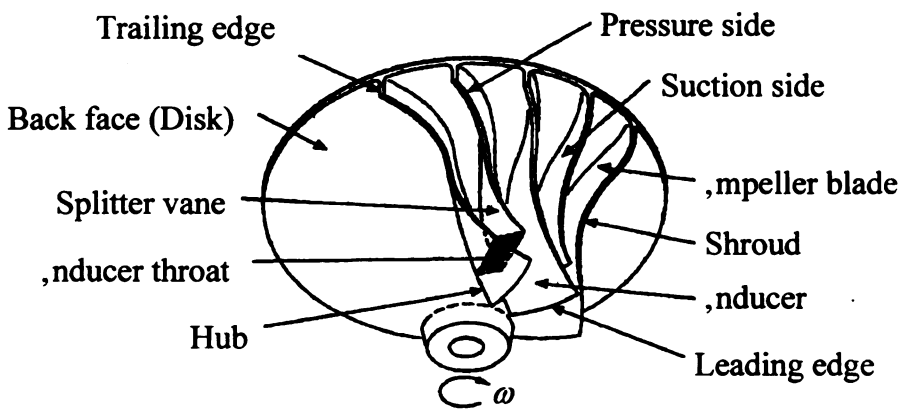

Figure 1-4 Impeller nomenclature[2]

The hub is the curve surface of revolution of the impeller, forming the inner boundary to the flow. The shroud is the curved surface, forming the outer boundary to the flow. At the entry of the impeller, the relative flow has a velocity in radial direction. And the relative flow is turned into the axial direction since the entry section, which is defined as inducer section. The inducer generally starts at the eye of impeller and finishes in the region where the flow is beginning to turn into radial direction.[1] The side of an impeller with higher pressure is called pressure side or driving face. On the opposite, the side with lower pressure is called suction face. The pressure side, suction side, hub and shroud form the four sides of the boundary to the flow. The contours of them greatly effect the deflection of the flow. The effects of leading edge and trailing will be discussed in chapter 2. The less the number of the impeller is, the less blockage effects is. However, decreasing the number of impeller leads to the lager pressure load, which formed by the pressure gradient between pressure side and suction side, and also results in mechanical problems. An alternative solution is that splitter blades are added to avoid this problem. Inducer throat has the smallest area in the channel of the flow in the impeller. The maximum impeller inlet mass flow occurs when the fluid passes through the inducer throat section at sonic speed. Therefore, the calculation of throat area is required for the calculation of the maximum mass flow and flow range.

1.2.3 Diffuser

As mentioned before, the fluid is drawn in through the inlet casing into the eye of the impeller parallel to the axis of rotation. In order to add angular momentum, the impeller whirls the fluid outwards and turns it into a direction perpendicular to the rotation axis. As a result, the energy level is increased, resulting in both pressure and velocity. In centrifugal compressors, energy is transferred to the fluid by the impeller. Even though centrifugal impellers are designed for good diffusion within the blade

passage, approximately half of the energy imparted to the fluid remains as kinetic energy at the impeller exit. Therefore, for an efficient centrifugal stage, this kinetic energy must be efficiently converted into the static pressure. Thus, a diffuser, which is stationary and is located downstream of the impeller, is a very important element in a centrifugal compressor.

Since over the years the demands on the centrifugal compressors increased for higher pressure ratios and efficiency, different types of radial diffusers have been developed. These different types of radial diffusers can be classified as the vaneless diffusers, the vaned diffusers, and the low solidity vaned diffusers.

Vaneless diffusers consist of two radial walls that may be parallel, diverging, or converging. The flow entering a vaneless diffuser has a large amount of swirl. Thus, the tangential component of momentum at low flow rates can be more than twice the radial component. The radial component of the flow diffuses due to the area increase (conservation of mass), and the tangential component diffuses inversely proportional to the radius (conservation of angular momentum). The vaneless diffuser is widely used in automotive turbochargers because of the broad operating range it offers. It is also cheaper to manufacture and more tolerant to erosion and fouling than the vaned diffusers. However, the vaneless diffuser needs a large diameter ratio because of its low diffusion ratio. The flow in a vaneless diffuser follows an approximate logarithmic spiral path. The flow in a vaneless diffuser with a radius ratio of 2 and an inlet flow angle of 6 degrees makes a full revolution before leaving the diffuser. This will result in high friction loss due to viscous drag on the walls and accordingly its pressure recovery is significantly lower than is found with vaned diffusers.

Generally the vaneless diffuser demonstrates lower pressure recovery by as much as 20% and lower stage efficiency by 10% compared to a vaned diffuser.

The role of vanes in a vaned diffuser is to shorten the flow path by deswirling the flow, allowing a smaller outlet diameter to be used. A vaneless space precedes the vaned diffuser to help reduce flow unsteadiness and Mach number at the leading edge of the vanes so as to avoid shock waves. Boundary layer develops and generates appreciable blockage at the vane leading edge. In order to reduce this blockage, the vaneless space should be minimized until it doesn't give any unfavorable effects such as increase in noise level or pressure fluctuations due to interaction of the impeller and diffuser. The flow exiting the impeller follows an approximate logarithmic spiral path to the vane leading edge and is guided by the diffuser channels. The semi-vaneless space follows the vaneless space, ending in a passage throat, which may limit the maximum flow rate in a compressor. The number of diffuser vanes has a direct bearing on the efficiency. With large number of vanes, the angle of divergence is smaller and the efficiency rises until friction and blockage overcomes the advantage of more gradual diffusion.

Although the vaned diffuser typically exhibits higher pressure recovery, the flow range is limited at low flow rate due to vane stall. At high flow rates, flow choking at the throat may also limit flow range.

1.2.4 Volute

Outside the diffuser is a scroll or volute whose function is to collect the flow from the diffuser and deliver it to the discharge pipe. It is possible to gain a further deceleration and thereby additional pressures rise. Volute plays an important role in influencing the overall performance of the centrifugal compressor. The flow leaving the impeller has the logarithmic spiral path. Therefore the volute has to be designed to match with the flow of the impeller. The volute affects the circumferential pressure distribution downstream the impeller, and then influence the impeller efficiency, off-design operation, static and dynamic pressure and flow range.[4]

1.3 Objectives of Research

The conventional design, which is based on trial and error and still greatly depends on the expertise of designers and existed database of companies, is widely used in the industrial compressor companies.

Due to the wide applications of centrifugal compressors, only a small improvement on centrifugal compressor performances will result in the significant savings in expenditure. Furthermore, more stringent criteria such as higher efficiency, wider flow operating range and shorter design cycle are required by consumers. Fortunately, as the increase of computing capacity and the application of Computational Fluid Dynamics (CFD) software, simulations has been widely applied, become a useful designing tool and substitute experiments to a large extent. This greatly decreases the design cycle time and makes the computer-aided design become possible. Therefore, developing of a design and optimization tool or methodology for centrifugal compressor impellers has attracted great attention and interest.

The conventional design process widely used in industry is a very complex procedure and can be broadly divided into three loops: One Dimensional (1D) Preliminary Design and Analysis, Two Dimensional (2D) Design and Aerodynamic Analysis, and Three Dimensional (3D) Design and Aerodynamic/Mechanical Analysis. Actually, these three steps are also closely related each other. 1D design is essential and a good 1D design can fasten the following 2D and 3D design. Defective 2D design cannot be expected to obtain the good 3D performance. If the performance of 2D or 3D design is unsatisfied, designers probably need to make modifications not only on 2D or 3D design but also on 1D design.

Even for experienced designers, it will still take several weeks or months to modify and analyze geometry to achieve customers' requirements. Therefore, it will not be realistic to expect that one automatic numerical optimization method can substitute

designers and be applied on total design and optimization procedure. In this study, an optimization tool, working as a fast assistant tool aimed at improving 2D design and analysis of industrial centrifugal compressor impellers is developed using quasi-3D flow solver and Genetic Algorithm (GA). The objectives of the present research are to improve the conventional design method procedure for the centrifugal compressor impellers and the project is accomplished systematically with the following steps:

1) Developing a geometry generation tool (BladeCAD) including the following functions:

a) Creating a new centrifugal compressor design, including an inlet casing, an impeller, and a diffuser. All the geometric variables can be edited.

b) Loading existed centrifugal compressor design files and also geometry files, e.g. geometry files in meridional plane or blade-to-blade plane.

c) Generating 3D model, which allow the designers to visually observe the impeller modeling.

2) Revising and linking the codes of Quasi-three dimensional (3D) flow solvers MERIDL and TSONIC to the geometry generation tool BladeCAD. Comparing the calculating results between Quasi-3D flow solvers and commercial software ANSYS CFX using Naiver-Stroker equations to evaluate the accuracies of MERIDL and TSONIC.

3) Developing an optimization procedure for centrifugal compressor impellers. Creating a performance map by using an Artificial Neural Network (ANN) and employing a Genetic algorithm (GA) as the optimization method.

4) Combing a Principle Component Analysis (PCA) and an Independent Component Analysis (ICA) with the ANN and studying their influences on the ANN. Presenting

an improved centrifugal compressor impeller optimization procedure using the PCA and GA.

5) Presenting a new online flow solver optimization procedure, in which the flow solvers are directly used to eliminate the errors caused by created performance map. Comparing this new one with the traditional optimization procedure which is called offline flow solver optimization procedure in this study.

6) Using developed fast optimization procedures to find the optimal and ANSYS CFX to evaluate the optimum as well as these optimization procedures eventually.

CHAPTER 2

THEORY OF CENTRIFUGAL COMPRESSORS

2.1 Introduction

Before introducing centrifugal compressor optimization, some basic theories on evaluating the centrifugalt compressors have to be introduced firstly. There are hundreds of formulas have been developed and used during decades of years of work for design and performance analysis of centrifugal compressors. Only the theory and equations related to the present research were presented here. Because of the complex process happened in compressor, these formulas remains relative accurate. To bring better accuracy, complex equations and practical interpretations have to be applied. Besides, the combination of gases and operating conditions are also required to consider.[2]

2.1.1 Gas Properties

The ideal equation of state for the perfect gas is:

$$pv = RT \tag{2-1}$$

If the fluid is perfect gas, the enthalpy can be expressed as a linear function of temperature T :

$$h = C_p T \tag{2-2}$$

The relationship between specific heat at a constant pressure C_p and specific gas constant R is:

$$C_p = \frac{\gamma \cdot R}{\gamma - 1} \tag{2-3}$$

However, the real equation of state is preferred to use in the industry for better accuracy in the industry in Eqn. (2-4). And the deviation from perfect gases counts on the compressibility fact Z.

$$pv = ZRT \tag{2-4}$$

One simple and approximate equation for calculating compressibility factor Z is:

$$Z \approx 1 + \left(\frac{0.188}{Tr} - \frac{0.468}{Tr^2} - \frac{0.887 e^{-5Tr}}{Tr^2} \right) Pr \text{ [5]} \tag{2-5}$$

Besides Eqn. (2-5), there are many methods have been proposed to calculate the compressibility factor. please see reference [6] for others formulas.

2.1.2 The First Law of Thermodynamics

The first law of thermodynamics is introduced in Eqn. (2-6).

$$\oint (dW - dQ) = 0 \tag{2-6}$$

dQ denotes the heat supplied by the system to the surrounding, while dW denotes the work done to the system. For a centrifugal compressor, the first law of thermodynamics can be rewritten into:

$$\dot{W} - \dot{Q} = \dot{m} \left[(h_2 - h_1) + \left(\frac{C_2^2}{2} - \frac{C_1^2}{2} \right) + (gz_2 - gz_1) \right] \tag{2-7}$$

The fluid in the centrifugal compressor is gas; therefore the potential energy gz is negligible. Most turbomachinery processes are or very close to adiabatic process, therefore the heat transfer is zero. The Eqn. above can be rewritten into as a function of stagnation enthalpy:

$$\dot{W} = \dot{m}\left[\left(h_2 + \frac{C_2^2}{2}\right) - \left(h_1 + \frac{C_1^2}{2}\right)\right] = \dot{m}(h_{02} - h_{01}) \tag{2-8}$$

Work done in Eqn. (2-8) is from the surrounding to the fluid.

2.1.3 The Second Law of Thermodynamics

$$Tds = dh - \frac{dp}{\rho} \tag{2-9}$$

The definition of isentropic process is:

$$pv^{\gamma} = \text{constant} \tag{2-10}$$

Therefore, by combining Eqns. (2-1) and (2-10), the relationship among pressure, temperature and density in the isentropic process, which mean $ds = 0$, are give as in the Eqns. (2-11) and (2-12):

$$\frac{p_1}{p_2} = \left(\frac{T_1}{T_2}\right)^{\gamma/\gamma-1} \tag{2-11}$$

$$\frac{\rho_1}{\rho_2} = \left(\frac{T_1}{T_2}\right)^{1/(\gamma-1)} \tag{2-12}$$

2.1.4 Compressible Gas Flow Relations

The stagnation enthalpy (total enthalpy) is defined by combined static enthalpy h and kinetic energy $\frac{c^2}{2}$:

$$h_0 = h + \frac{c^2}{2} \tag{2-13}$$

If the fluid is a perfect gas, combining Eqns. (2-2), (2-3) and (2-13) gives the relationship between stagnation temperature and static temperature:

$$\frac{T_0}{T} = 1 + \frac{c^2}{2C_p T} = 1 + (\gamma - 1)\frac{c^2}{2\gamma RT} = 1 + \frac{(\gamma - 1)}{2} M^2 \tag{2-14}$$

Where the Mach number M is defined by:

$$M = c / a = c / \sqrt{\gamma RT} \tag{2-15}$$

If the flow rest adiabatically and isentropically, combining Eqns. (2-1), (2-2), (2-3) and (2-9) gives Eqns. (2-16) and (2-17):

$$\frac{p_0}{p} = \left(\frac{T_0}{T}\right)^{\frac{\gamma}{\gamma-1}} = \left[1 + \frac{(\gamma - 1)}{2} M^2\right]^{\frac{\gamma}{\gamma-1}} \tag{2-16}$$

$$\frac{\rho_0}{\rho} = \left(\frac{T_0}{T}\right)^{\frac{1}{\gamma-1}} = \left[1 + \frac{(\gamma - 1)}{2} M^2\right]^{\frac{1}{\gamma-1}} \tag{2-17}$$

2.2 Basic Theories for Centrifugal Compressors

2.2.1 Velocity Triangle

Both inlet and outlet velocity triangles play an important role on the performance of centrifugal compressors. Therefore, they are paid great attention and carefully designed.

The blade velocity is calculated from:

$$U = NR \tag{2-18}$$

Therefore the blade velocity at inducer tip is:

$$U_{1S} = NR_{1S} \tag{2-19}$$

The relative velocity W of the fluid is a very important factor in analyzing the performance of the centrifugal compressor. The relationship between relative velocity W, blade velocity U and absolute velocity C is expressed by:

$$C = U + W \tag{2-20}$$

C, U, W are velocity vectors. Because inlet casings and diffusers are stationary, $U = 0$. Therefore, relative velocity W is equivalent to absolute velocity C in inlet casing and diffusers.

2.2.2 Mass Flow

The mass flow can be calculated by using of the integral form:

$$\dot{m} = \int_A \rho C_m dA \tag{2-21}$$

If the inlet mass flow is uniform with a constant pre-rotation, and the meridional flow velocity is normal to the blade leading edge, the then the mass flow at the inducer inlet is defined by:

$$\dot{m} = \rho_1 \pi \left(R_{1S} + R_{1H} \right) \left| Z_{1S} - Z_{1H} \right| C_{1m} \tag{2-22}$$

The volume flow is defined by:

$$\dot{Q} = \frac{\dot{m}}{\rho} \tag{2-23}$$

However, the equation above needs to be revised because of the effect of blade blockage, which is introduced in Section 2.6.2.

2.2.3 Dimensionless Variables and Similitude

The dimensionless variables are very useful in the analysis of turbomachinery performance, The important variables in turbomachine performance included volume flow $\dot{Q}$, angular speed N and rotor diameter D.

The flow coefficient is defined as:

$$\varphi = \frac{Q}{ND^3} \tag{2-24}$$

The head coefficient is defined as:

$$\psi = \frac{gH}{N^2 D^2} \tag{2-25}$$

The specific speed is defined as:

$$Ns = \frac{\varphi^{\frac{1}{2}}}{\psi^{\frac{3}{4}}} = \frac{\left(\frac{Q}{ND^3}\right)^{\frac{1}{2}}}{\left(\frac{gH}{N^2D^2}\right)^{\frac{3}{4}}} = \frac{NQ^{\frac{1}{2}}}{(gH)^{\frac{3}{4}}} \tag{2-26}$$

The equality of dimensionless groups resulting from similitude plays an important role in analysis of compressor performances. The similarity velocity triangle gives equal flow coefficient:

$$\frac{Q_1}{N_1 D_1^3} = \frac{Q_2}{N_2 D_2^3} \tag{2-27}$$

While the similar force triangle gives equal head coefficient:

$$\frac{H_1}{N_1^2 D_1^2} = \frac{H_2}{N_2^2 D_2^2} \tag{2-28}$$

For same compressor with different running speed, Eqns. (2-27) and (2-28) can be rewritten into:

$$\frac{Q_1}{N_1} = \frac{Q_2}{N_2} \tag{2-29}$$

$$\frac{H_1}{N_1^2} = \frac{H_2}{N_2^2} \tag{2-30}$$

For the trimmed diameter D_2 from the original diameter D_1 while keeping the rotating speed, Eqns. (2-27) and (2-28) can be rewritten into:

$$\frac{Q_1}{D_1^3} = \frac{Q_2}{D_2^3} \tag{2-31}$$

$$\frac{H_1}{D_1^2} = \frac{H_2}{D_2^2} \tag{2-32}$$

2.3 Head and Efficiency

2.3.1 Rise of Stagnation Enthalpy

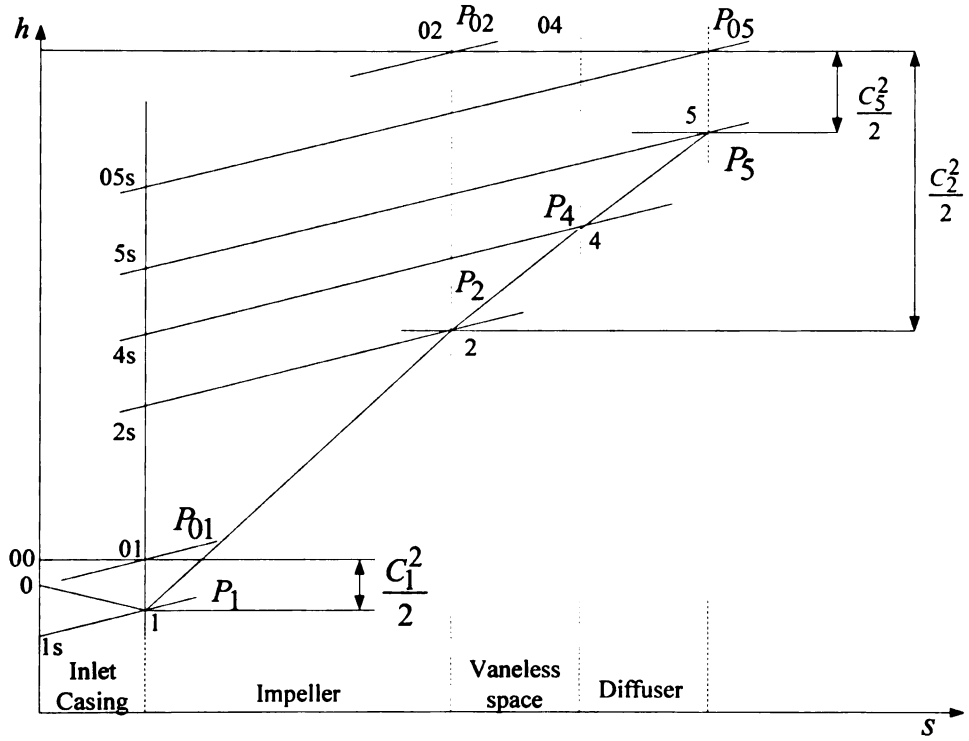

Figure 2-1 h-s diagram for the centrifugal compressor stage[5]

The contribution of each element of the compressor is as shown in Figure 2-1. In Figure 2-1, in the inlet casing, the fluid is accelerated from velocity c_0 to c_1 while the static pressure decreased from p_0 to p_1. Since there is no shaft works in inlet casing. The loss in the inlet casing is small and negligible compared to others elements. Therefore the stagnation enthalpy is constant in adiabatic flow:

$$h_{00} = h_0 + \frac{c_0^2}{2} = h_1 + \frac{c_1^2}{2} = h_{01} \tag{2-33}$$

In the impeller, the rise of stagnation enthalpy is equivalent to:

$$\Delta h = h_{02} - h_{01} = \left(h_2 + \frac{c_2^2}{2} \right) - \left(h_1 + \frac{c_1^2}{2} \right) \tag{2-34}$$

The flow is decelerated adiabatically from c_4 to c_5 in the diffuser. The static pressure rises from p_4 to p_5 (Figure 2-1). The stagnation enthalpy in steady adiabatically flows without shaft work is constant. However, in the real situation, the stagnation enthalpy decreases because of the losses in the diffusers.

$$h_{04} = h_4 + \frac{c_4^2}{2} = h_5 + \frac{c_5^2}{2} = h_{05} \tag{2-35}$$

2.3.2 Specific Work and Head

The specific energy transfer can be derived from the velocity triangle at inlet and outlet from the impeller as shown in Figure 2-2 and Figure 2-3.

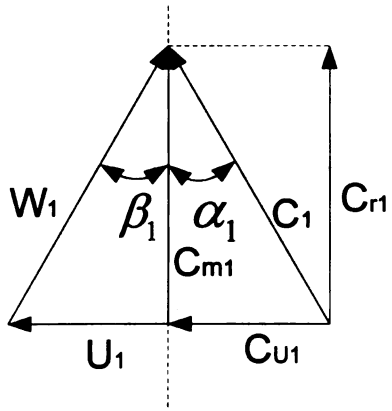

Figure 2-2 Velocity triangle at inlet

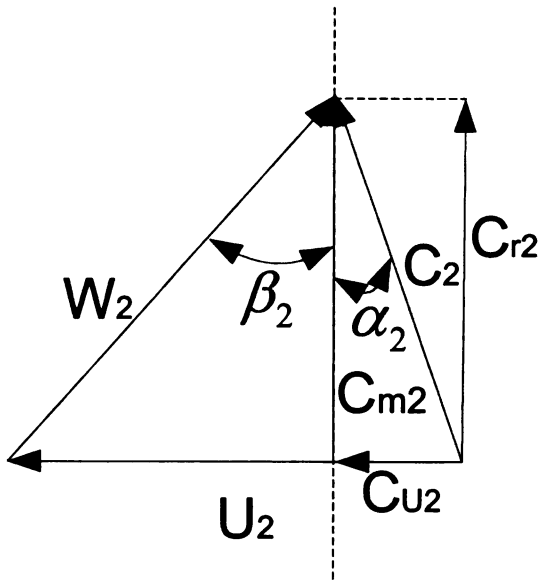

Figure 2-3 Velocity diagram at outlet

The rate of change of angular momentum will equal the sum of the moments of the external forces T_q. When applied angular momentum theorem to an impeller, the torque T_q, is given by:

$$T_q = \dot{m}(r_2 C_{u2} - r_1 C_{u1}) \tag{2-36}$$

Multiplying compressor rotating angular velocity N on both sides of Eqn. (2-28) gives work of rotor done on the fluid per unit of time is:

$$\dot{W} = NT_q = N\dot{m}(r_2 C_{u2} - r_1 C_{u1}) = \dot{m}(U_2 C_{u2} - U_1 C_{u1}) \tag{2-37}$$

Applying the law of trigonometry to the velocity triangles of exit and inlet of the impeller yields

$$U_2 C_{u2} = \tfrac{1}{2}(U_2^2 + C_2^2 - W_2^2) \tag{2-38}$$

$$U_1 C_{u1} = \tfrac{1}{2}(U_1^2 + C_1^2 - W_1^2) \tag{2-39}$$

Then by combing Eqns. (2-28) and (2-39), Eqn. (2-39) can be rewritten into:

$$\dot{W} = \frac{\dot{m}}{2}\left[\left(U_2^2 - U_1^2\right) + \left(C_2^2 - C_1^2\right) - \left(W_2^2 - W_1^2\right)\right] \tag{2-40}$$

The work done on the fluid per unit mass or specific work per unit time is:

$$\dot{w} = \frac{\dot{W}}{\dot{m}} = \frac{\dot{m}(U_2 C_{u2} - U_1 C_{u1})}{\dot{m}} = (U_2 C_{u2} - U_1 C_{u1})$$

$$= \frac{1}{2}\left[\left(U_2^2 - U_1^2\right) + \left(C_2^2 - C_1^2\right) - \left(W_2^2 - W_1^2\right)\right] \quad (2\text{-}41)$$

The head is defined as:

$$H = \frac{\Delta h_0}{g} = \frac{(U_2 C_{u2} - U_1 C_{u1})}{g} = \frac{\left(U_2^2 - U_1^2\right) + \left(C_2^2 - C_1^2\right) - \left(W_2^2 - W_1^2\right)}{2g} \quad (2\text{-}42)$$

2.3.3 Conservation of Rothalpy

In the centrifugal compressor, the specific work done on the fluid per unit time equals to the rise of the stagnation enthalpy. Therefore combining Eqns. (2-34) and (2-41) gives:

$$\Delta h_0 = h_{02} - h_{01} = \left(h_2 + \frac{c_2^2}{2}\right) - \left(h_1 + \frac{c_1^2}{2}\right) = (U_2 C_{u2} - U_1 C_{u1}) \quad (2\text{-}43)$$

The Eqn. (2-43) can be also rewritten into:

$$h_{02} - U_2 C_{u2} = h_{01} - U_1 C_{u1} \quad (2\text{-}44)$$

or:

$$h_2 - \frac{U_2^2}{2} + \frac{W_2^2}{2} = h_1 - \frac{U_1^2}{2} + \frac{W_1^2}{2} \quad (2\text{-}45)$$

In the Eqns. (2-44) and (2-45), the sum of all the variables in the left side are at the entry equals to that in the right side at the exit of impeller. Therefore, a new function rothalpy I is introduced. And value of rothalpy I is unchanged between the entry and the exit of the impeller. However, some researchers found that an increase in rothalpy was possible for steady, rothalpy flow without heat transfer or body forces. And the increased rothalpy is because of the fluid friction acting on the stationary wall, such as the shroud of centrifugal compressors. Therefore, a revised equation for rothalpy has been proposed [6]:

$$h_{02} - U_2 C_{u2} = h_{01} - U_1 C_{u1} + \dot{W}_f / \dot{m} \tag{2-46}$$

Where $\dot{W}_f$ denotes the power loss due to the fluid friction on the stationary shroud.

2.3.4 Efficiency

The overall efficiency of an adiabatic compressor is defined as the ratio of minimum adiabatic work input per unit time to actual adiabatic work input to rotor per unit time, or one of the isentropic head to actual head:

$$\eta_s = \frac{h_{05s} - h_{01}}{h_{05} - h_{01}} = \frac{H_s}{H_{act}} \tag{2-47}$$

The Eqn. (2-47) can be rewritten into:

$$\eta_c = \frac{h_{05s} - h_{01}}{h_{05} - h_{01}} = \frac{h_{05s} - h_{01}}{h_{02} - h_{01}} = \frac{C_p T_{01}\left(\frac{T_{05s}}{T_{01}} - 1\right)}{U_2 C_{u2} - U_1 C_{u1}}$$

$$\eta_c = \frac{C_p T_{01}\left(\frac{T_{05s}}{T_{01}} - 1\right)}{C_p T_{05} - C_p T_{01}} = \frac{\left(\frac{P_{05}}{P_{01}}\right)^{\frac{\gamma-1}{\gamma}} - 1}{\frac{T_{05} - T_{01}}{T_{01}}} \tag{2-48}$$

The efficiency of an impeller is defined as the same overall efficiency of a compressor:

$$\eta_i = \frac{h_{02s} - h_{01}}{h_{02} - h_{01}} \tag{2-49}$$

The efficiency of a diffuser is defined as ratio of the actual enthalpy change to the isentropic enthalpy change.

$$\eta_d = \frac{h_{5s} - h_4}{h_5 - h_4} \tag{2-50}$$

For steady and adiabatic flow in stationary diffusers, the stagnation enthalpy remains constant $h_{04} + \frac{c_4^2}{2} = h_{05s} + \frac{c_{5s}^2}{2}$; therefore the efficiency of a diffuser can be also rewritten into:

$$\eta_d = \frac{c_4^2 - c_{5s}^2}{c_4^2 - c_5^2} \tag{2-51}$$

2.3.5 Pressure Ratio

The overall pressure ratio is defined by:

$$\frac{P_{05}}{P_{01}} = \left(\frac{T_{05s}}{T_{01}} \right)^{\frac{\gamma}{\gamma - 1}} \tag{2-52}$$

Combine Eqns. (2-48) and (2-52) and get the overall pressure ratio

$$\frac{P_{05}}{P_{01}} = \left(1 + \frac{(\gamma - 1)\eta_c (U_2 C_{u2} - U_1 C_{u1})}{a_{01}^2} \right)^{\frac{\gamma}{\gamma - 1}} \tag{2-53}$$

2.4 The Choking Mass Flow

When the flow velocity in a passage reaches at the sonic speed at some cross-section, the flow chokes. Once the flow chokes, the mass flow cannot be increased further either by decreasing the backpressure or increasing the rotational speed. For centrifugal compressors, the behavior of choking can happen in an impeller or a diffuser. However, the theories are different for rotating component and stationary component. In the rotating component, choking occurs when the relative velocity is equivalent to sonic speed at some cross-section, while when absolute velocity reaches to speed of sound in the stationary component. An Eqn. is used to calculate in choking mass flow is proposed in [1]:

$$\dot{m}_{th} = \rho_{th} W_{th} A_{th} \tag{2-54}$$

And when W_{th} reaches the sound of speed, the choking occurs. This equation is only approximate equation to calculate choking mass flow. Because the actual choking may occur at lower mass flows because the whirl of the flow cannot provide the uniform velocity for the throat section. Therefore the supersonic part of the throat may

result in a choking mass flow while the left part still remain subsonic, which leads to the actual choking mass flow is below the theoretical maximum value. A revised equation for calculating choking mass flow has been supposed [3]:

$$\dot{m}_{th} = \int_{R_{th,h}}^{R_{th,s}} \rho_{th}\left(R_{th}\right) \cdot W_{th}\left(R_{th}\right) \cdot D_{th}\left(R_{th}\right) dR_{th} \qquad (2\text{-}55)$$

2.5 The Influences of Inlet Guidancing Vanes (IGV)

The IGV has several important functions. The first function is to modify the Mach number. The supersonic Mach number will lead to strong shock losses. Moreover, supersonic Mach number will also induce early flow separation as well as higher losses. Reducing the rotating speed is one possible method for this problem, which is as shown in Figure 2-4. However, a lot of variables were required to redesign if the designed speed changed. Another possibility is to induce preswirl vanes, which is as shown in Figure 2-5 . The increase of turning of the flow results in a lower relative velocity W and also lower Mach number. Besides, the increase of turning of the flow from zero to positive prerotation results in the gradual increase of C_{u1} obviously. The Eqns. (2-43) and (2-53) explained that this also decreases the enthalpy rise as well as the specific work.

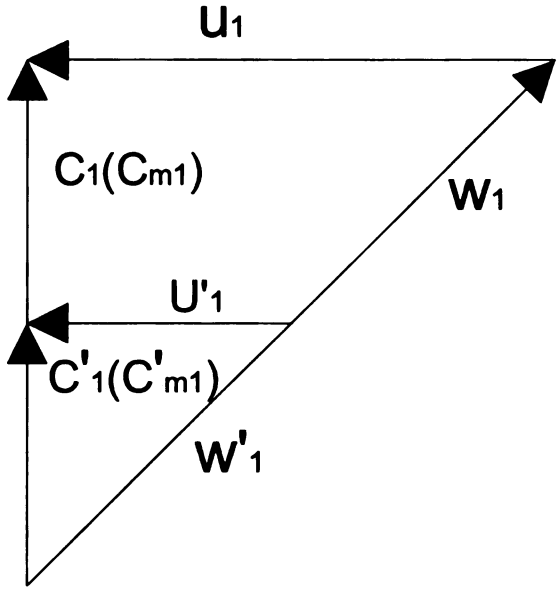

Figure 2-4 Illustration of influence of rotation speed on C_m

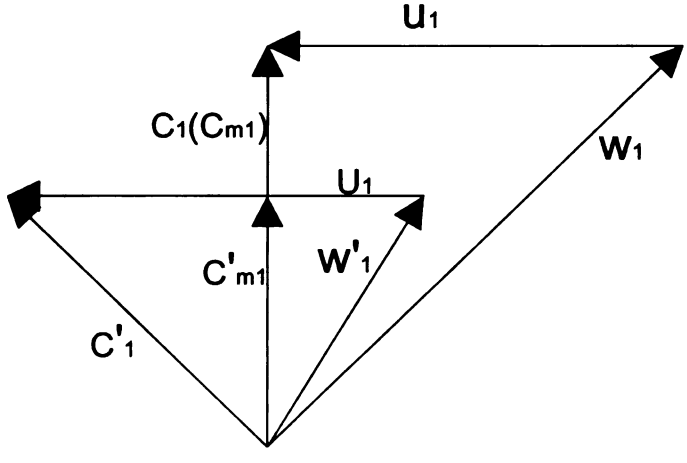

Figure 2-5 Illustration of influence of preswirl on C_m

The second important function of IGV is to modify the mass flow. Mass flow variation is limited by choking losses, incidence. The C_{1m} varies as the change of preswirl shown in the figure 2.4, which can change mass flow based on Eqn. (2-22).

The third influence of IGV is on the pressure ratio. The increase of prerotation C_{u1} decreased the overall pressure ratio based on Eqn. (2-53).

2.6 The Influences of Inducer

2.6.1 Influences of Blade Blockage

The inducer plays a very important role in the impeller performance. The good design of an inducer should minimize the inlet relative Mach number and keep it subsonic if possible.

The effect of leading edge blade angle on throat area is as shown in Figure 2-6. Smaller value of leading edge blade angle β_1 leads to the larger throat area and larger operating flow range.

When the flows enter the inducer, the real free area is not $\pi\left(R_{1S}^2 - R_{1H}^2\right)$, but smaller than this value because of the blockage by the presence of the blades.

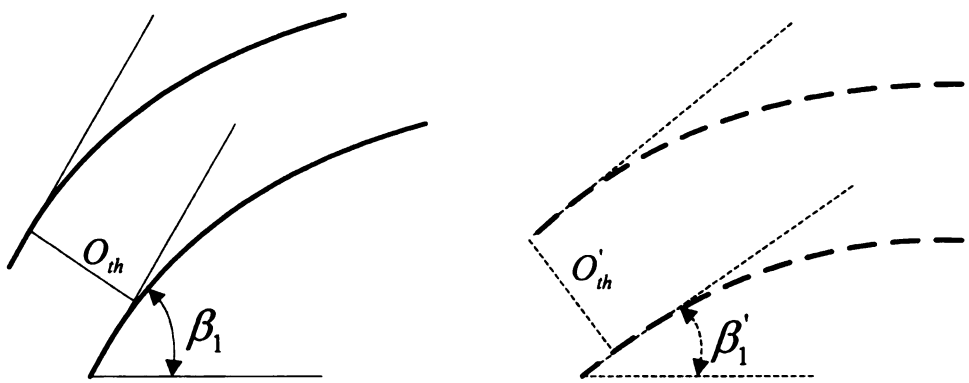

Figure 2-6 Influence of leading blade angle on throat area

The calculation of the zero loading incidence i_{kb} has been proposed: [7]

$$\tan\left(i_{kb}\right) = \frac{\varepsilon_{kb} \sin \beta_{1kb}}{1 - \varepsilon_{kb} \sin \beta_{1kb} \cdot \tan \beta_{1kb}} \tag{2-56}$$

Where the relative blade blockage ε_{kb} is defined by:

$$\varepsilon_{kb} = \frac{Z \cdot Tn}{2\pi R} \tag{2-57}$$

R_h of the inducer is much smaller than R_s. Therefore the large value of zero loading incidence at the hub occurs due to the larger value of the relative blade blockage ε_{kb}. It was supposed the lower value at the shroud because of the lower value of ε_{kb} at shroud. However, β_1 at shroud is larger than β_1 at hub, which results in the large zero loading incidence. The influence of β_1, V_{m1}, T_1 and R_1 were discussed as following:

The relationship between new blade angle due to blockage and the designed blade angle is:

$$\beta_{1kb} = \beta_1 - i_{1kb} \tag{2-58}$$

Assume there is no work done on the leading edge, therefore the tangential velocity remains the same, which means the tangential component of relative velocity is unchanged which is as shown in Figure 2-7.

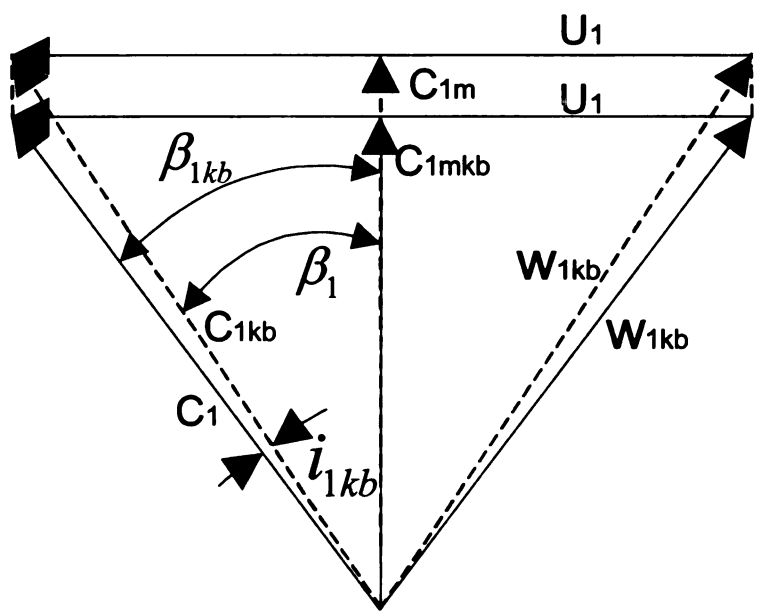

Figure 2-7 Influence of blade blockage on velocity triangle

Therefore the new relative velocity is:

$$W_{1kb} = \frac{W_1 \sin \beta_1}{\sin \beta_{1kb}} \tag{2-59}$$

The new axial velocity component is:

$$C_{1mkb} = \frac{C_{1m} \cdot \tan(\beta_1)}{\tan(\beta_{1kb})} \tag{2-60}$$

The new absolute velocity is:

$$C_{1mkb} = \sqrt{W_{1mkb}^2 + U_1^2 + 2W_{1mkb}U_1 \sin \beta_{1kb}} \tag{2-61}$$

Supposing there is no work done during the contraction of the fluid, the new static temperature due to the blockage of the blades is:

$$T_{1kb} = T_1 + \frac{C_1^2 - C_{1kb}^2}{2C_p} \tag{2-62}$$

Supposing an isentropic process, therefore the new static pressure can be calculated by:

$$P_{kb} = P_1 \left(\frac{T_{1kb}}{T_1} \right)^{\frac{\gamma-1}{\gamma}} \tag{2-63}$$

CHAPTER 3

GEOMETRY GENERATION TOOL

3.1 Impeller Geometry Specification

The impeller geometry parameters are introduced in this chapter. The most common coordinate system to describe impellers is (z,r,θ) which is as shown in Figure 3-1.

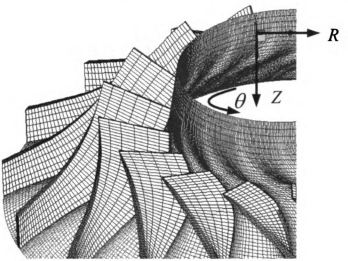

Figure 3-1 Illustration of coordinate system (z,r,θ)

Theoretically, coordinates of all points on each blade surface are required to specify the geometry shape of an impeller. However, the impeller is axial symmetrical and information on one blade shape is sufficient if the blade number is known.

If it is assumed that blade surface from hub to shroud can be approximated in polynomials, then only several section curves (Figure 3-3) are required to be specified instead the whole blade surface (Figure 3-2).

Figure 3-2 Whole blade surface[10]

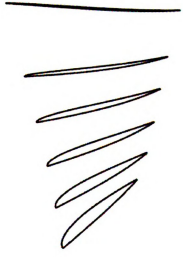

Figure 3-3 several section curves[10]

To calculate the points among these section curves, another coordinate system have to be introduced here. Besides the coordinate system (r,z,θ), all the points on surface blade can also be defined in a relative coordinate system (u,v,w) shown in Figure 3-4.

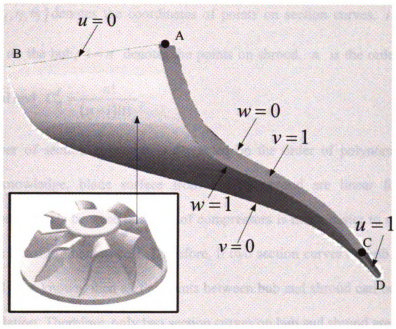

Figure 3-4 Illustration of coordinate system (u,v,w)[11]

Along the streamline from leading edge (AB) to trailing edge (CD), u increased from 0 to 1 while u=0 at the leading edge and u=1 at the trailing edge. Along the quasi-normal lines, v increased from 0 to 1 while v=0 at the hub and v=1 at the shroud. Along the pressure surface to suction surface, w increased from 0 to 1 while w=0 at the pressure surface, w=1 at the suction surface and w=0.5 at the camber surface. Physically, u can be viewed as normalized arc length of streamlines and v as normalized arc length of quasi-normal lines. As we mentioned above, if blade surface from hub to shroud can be approximated in polynomials, then the calculation of coordinates of any points on blade surface can be expressed by:

$$[z,r,\theta]^T = \sum_{i=0}^{n} C_n^i (1-v)^{n-i} v^i [z_i, r_i, \theta_i]^T \qquad (3\text{-}1)$$

Where (z_i, r_i, θ_i) denotes the coordinates of points on section curves, $i = 0$ denotes the points on the hub, $i = n$ denotes the points on shroud. n is the order of Bezier polynomial and $C_n^i = \frac{n!}{(n-i)!i!}$.

The number of section curves i is depended on the order of polynomial. To the author's knowledge, blade surface from hub to shroud are linear for most of compressors. This is because this type of compressors is much easier to manufacture and save a lot of production cost. Therefore, if two section curves on hub and shroud respectively are known, then all the points between hub and shroud can be calculated by interpolation. Therefore, only two section curves on hub and shroud are required to be specified. And coordinates of other points between hub and shroud can be interpolated by coordinates of these points on hub and shroud. Eqn. (3-1) can be also simplified into:

$$[z, r, \theta]^T = (1-v)[z_H, r_H, \theta_H]^T + v[z_S, r_S, \theta_S]^T \tag{3-2}$$

The shape of one section curves (Figure 3-3) can be further divided into the camber lines and thickness t which is normal to camber lines (Figure 3-5). The mean line of the section curve is called as camber line. Then only the camber lines on shroud and hub as well as their corresponding thickness distributions normal to camber lines, which are called as normal thickness distributions (Figure 3-6), are required to be defined instead of whole section curves. The definition of s in Figure 3-5 is expressed by:

$$ds = \sqrt{dr^2 + dz^2 + r^2 d\theta^2} \tag{3-3}$$

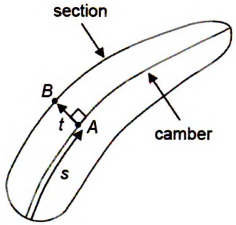

Figure 3-5 Illustration of camber line

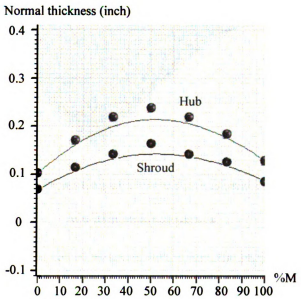

Figure 3-6 normal thickness distribution on shroud and hub

The camber line is a three dimensional curve in coordinate system (r,z,θ). If all points on the camber line are project onto the cross-sections in meridional plane, which is shown in Figure 3-7, then there is no change of θ in the projected plane. Therefore, this three dimensional curve can be transformed into two curves in two dimensional planes: one is (r,z) coordinate system while another is (r,θ) or (z,θ).

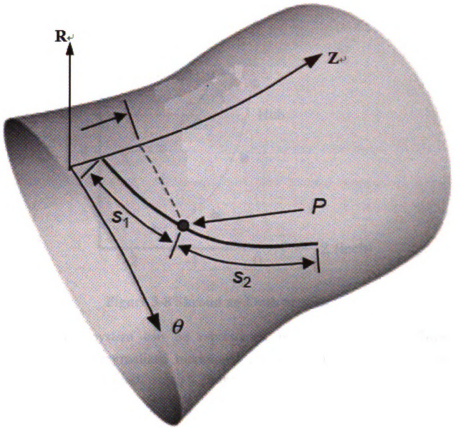

Figure 3-7 Transformation of a three dimensional curve into two two-dimensional planes

(r,z) coordinate system is called as meridional plane, the projected curve of camber line on hub is called as hub profile while one on shroud is called as shroud profile (Figure 3-8). The impeller outline which includes the shroud profile, hub profile, leading edge and trailing edge is called as contour in turbomachinery.

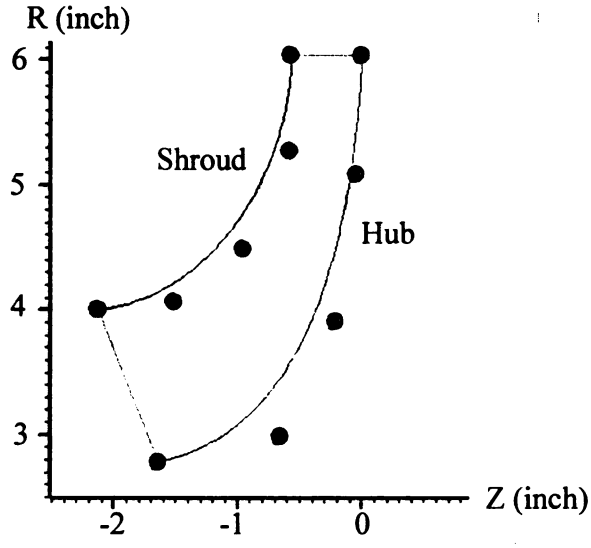

Figure 3-8 Shroud and hub profiles

Another coordinate system can be represented by (r,θ) or (z,θ). However, coordinate system of normalized meridional distance and beta angle distribution $(\%m,\beta)$ are commonly used, which is shown in Figure 3-9.

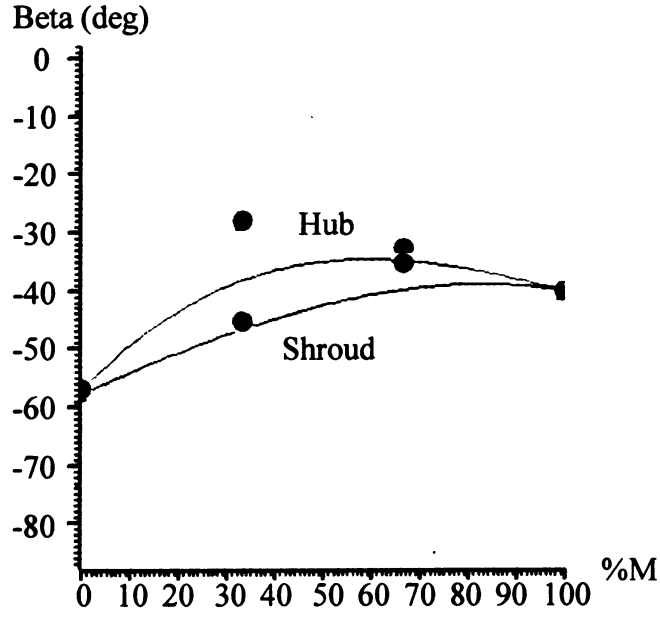

Figure 3-9 Blade angle distributions on shroud and hub

The derivative from, the continuous and discrete integer forms of calculation on meridional distance are respectively expressed by:

$$dm(u)=\sqrt{dr(u)^2+dz(u)^2} \tag{3-4}$$

$$m(u) = \int_0^u \sqrt{r'(u_1)^2 + z'(u_1)^2}\, du_1 \tag{3-5}$$

$$m_i = \sum_{j=2}^{i} \left(r_j - r_{j-1}\right)^2 + \left(z_j - z_{j-1}\right)^2 \tag{3-6}$$

Normalized meridional distance is ratio between current meridional distance from leading edge and whole meridional distance. The discrete normalized meridional distance is expressed by:

$$\%m_i = \frac{\sum_{j=1}^{i} m_j}{\sum_{j=1}^{n} m_j} \tag{3-7}$$

Normalized meridional distance $\%m$ or meridional distance m are monotonically increasing variables. Therefore each coordinates z, r and $\%m$ or m is correlated each other.

The wrap angle, also called theta angle θ represented the blade angle in an absolute coordinate system. And the definition of blade angle (β) is the angle between the camber line and axial cross section, which is actually impeller blade angle in the relative coordinate system and illustrated in Figure 3-10.

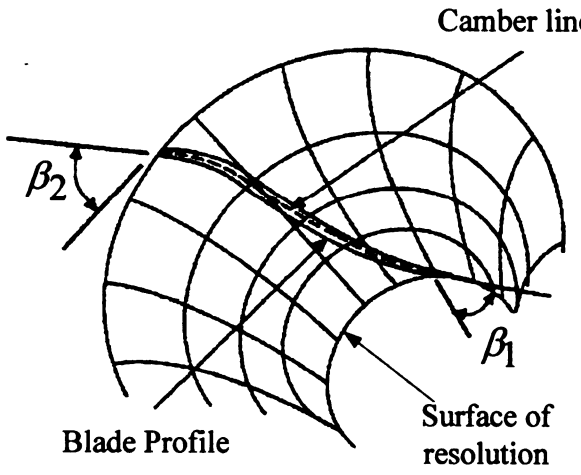

Figure 3-10 Illustration of blade angle

The equation to calculate blade angle distribution from wrap angle distribution is expressed by:

$$\beta_i = \tan^{-1}\left(r_i \frac{d\theta_i}{dm_i}\right) = \tan^{-1}\left(r_i \frac{d\theta_i}{\sqrt{dr_i^2 + dz_i^2}}\right) \tag{3-8}$$

The Eqns. to calculate wrap angle distribution from blade angle are expressed by:

$$\theta_i = \int_{j=0}^{i} \frac{\tan(\beta_j)\, dm_j}{r_j} + \theta_{LE} \tag{3-9}$$

We can see that once normal thickness distributions, blade angle distributions, hub profile and shroud profile, which are called contour in this study, are specified, then the whole impeller geometry can be fixed.

3.2 Geometry Parameters

3.2.1 One-dimensional Geometry Parameters

All inlet and exit variables of these three two-dimensional distributions are defined as one-dimensional parameters, which are listed in

Table 3-1. Besides, blade number can be also considered as one-dimensional parameter.

Table 3-1 One dimensional impeller geometry parameters

Area	Symbols
Contours (R-Z coordinates system)	$R_{1S}, R_{1H}, R_{2S}, R_{2H}, Z_{1S}, Z_{1H}, Z_{2S}, Z_{2H}$
Angle Distribution	$\beta_{1S}, \beta_{1H}, \beta_{2S}, \beta_{2H}, \theta_{1S}, \theta_{1H},$
Thickness Distribution	$Tn_{1S}, Tn_{1H}, Tn_{2S}, Tn_{2H}$
Number of full blade	Z

Design on these geometry parameters in Table 3-1 is called as one preliminary design, which is basis of the design. There is no good performance of compressor can be obtained without a good 1D design.

3.2.2 Two-dimensional Geometry Parameters

Design on contour, blade angle distribution or normal thickness distribution can be considered as two-dimensional design. Bezier polynomials are used to describe the profiles of contours and distributions because of the characteristics of Bezier polynomials including flexibility, smoothes and continuity. The general formulation of Bezier polynomial is expressed by:

$$x(u) = \sum_{i=0}^{n} C_n^i u^i (1-u)^{n-i} x_{node,i} \tag{3-10}$$

Where $C_n^i = \frac{n!}{(n-i)!i!}$; n is the order of Bezier polynomial and $n = n_{node} - 1$, n_{node} is the number of node points.

The equations of Bezier polynomial used to calculate contour are expressed by:

$$\begin{cases} z(u) = \sum_{i=0}^{n} C_n^i u^i (1-u)^{n-i} z_{node,i} \\ r(u) = \sum_{i=0}^{n} C_n^i u^i (1-u)^{n-i} r_{node,i} \end{cases} \tag{3-11}$$

After the preliminary design, there are only two node points. The order of Bezier polynomial is one and the Eqn. (3-11) for calculating R and Z can be rewritten into Eqn. (3-12) and the contour is also as shown in Figure 3-11.

$$\begin{cases} z(u) = \sum_{i=0}^{1} C_1^i u^i (1-u)^{1-i} z_{node,i} = (1-u) z_1 + u z_2 \\ r(u) = \sum_{i=0}^{1} C_1^i u^i (1-u)^{1-i} r_{node,i} = (1-u) r_1 + u r_2 \end{cases} \tag{3-12}$$

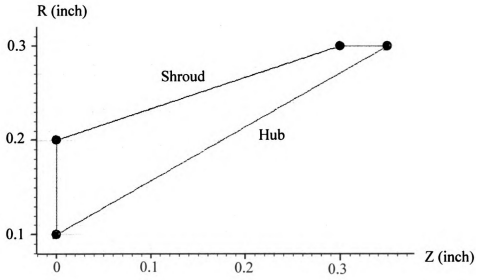

Figure 3-11 Illustration of one-order Bezier polynomial with only inlet and outlet control node points

To change contours to achieve the desired curves, more node points are required to add to Bezier polynomials. Without changing the profiles of contours, the new coordinates of node points are expressed by:

$$\begin{cases} z'_{node,i} = \dfrac{i \cdot z_{node,i-1} + (n+1-i) \cdot z_{node,i}}{n+1} \\ r'_{node,i} = \dfrac{i \cdot r_{node,i-1} + (n+1-i) \cdot r_{node,i}}{n+1} \end{cases} \quad i = 0,1,\cdots,n+1 \tag{3-13}$$

Where $\left(z'_{node,i}, r'_{node,i}\right)$ is the coordinates of new node points while $\left(z_{node,i}, r_{node,i}\right)$ is the coordinate of old node points. n is the original order of Bezier polynomial before adding one node and $n+1$ is the new order.

From the Eqn. (3-14), it can be seen that when $i=0$, $z_{node,i-1}=z_{node,-1}$ doesn't exist. However the weight factor in front of $z_{node,-1}$ is zero. Therefore, the whole term $i \cdot z_{node,i-1}$ goes to zero and has no influence on the result. The similarity also occurred when $i=n+1$.

During the editing of contour, the order of Bezier polynomial may be required to reduce if too many node points have been added; the coordinates of new node points are expressed by without significant changes on the profile of Bezier curves:

$$\begin{cases} z'_{node,i} = \dfrac{(n-1-i)\cdot z_{node,i-1} + i \cdot z_{node,i}}{n-1} \\ r'_{node,i} = \dfrac{(n-1-i)\cdot r_{node,i-1} + i \cdot r_{node,i}}{n-1} \end{cases} \quad i=0,1,\cdots,n-1 \qquad (3\text{-}14)$$

When the coordinates of node points of Bezier curves are changed, the profile of Bezier curves is also changed correspondingly. The adding and moving of node points on hub profile is as shown in Figure 3-12.

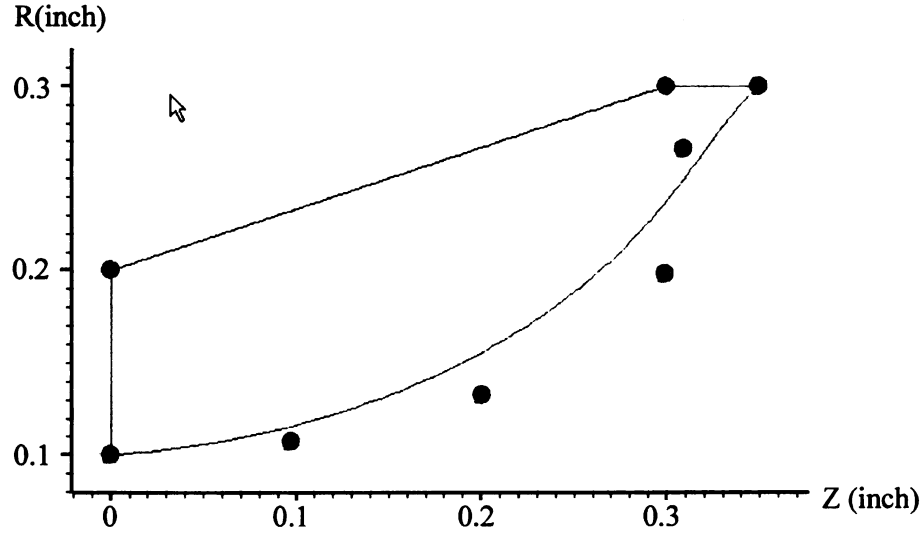

Figure 3-12 Illustration of adding and moving node points on hub profile

3.3 Calculation of Lean Angle

The definition of lean angle is illustrated in Figure 3-13, which is the view from axis direction. The calculation of lean angle is expressed by:

$$\theta_{Lean,i} = \theta_{S,i} - \theta_{H,i} \tag{3-15}$$

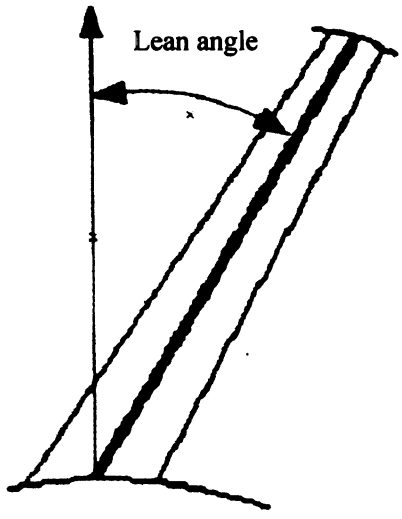

Figure 3-13 Illustration of lean angle

Because $\theta_{S,i}$ and $\theta_{H,i}$ belongs to two different Bezier polynomials and how to

decide a pair of θ_i on shroud and hub is the difficulty of calculating $\theta_{Lean,i}$. This depends on the definition of quasi-normal lines in the meridional plane. Different definitions lead to different results of lean angle distribution. Two different definitions of quasi-normal lines are discussed here.

The first definition is that quasi-normal lines have same values of u on shroud and hub (Figure 3-14); the second definition is that quasi-normal lines are normal to mean lines of blades (Figure 3-15). Lean angle distributions based on first definition and second definition of quasi-normal lines are as shown in Figure 3-16 and Figure 3-17. And the lean angle at exit is named as rake angle.

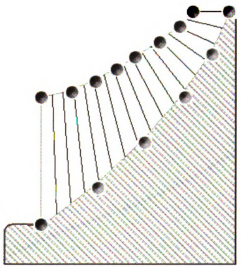

Figure 3-14 First definition of quasi-normal lines

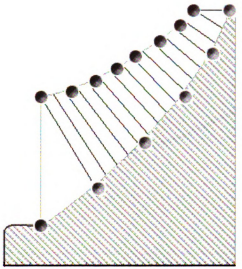

Figure 3-15 The second definition of quasi-normal lines

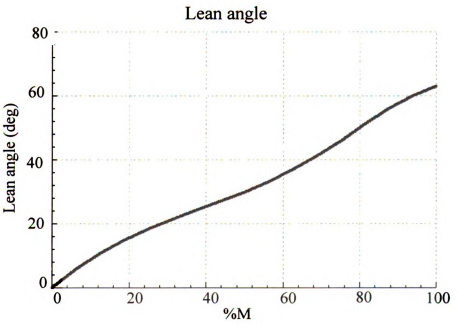

Figure 3-16 Lean angle distribution based on first definition of quasi-normal lines

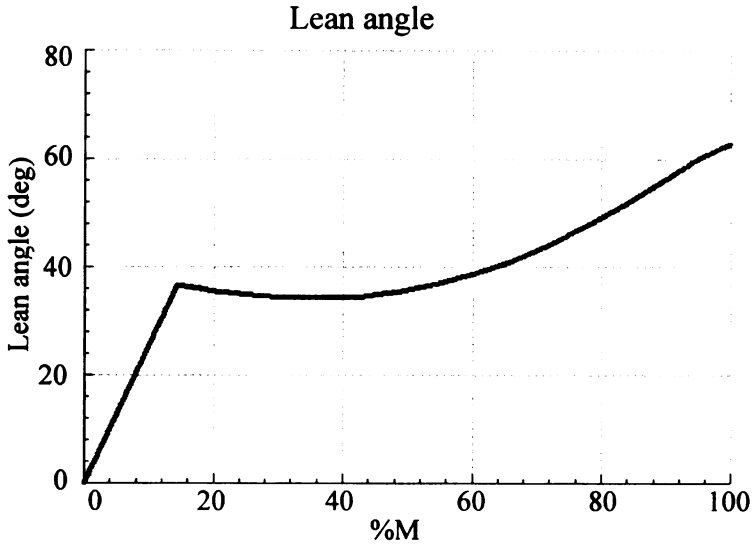

Figure 3-17 Lean angle distribution based on second definition of quasi-normal lines

In Figure 3-16 and Figure 3-17, X coordinate denotes normalized meridional distance. The value changes from 0% to 100%. Y coordinate denotes lean angle. The unit is degree. In these two figures, lean angle changes from 0 to 63 as %M changes from 0% to 100%.

The great difference between first method and second method is that the quasi-normal lines are vertical to mean lines in the second method. Because this definition, we can see that at the leading edge and trailing edge, lean angle distribution is not continuous. Moreover, the values of u of the intersection point between quasi-normal lines and shroud or hub are not equal. Generally we count the leading edge and trailing edge as the first and the last Quasi-Normal lines in second method, although these two lines are not vertical to the corresponding mean line.

As mentioned above, lean angle distribution greatly depends on quasi-normal lines distribution. Therefore, the comparison of first method and second method to define quasi-normal lines are introduced here, which is as shown in Figure 3-18 and Figure

3-19. S_iH_i are lines which are used to calculate lean angle distribution. In the first method, lengths of arcs S_1S_2, S_2S_3, S_3S_4 are equal while those of H_1H_2, H_2H_3,H_3H_4 are equal. If there are 11 points on each shroud and hub, then corresponding u of each points on shroud and hub are 0, 0.1, 0.2, ...,0.9,1.0. The determination of lines in second method is as shown in Figure 3-19. Each quasi-normal line is normal to the mean line at the intersection.

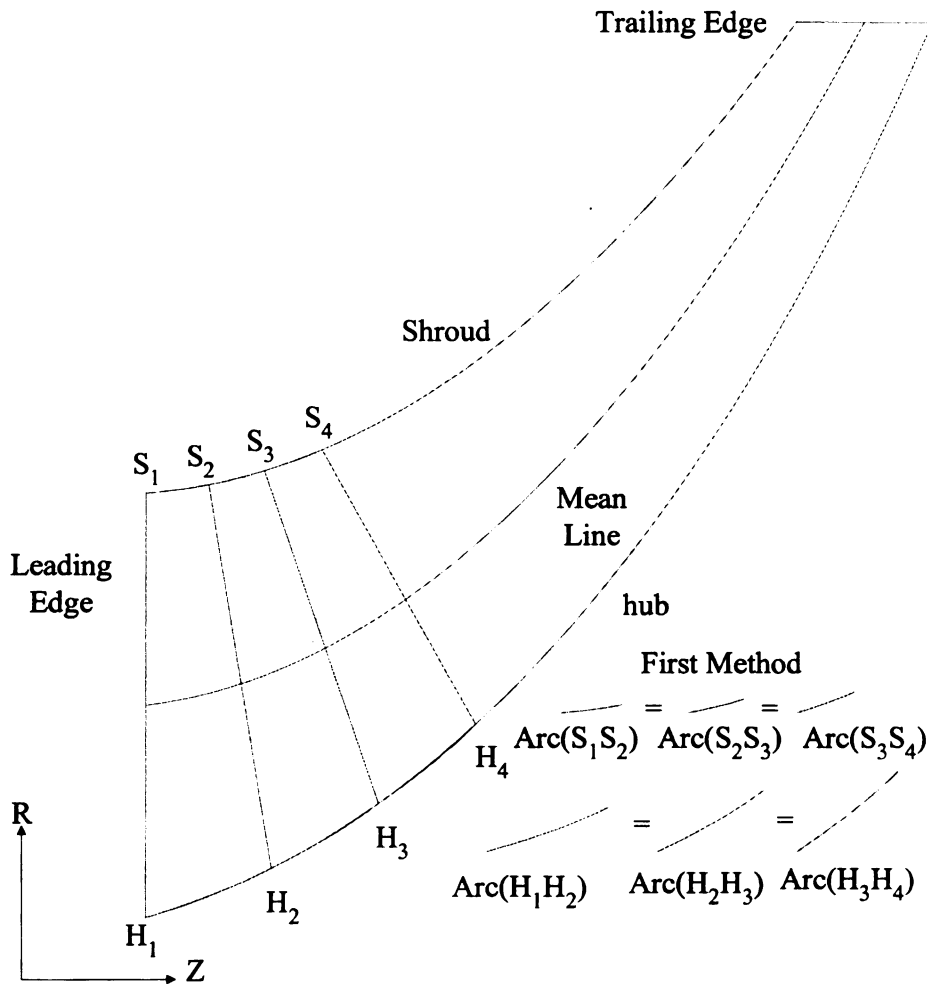

Figure 3-18 Generations of quasi-normal lines of first method

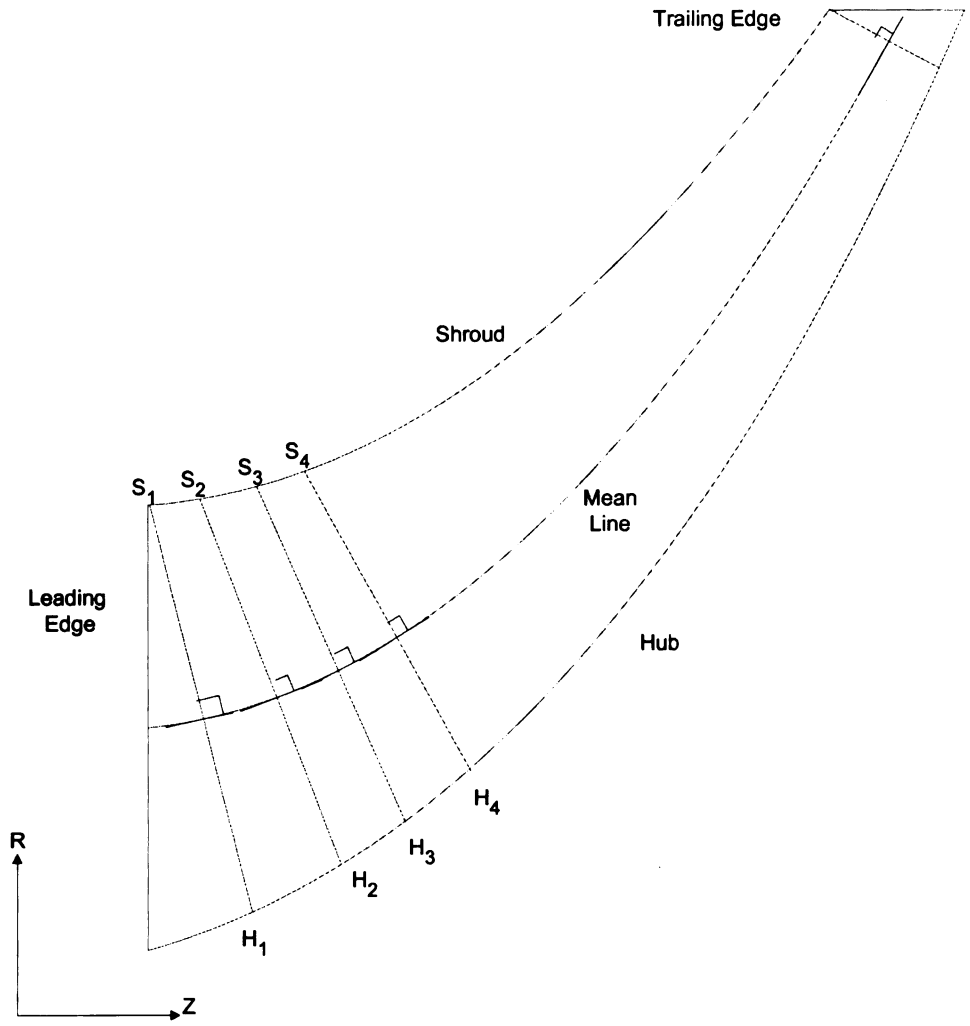

Figure 3-19 Generations of quasi-normal lines of second method

Generally, we define the leading edge as the 1st Quasi-Normal line. But we need to find 2nd Quasi-Normal line. The difficulty in finding that is because the contour of shroud, hub and mean line are not standard equations. Therefore, we have to use iteration method to search. At the first, we calculate angle of leading edge α_1. Then we calculate the angle α_2 of normal line at the beginning of mean line. If $\alpha_1 < \alpha_2$, then we can see that the position of 2nd Quasi-Normal line depends on shroud. On the contrary, it would depend on hub. S1H1 is the 2nd Quasi-Normal as shown in Figure 3-20. The next step is to find the foot of perpendicular from one point on shroud to

mean line. However, the contour of mean line is not standard equation either. Therefore, iteration method is applied. If we want to find the point M2 which is the foot of perpendicular from point S2 to the mean line. M2Lef and M2Rig are points which are left and right of M2, but very close to. The intersection angle between S2M2 and normal line at point M2 should be zero, which means S2M2 is normal to mean line at point M2. However, one intersection angle of M2Lef and M2Rig should be positive and another one should be negative. Which one is positive depends on the definition of intersection angle. Hence, once we find M2Lef and M2Rig by iteration method, it will be very easy to find M2. The accuracy of coordinates of M2 depends on resolution. However, high resolution will higher computational time.

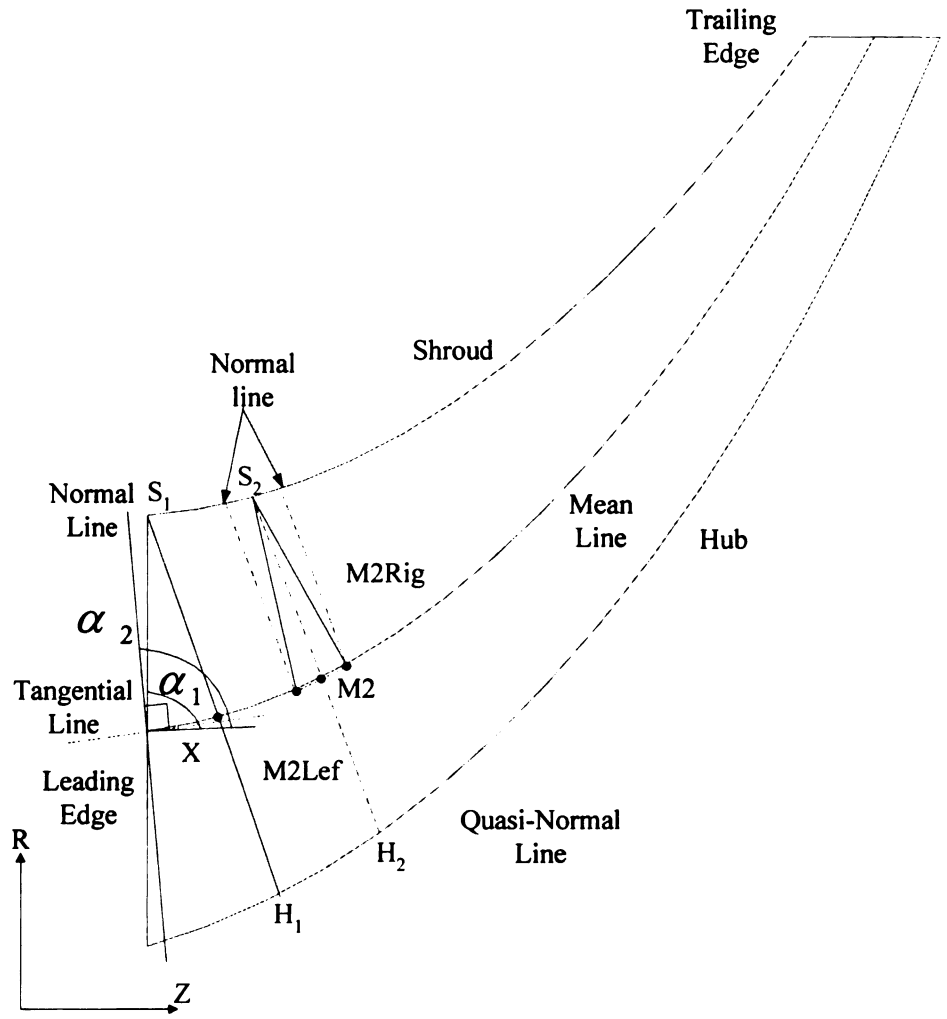

Figure 3-20 Illustration of generating quasi-normal line in second method

The equation for the calculation of lean angle distribution in BladeCAD:

$$\theta_{i,Lean} = \frac{R_{i,shr}\left(\theta_{i,shr} - \theta_{i,hub}\right)}{\sqrt{\left(R_{i,shr} - R_{i,hub}\right)^2 + \left(Z_{i,shr} - Z_{i,hub}\right)^2}} \tag{3-16}$$

The calculation of mean line in meridional plane:

$$R_{i,ML} = \frac{R_{i,shr} + R_{i,hub}}{2} \tag{3-17}$$

$$Z_{i,ML} = \frac{Z_{i,shr} + Z_{i,hub}}{2} \tag{3-18}$$

3.4 Calculation of Theta and Beta angle

If the rake angle is known, the equations of calculating Theta Angle are expressed as following:

$$\theta_{LE,shr} = 0 \tag{3-19}$$

$$\theta_{i,shr} = \theta_{i-1,shr} + \frac{\tan(\beta_{i,shr})}{R_{i,shr}} \mathrm{d}m_i \quad i = 1,2,.....,m \tag{3-20}$$

$$\theta_{TE,hub} = \tan(\theta_{Rake}) \frac{Z_{TE,hub} - Z_{TE,shr}}{R_{TE,shr}} + \theta_{TE,shr} \tag{3-21}$$

$$\theta_{i,hub} = \theta_{i+1,hub} - \frac{\tan(\beta_{i,hub})}{R_{i,hub}} \mathrm{d}m_i \quad i = 1,2,.....,m \tag{3-22}$$

If the inlet shroud theta angle and hub inlet theta angle are known, then the Eqns. to calculate the theta angle distribution are:

$$\theta_{i,shr} = \theta_{i-1,shr} + \frac{\tan(\beta_{i,shr})}{R_{i,shr}} \mathrm{d}m_i \quad i = 1,2,.....,m \tag{3-23}$$

$$\theta_{i,hub} = \theta_{i-1,hub} + \frac{\tan(\beta_{i,hub})}{R_{i,hub}} \mathrm{d}m_i \quad i = 1,2,.....,m \tag{3-24}$$

where

$\theta_{LE,shr}$, $\theta_{LE,hub}$ denote theta angles of leading edge on shroud and hub respectively

$\theta_{TE,shr}$, $\theta_{TE,hub}$ denote theta angles of trailing edge on shroud and hub respectively

$\theta_{i,shr}$ denotes theta angle at point i on shroud

$\theta_{i,hub}$ denotes theta angle at point i on hub

$\beta_{i,shr}$ denotes beta angle at point i on shroud

i denotes the number of Quasi-Normal lines

3.5 Calculation of Leading and Trailing Edge

The developed geometry design tool has the function of output geometry files, which can be used to generate mesh and calculate impeller performance using flow solver. Variables $(R, Z, \%m, \theta, \beta, tn)$ of points are output in this geometry output files. R and Z are calculated from Eqn. (3-11). $\%m$ is calculated based on Eqn. (3-7). The β, tn are calculated from node points on blade angle distribution and normal

thickness distribution. Eqns. to calculate β_i, tn_i are respectively expressed by:

$$\beta(u) = \sum_{i=0}^{n} C_n^i (u)^i (1-u)^{n-i} \beta_{node,i} \tag{3-25}$$

$$Tn(u) = \sum_{i=0}^{n} C_n^i (u)^i (1-u)^{n-i} tn_{node,i} \tag{3-26}$$

However, it should be emphasize that each variable $(R, Z, \%m, \theta, \beta, tn)$ should be correlated to one point, which also means $R, Z, \%m, \theta, \beta, tn$ should be related to the same value of u. If R, Z are calculated based on node points in contour, β_i is calculated based on node points in blade angle distribution, and tn_i are calculated based on node points in normal thickness distribution. Then the same distributions of u have to choose. Otherwise, u are required to interpolate in blade angle distribution and normal thickness distribution to obtain the same distribution as u distribution in the contour. After $(R, Z, \%m, \beta, tn)$ are calculated, then θ could be calculated based on Eqn. (3-23) and (3-24).

The surface file contains variable (x, y, z, r, θ) on pressure side (leading surface) and suction side (trailing surface) of section curves. And these data are calculated based on data of camber line. As mentioned before, every point can be denotes in coordinate system (z, r, θ) and x, y can be calculated from r, θ, which are expressed by:

$$x = r\sin(\theta) \tag{3-27}$$

$$y = r\cos(\theta) \tag{3-28}$$

Pressure and suction side should be calculated in the $(m, \theta r)$ coordinate system as shown in Figure 3-21. The calculation of $(z_{suc}, r_{suc}, \theta_{suc})$ on the suction side based on data of camber lines has three steps.

The first step is to calculate $z_{suc}(u)$ and $\theta_{suc}(u)\cdot R_{suc}(u)$, which are expressed by:

$$z_{suc}(u)=z(u)-0.5Tn(u)\sin(\alpha) \tag{3-29}$$

$$\theta_{suc}(u)\cdot R_{suc}(u)=z(u)+0.5Tn(u)\cos(\alpha) \tag{3-30}$$

The second step is to calculate $R_{suc}(u)$ based on the value of $Z_{suc}(u)$. If $Z_{suc}(u)=Z(u)$, then $R_{suc}(u)=R(u)$.

The third step is to calculate $\theta_{suc}(u)$ after the $R_{suc}(u)$ has been obtained by

$$\theta_{suc}(u)=\frac{\theta_{suc}(u)\cdot R_{suc}(u)}{R_{suc}(u)}$$

The method of calculating $(z_{pre},r_{pre},\theta_{pre})$ on the pressure side is similar to the Eqns. for calculating $(z_{pre},r_{pre},\theta_{pre})$, while calculation of $z_{pre}(u)$ and $R_{pre}(u)\cdot\theta_{pre}(u)$ are different:

$$z_{pre}(u)=z(u)+0.5Tn(u)\sin(\alpha) \tag{3-31}$$

$$\theta_{pre}(u)\cdot R_{pre}(u)=z(u)-0.5Tn(u)\cos(\alpha) \tag{3-32}$$

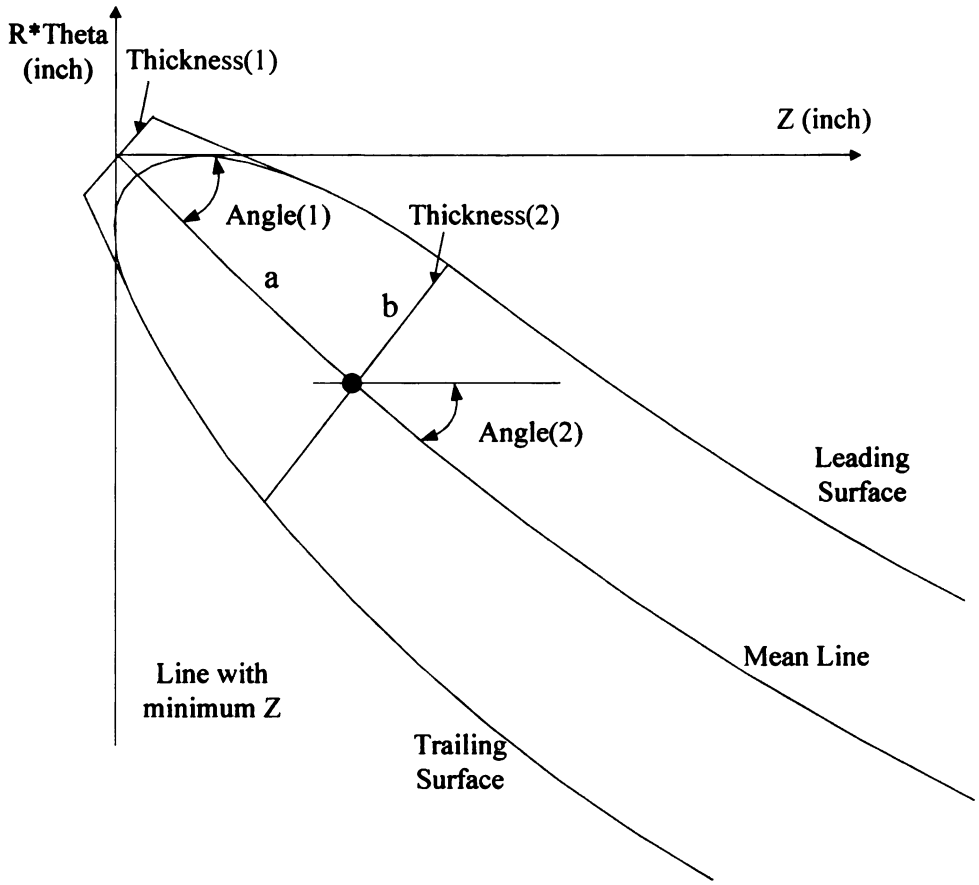

Figure 3-21 Illustration of calculation of leading edge

To calculating all points on pressure side and suction side are not sufficient, because the leading edge and trailing edge has to be designed to reduce blockage and separation, especially for leading edge. Therefore, the semi-ellipse is used to substitute the blunt leading edge, which is also as shown in Figure 3-21. The ellipse ratio is specified by designers. Therefore the center of ellipse is the most important factor to be determined. The calculation of center of ellipse is based on trail-and-error method and under the assumption that the blade angle is a constant in the leading edge, which has several steps as following:

The first step is to choose a point as center of ellipse on the camber and then the ellipse function $Az^2 + Bzr + Cr^2 + Dz + Er + F = 0$ can be determined.

The second step is to calculate the number of intersection points between ellipse and line with minimum Z. Because the leading edge is assumed to be tangential to the line with minimum Z. To calculate the number of intersection points between ellipse and line with minimum Z, Z_{min} is input into the ellipse function and the values of R are calculated. If there is no real solutions for R, then there is no intersection points between ellipse and line with minimum Z, and the center of ellipse should be moved toward the line with minimum Z; if there are two different real solutions for R, then the center of ellipse should be moved away from the line with minimum Z. This iteration ends during the there are two same real solutions have been obtained.

In Figure 3-22 we can see that the leading and trailing surface begin at 3rd point instead of 1st point. In fact, this number is influenced by many factors including ratio of ellipse and the number of points to output. As shown in Figure 3-22, all calculation of points on leading edge or leading surface or trailing surface are depends on camber line. When the number of points P to output has been decided. BladeCAD divided mean line into P small parts, as shown by red points. The green points on leading surface or trailing surface output after the output of coordinates of blue points on leading edge. The beginning number represents the position where the leading surface and trailing surface begin. If the number for output is 50 instead, the space between two close points increased 100%, which is shown with square in Figure 3-22. Besides, if the ratio increases, the beginning number may also increases.

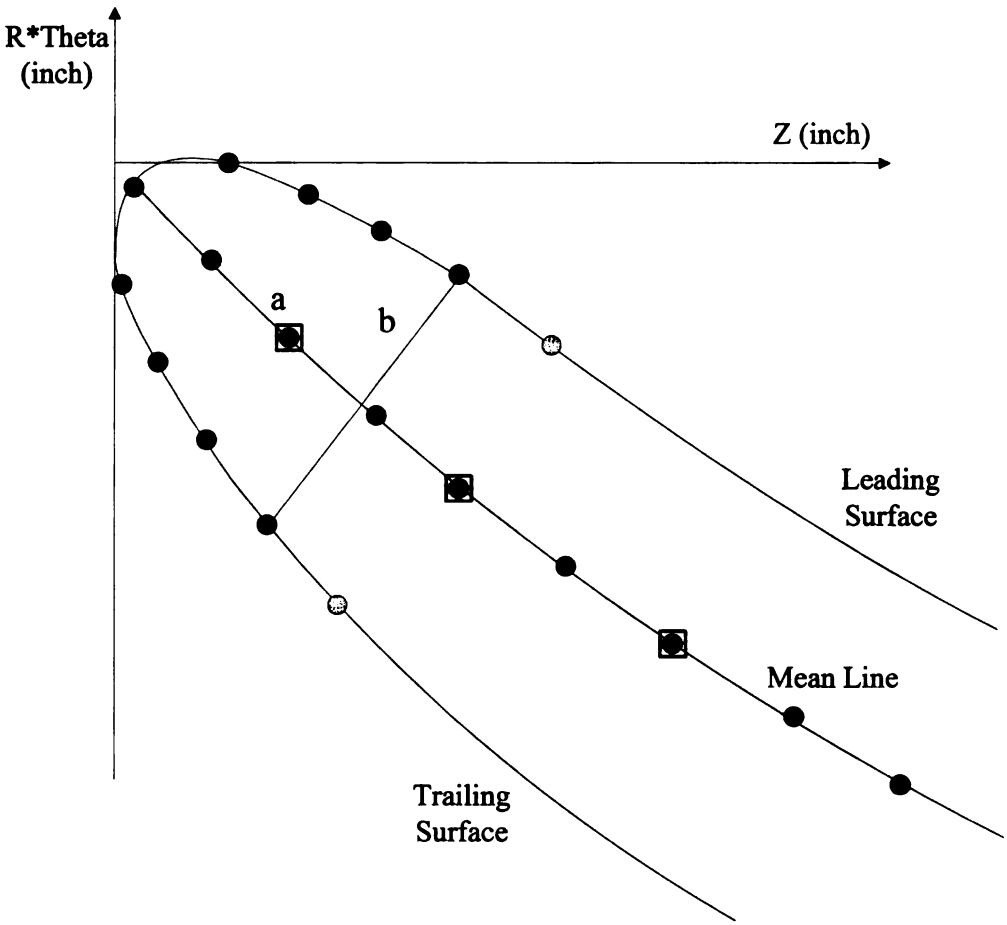

Figure 3-22 Illustration of starting point on leading edge

The condition at trailing edge is as shown in Figure 3-23. It can be seen that *Z* coordinate of last point on leading surface is already larger than 0 while that on the trailing surface is less than 0 although that of camber line is equal to 0 . This is the influences of thickness and exit blade angle. In BladeCAD, the shape of trailing edge is defined as blunt. The last point the leading surface is move left to the point with the same Z coordinate as the last point on the camber line. The same method is used for the last point on the trailing edge but in the inverse direction (Figure 3-23).

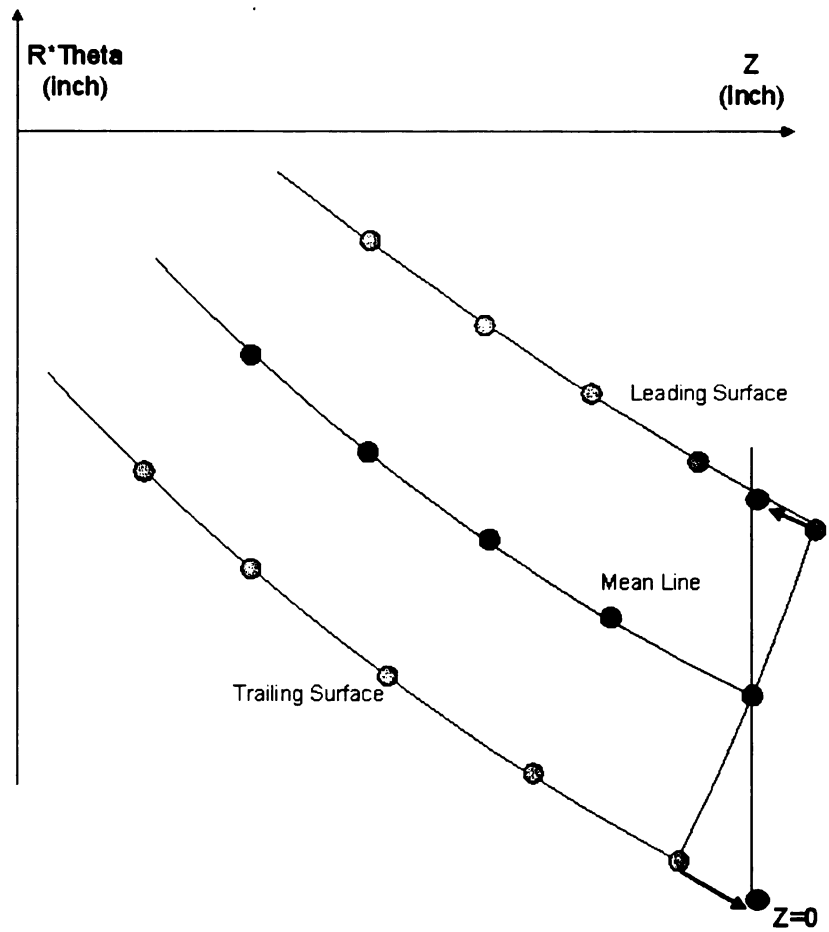

Figure 3-23 Illustration of trailing edge

3.6 Comparison of BladeCAD and CCAD

To compare the developed geometry tool, contour, blade angle distribution, normal thickness distribution, theta angle distribution, lean angle distribution, leading edge, leading and trailing surface of BladeCAD are compared with those of CCAD, commercial software.

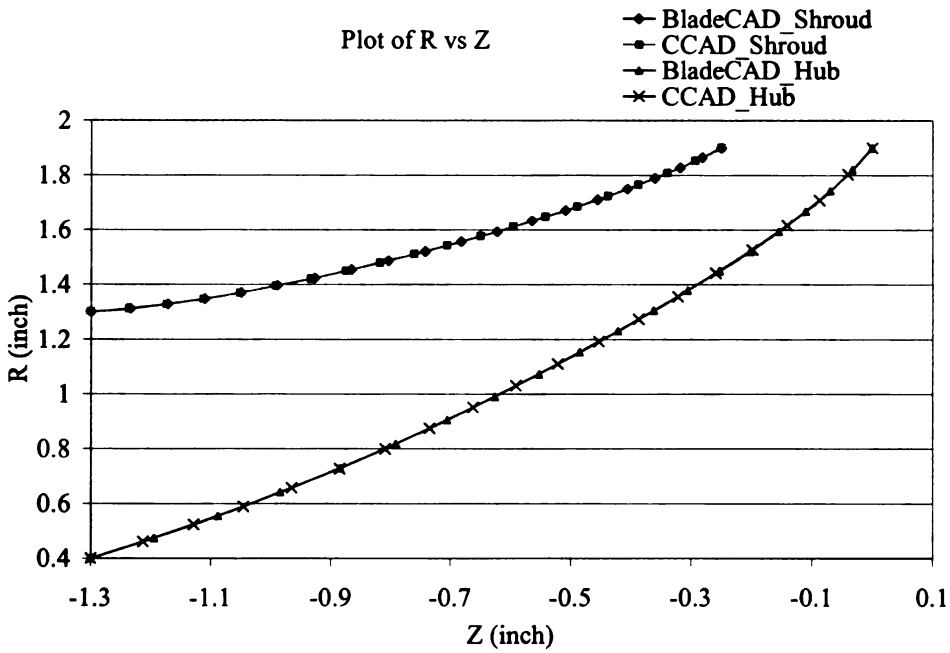

Figure 3-24 Comparison of Contours

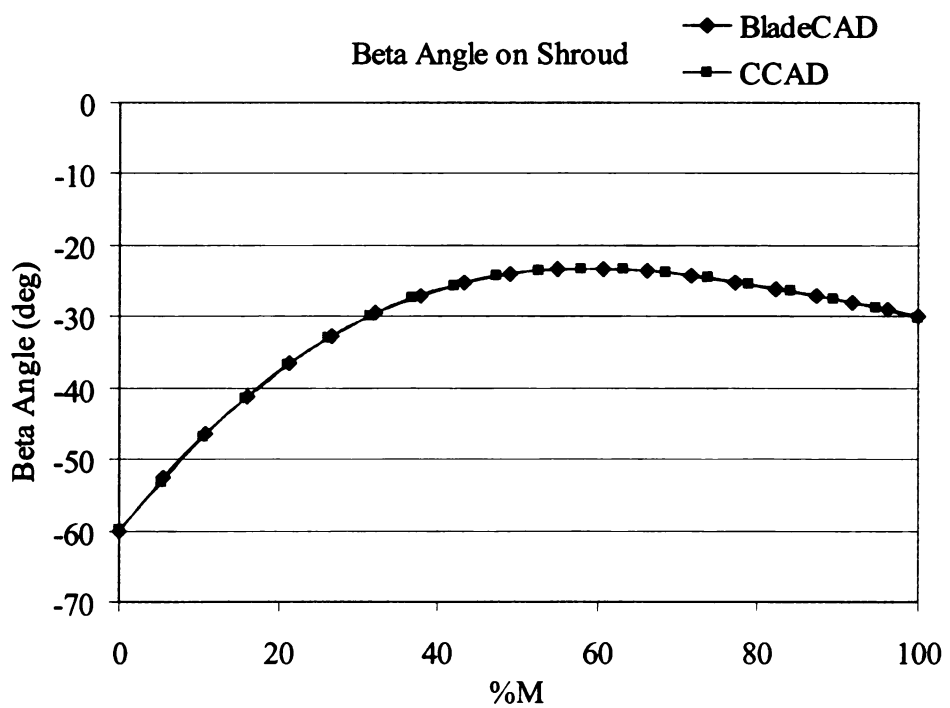

Figure 3-25 Comparison of beta angle distribution on shroud

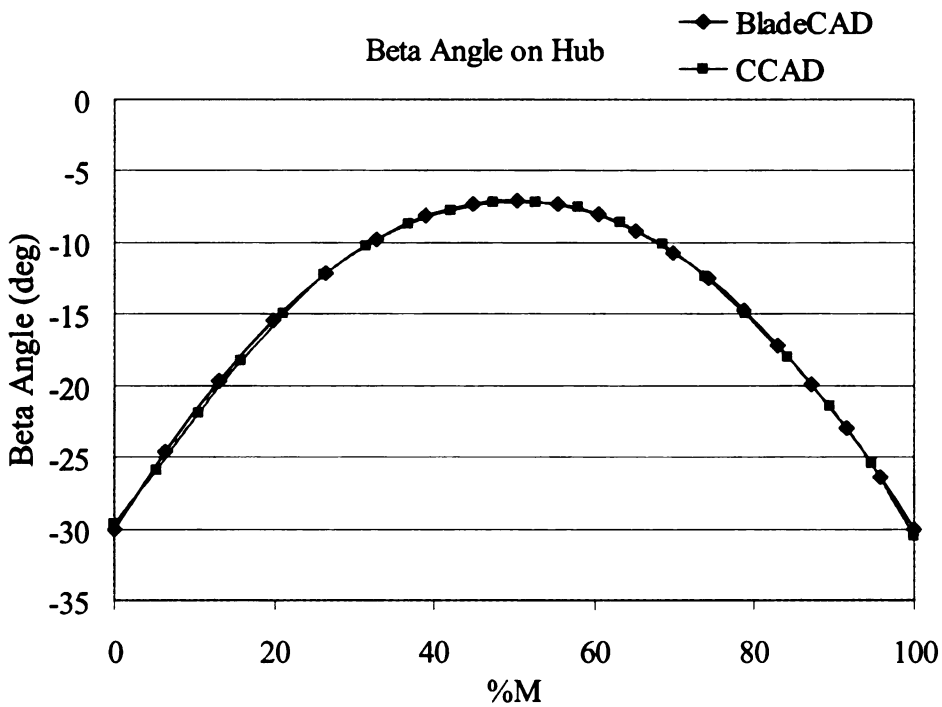

Figure 3-26 Comparison of beta angle distribution on hub

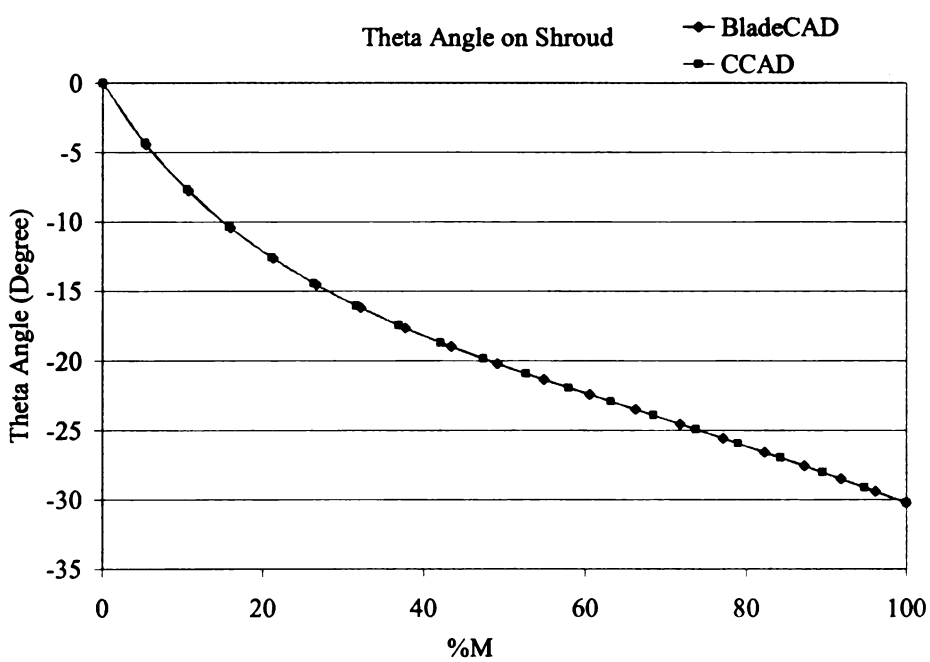

Figure 3-27 Comparison of theta angle distribution on shroud

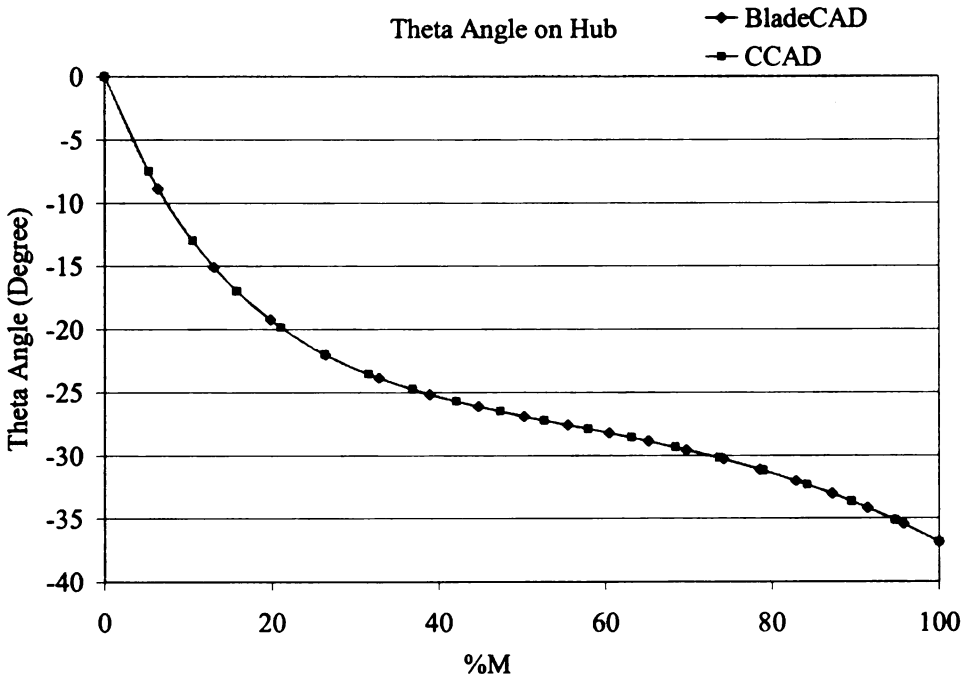

Figure 3-28 Comparison of theta angle distribution on hub

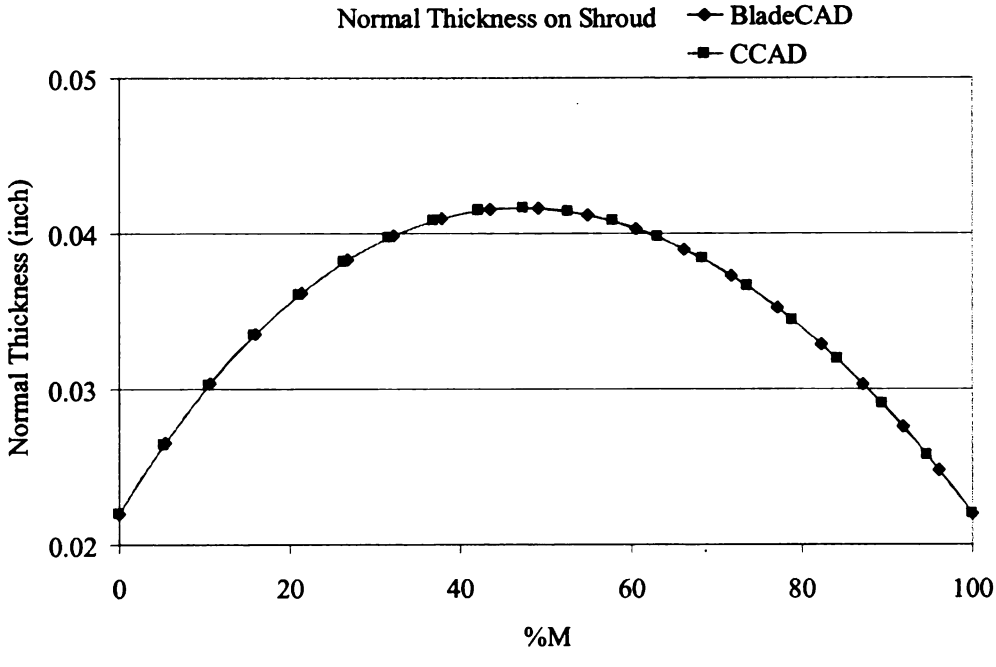

Figure 3-29 Comparison of normal thickness distribution on shroud

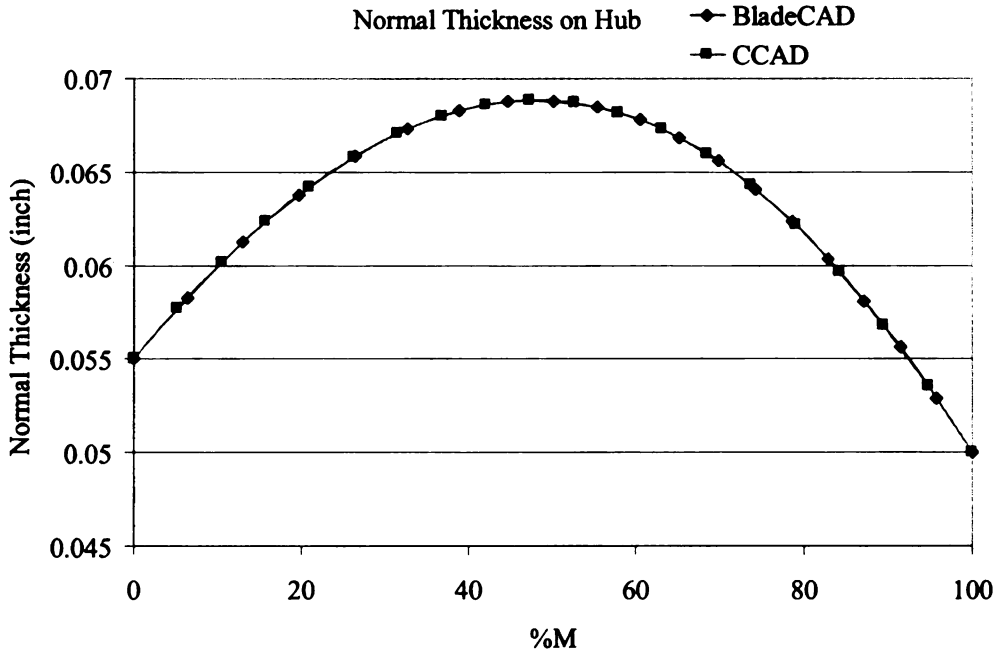

Figure 3-30 Comparison of normal thickness distribution on shroud

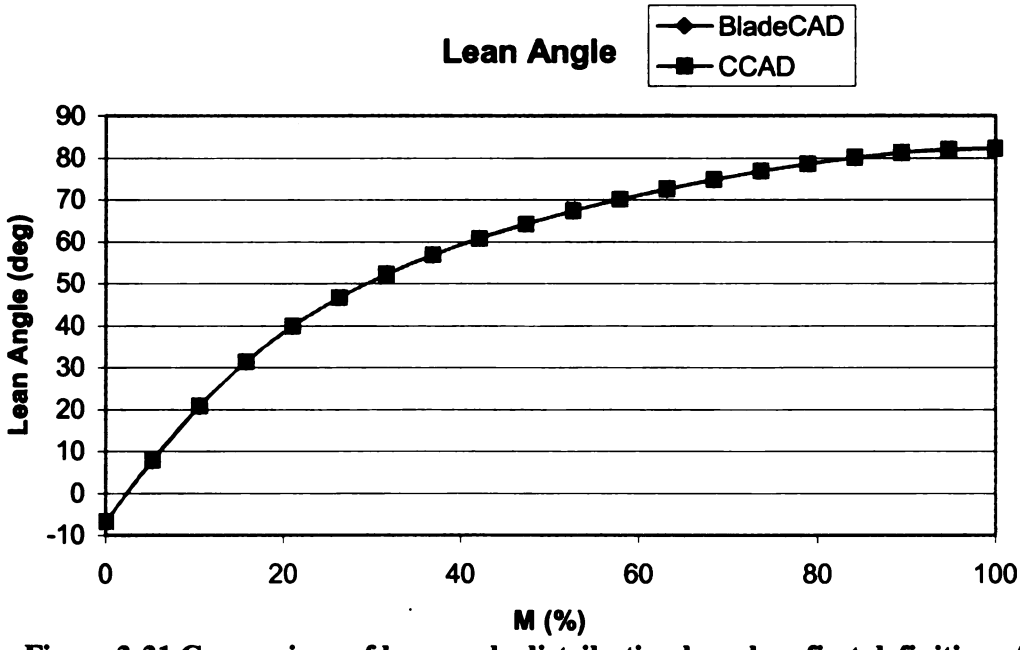

Figure 3-31 Comparison of lean angle distribution based on first definition of quasi-normal lines

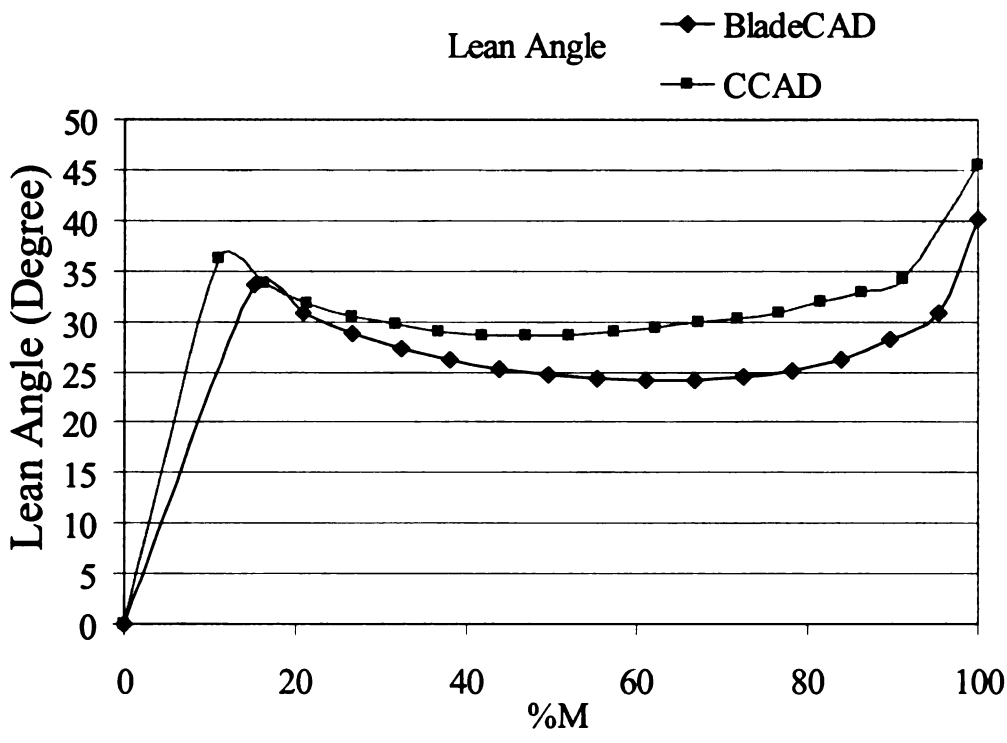

Figure 3-32 Comparison of lean angle distribution based on second definition of quasi-normal lines between BladeCAD and CCAD

The differences of lean angle distributions between BladeCAD and CCAD (Figure 3-32) are resulted from the different calculation method on quasi-normal lines.

Before we compare Leading Edge (L.E.), there are three parameters needed to be set. The type of L.E. has been set to semi-ellipse. The number of L.E. points has been set as 9. The L.E. ellipse aspect ratio has been set as two different values: 2 and 4, and the comparison results are shown as following:

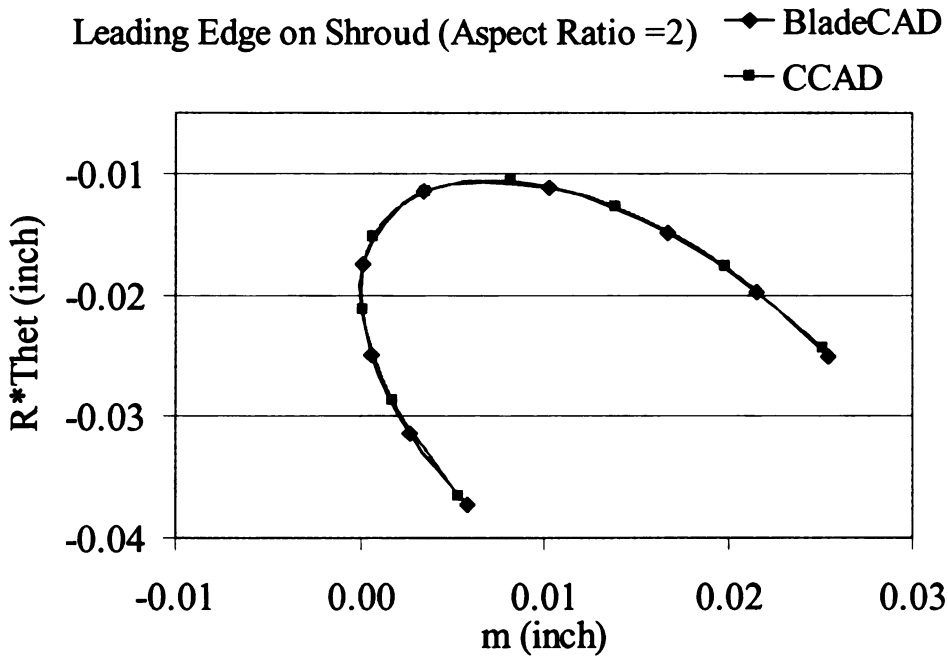

Figure 3-33 Comparison of lead edge on shroud (ellipse aspect ratio = 2)

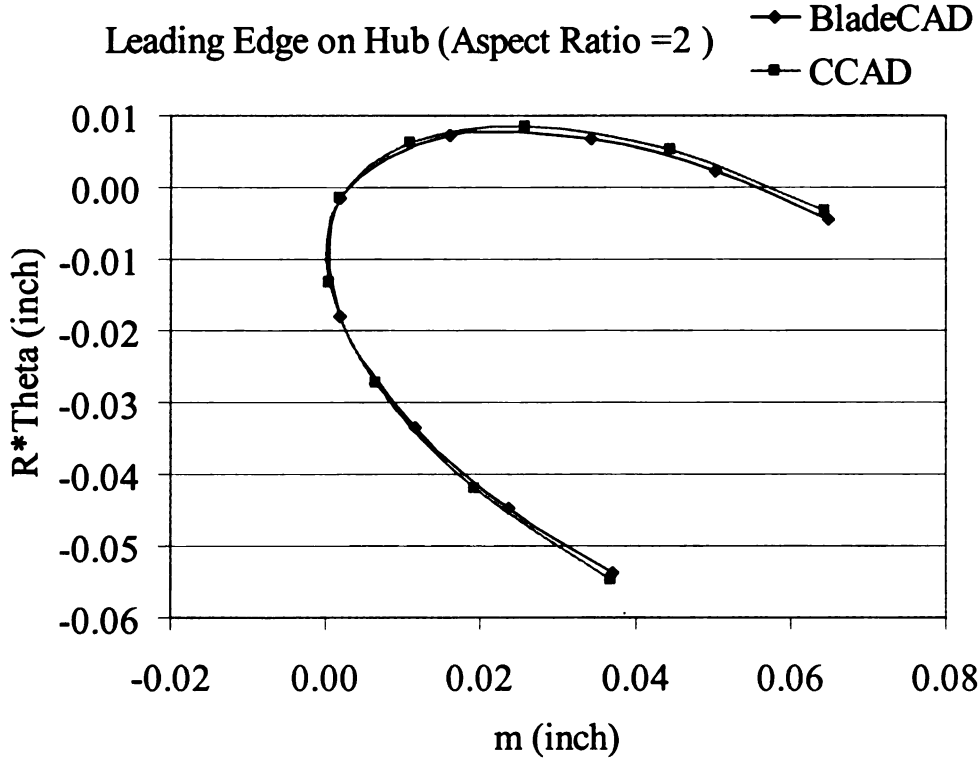

Figure 3-34 Comparison of lead edge on shroud (ellipse aspect ratio = 2)

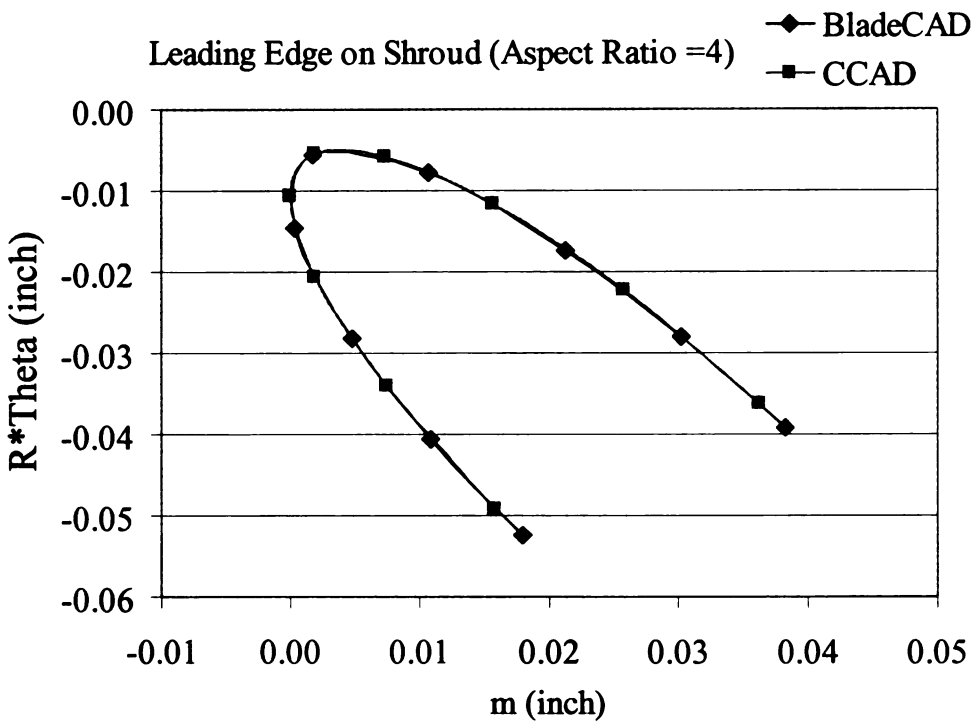

Figure 3-35 Comparison of lead edge on shroud (ellipse aspect ratio = 4)

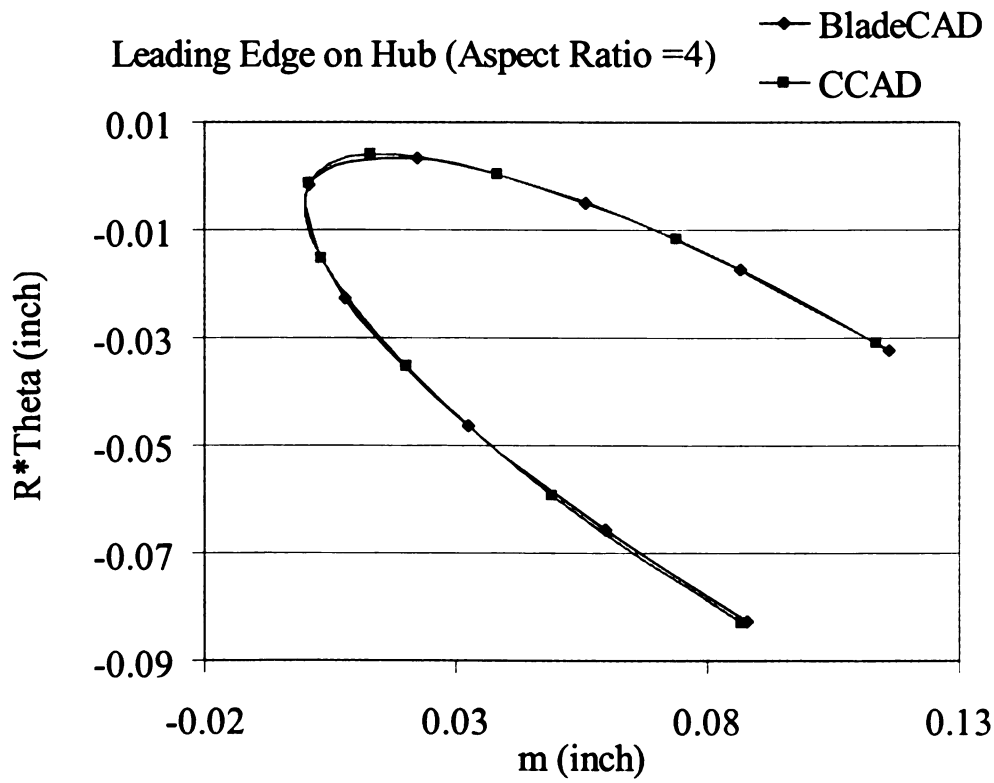

Figure 3-36 Comparison of lead edge on shroud (ellipse aspect ratio = 4)

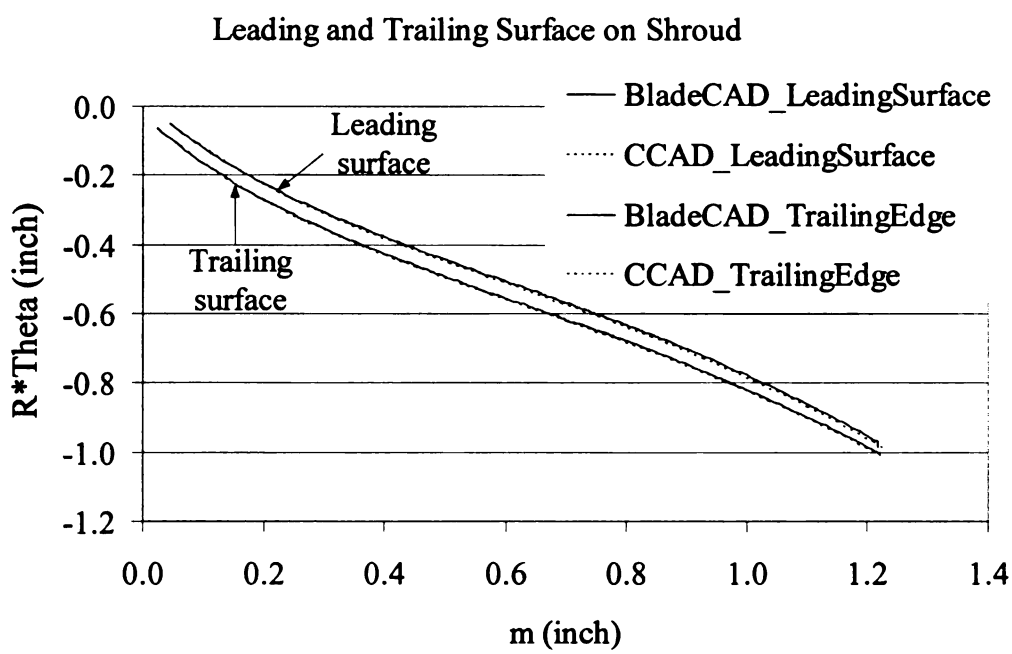

Figure 3-37 Comparison of leading and trailing surface on shroud (ellipse aspect ratio = 4)

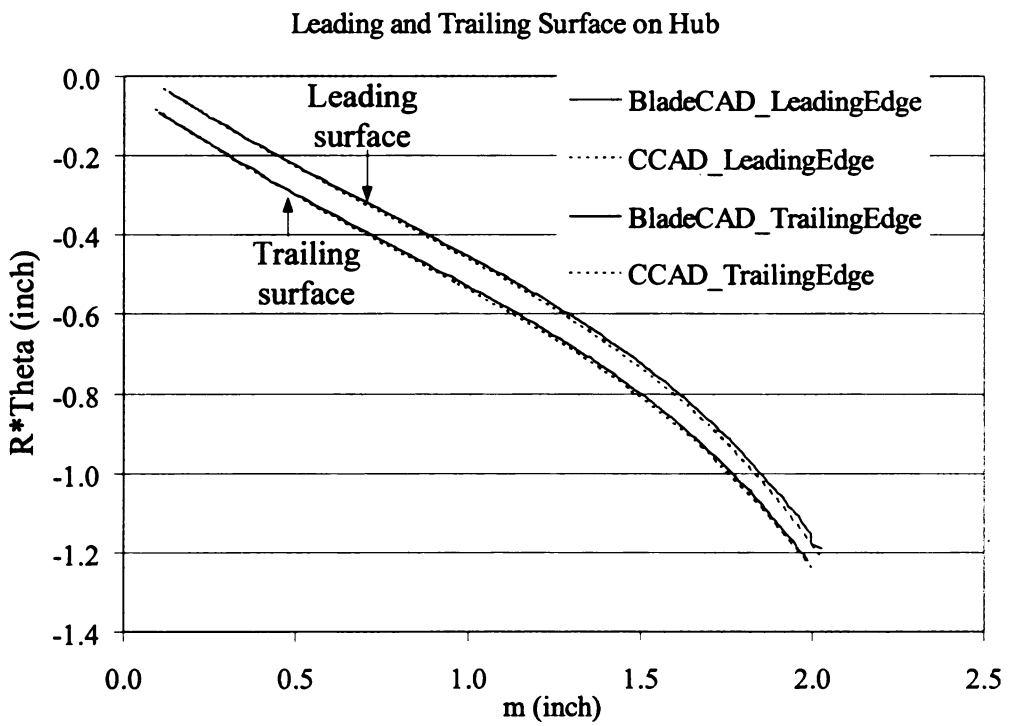

Figure 3-38 Comparison of leading and trailing surface on shroud (ellipse aspect ratio = 4)

3.7 Three-dimensional Design

There are two ways to calculate all points on surface of blades. The first method is to calculate all the points on the pressure sides and suction sides on section curves mentioned above, and then calculate all points on pressure surface and suction surface based on data of pressure sides and suction sides on section curves by Eqn. (3-29)-(3-32).

The second method is to calculate all the points on camber surface firstly, and then calculate corresponding points on pressure surface and suction surface. The method to calculate camber surface is the combination of Eqns. (3-1) and (3-10).

$$[z,r,\theta]^T = \sum_{i=0}^{n}\sum_{j=0}^{n} C_n^i C_n^j (1-u)^{n-i} u^i (1-v)^{n-j} v^j \left[z_{node,i}, r_{node,i}, \theta_{node,i}\right]^T \quad (3\text{-}33)$$

CHAPTER 4

FLOW SOLVER

4.1 Introduction

MERIDL and TSONIC, which are free CFD codes from NASA, are applied to calculate the performance of centrifugal compressors with cubic spline curve. The MERIDL is used to calculate meridional plane while TSONIC is applied to calculate the blade-to-blade plane. The basic theory used in MERIDL/TOSNIC is streamline curvature method and the basic idea for meshing is the use of arbitrary quasi-orthogonals. MERIDL and TSONIC are two-dimensional codes and very low time cost. The total time cost has been reduced to approximately 0.5 second per case using CPU Pentium 3.20GHz. The combination of MERIDL and TSONIC can provide quasi-three dimensional results. The detail introduction of MERIDL and TSONIC are in References [12-14] respectively. To combine MERIDL and TSONIC with the geometry generation tool BladeCAD, several changes are made to allow the MERIDL and TSONIC can be directly called by BladeCAD.

1) Modifying Katsainis's TSONIC to calculate geometry with Bezier polynomials instead of original spline curves.

2) Combing the MERIDL and TSONIC with BladeCAD

3) Generating a file which included geometry file and running condition from BladeCAD as the input for MERIDL and TSONIC.

To further improve the accuracy of results, five different meshing methods are compared and their corresponding results are analyzed.

Furthermore, to evaluate the accuracy of MERIDL and TSONIC, the calculation results from MERIDL and TSONIC are compared with results calculated by

TASCFlow. The calculation results of different flow solvers are solved under the same compressor geometry and running condition.

4.2 Influences of Meshing

4.2.1 Comparison of Five Different Meshing Methods

Five types of meshing are compared in this report. The aim is to study of the influences of mesh. Based on the last report, there are oscillations in the results. Based on the deep exploration on the codes, it has been found it occurs because of the undesired meshing. Therefore, five different types of meshing are changed and their corresponding influences are studied.

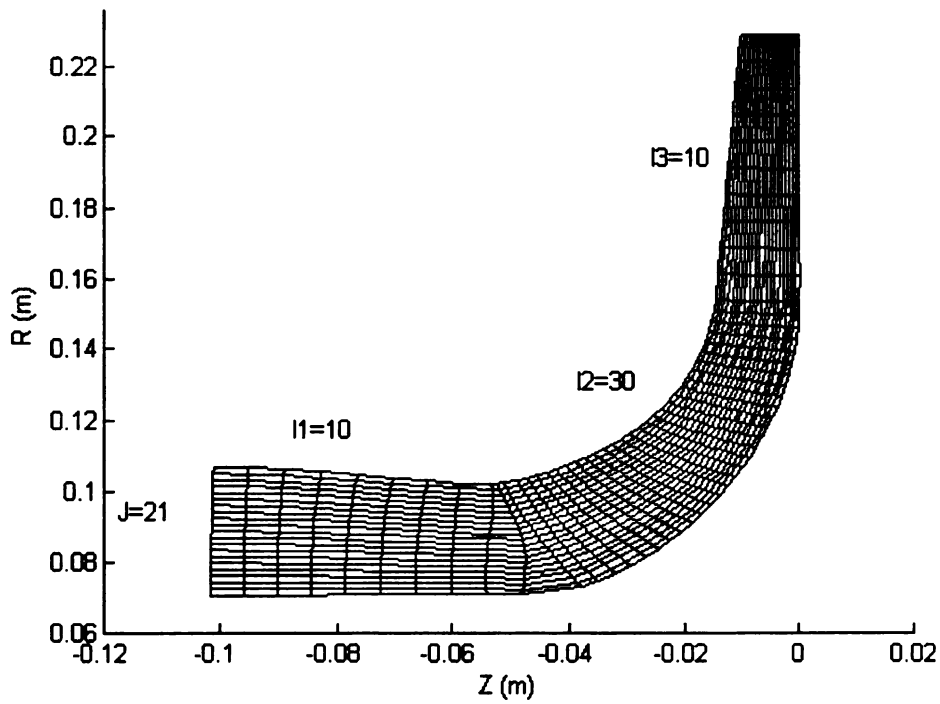

Figure 4-1 First meshing method

In the first meshing method, there are 50 grids from upstream line to downstream line along meridional direction (I=50), which includes inlet casing, impeller and diffuser. And there are 21 grids from hub to shroud along vertical direction (J=21). There are 10 grids in the inlet casing along meridional direction; while 30 grids in the impeller and 10 grids in the diffuser. In the middle line (J=11), the meridional distances in the inlet casing, impeller and diffuser are uniformly divided. Quasi-Normal lines are

created from middle line to shroud and hub to mesh. Therefore, the meridional distances are not equal to each other on shroud and hub. Please refer to [12, 14] for detail information on creating the arbitrary quai-orthogonals.

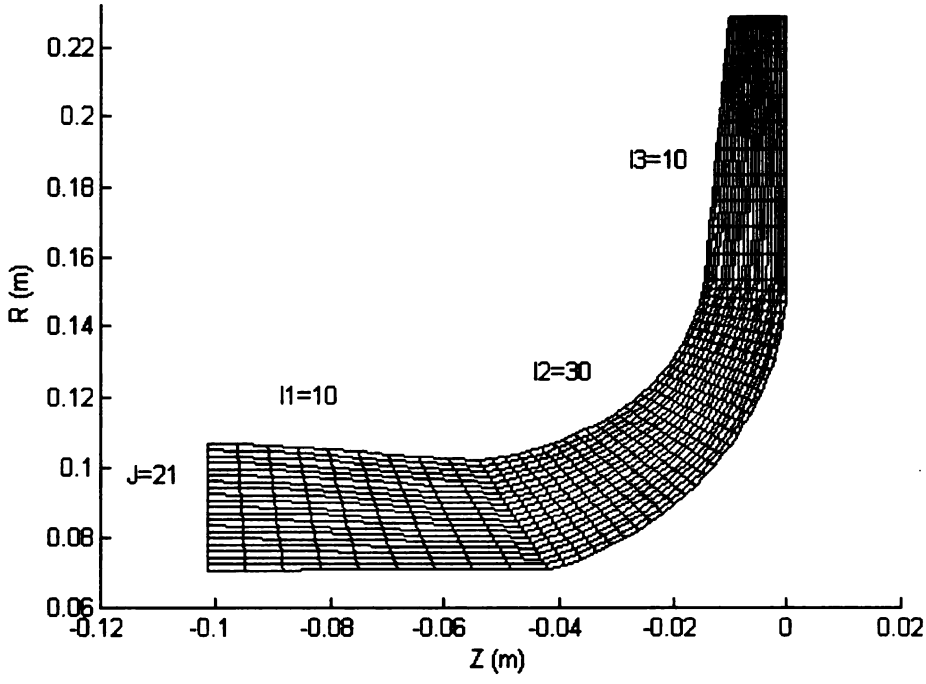

Figure 4-2 Second meshing method

In the second meshing method, I=50 and J=21. There are 10 grids in the inlet casing along meridional direction; while 30 grids in the impeller and 10 grids in the diffuser. The grids are divided based on the same normalized meridional distances on shroud and hub. However, meridional distances on the inlet casing, impeller and diffuser are not equal to each other.

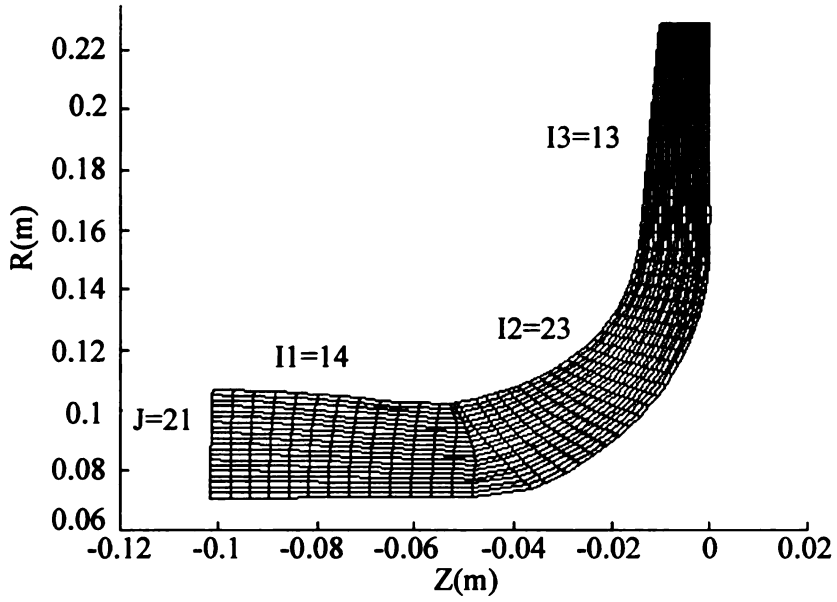

Figure 4-3 Third meshing method

In the third meshing method, I=50 and J=21. The method is similar to the first one. However, not only middle line of each component is uniformly divided, but also the whole middle line of compressor, which includes the inlet casing, impeller and diffuser, is uniformly divided.

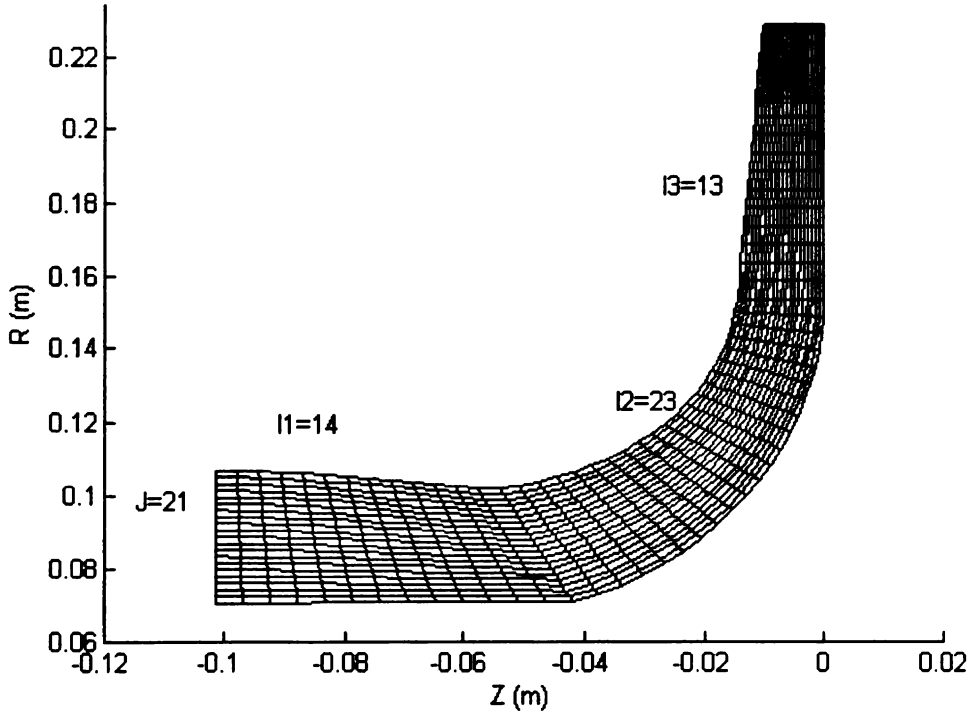

Figure 4-4 Fourth meshing method

In the 4th case of meshing, I=50 and J=21. The method is similar to the second method.

However, the whole shroud or hub of compressor instead of each component is uniformly divided.

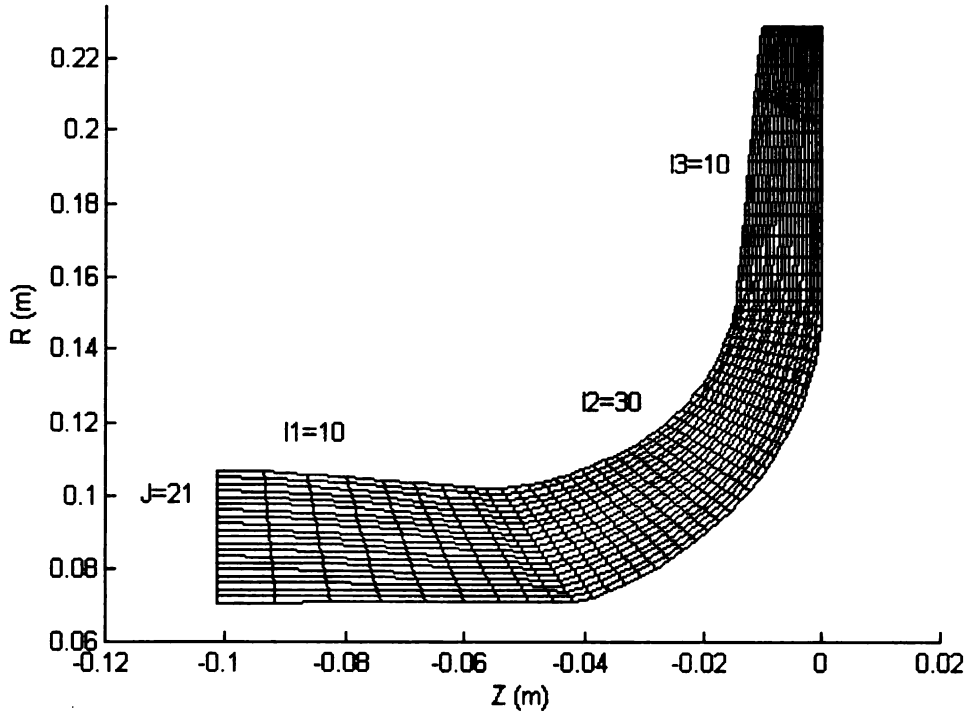

Figure 4-5 Fifth meshing method

In the 5th case of meshing, I=50 and J=21. There are 10 grids in the inlet casing along meridional direction; while 30 grids in the impeller and 10 grids in the diffuser. The grids are divided based on the same normalized meridional distances on shroud and hub in impeller. However, they are not uniform in the diffuser and inlet casing. The meridional distance on shroud and hub of inlet casing gradually decrease while the meridional distance on shroud and hub gradually increase.

4.2.2 Comparison of Relative Velocity Distribution

Results of five different meshing methods are introduced and their corresponding results are compared on the following compressor performance parameters: relative meridional velocity, relative flow angle, relative Mach number and static pressure.

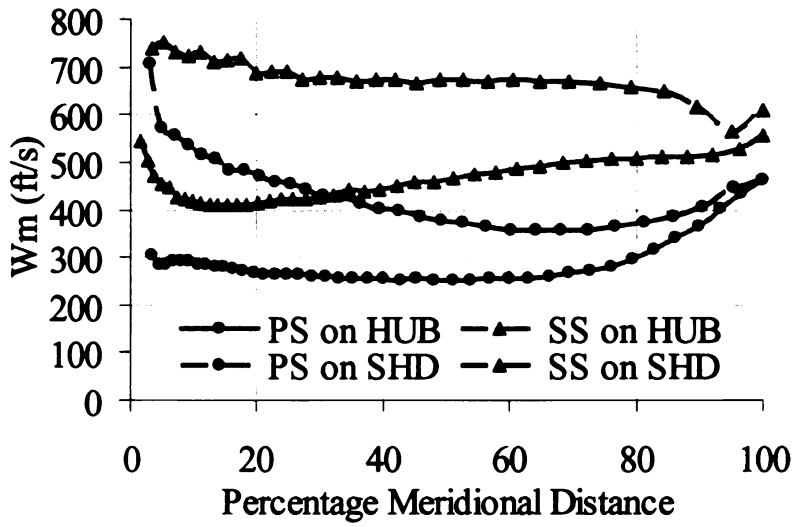

Figure 4-6 Relative velocity distribution based on first meshing method

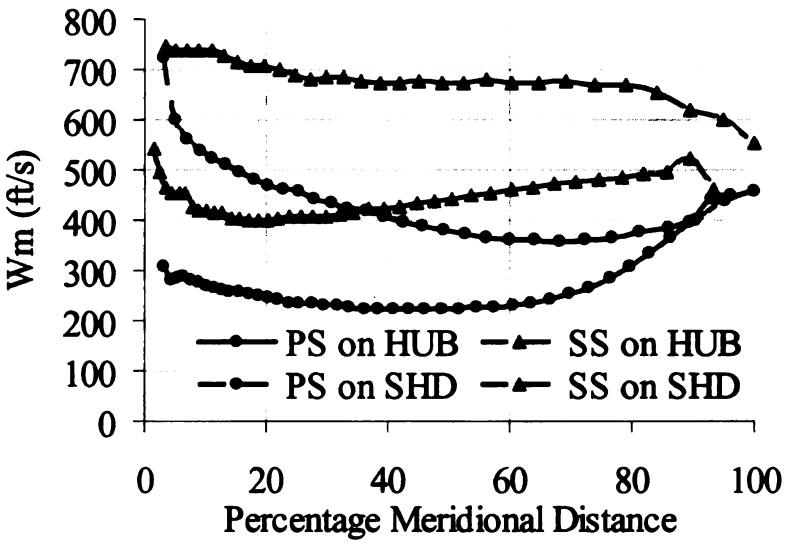

Figure 4-7 Relative velocity distribution based on second meshing method

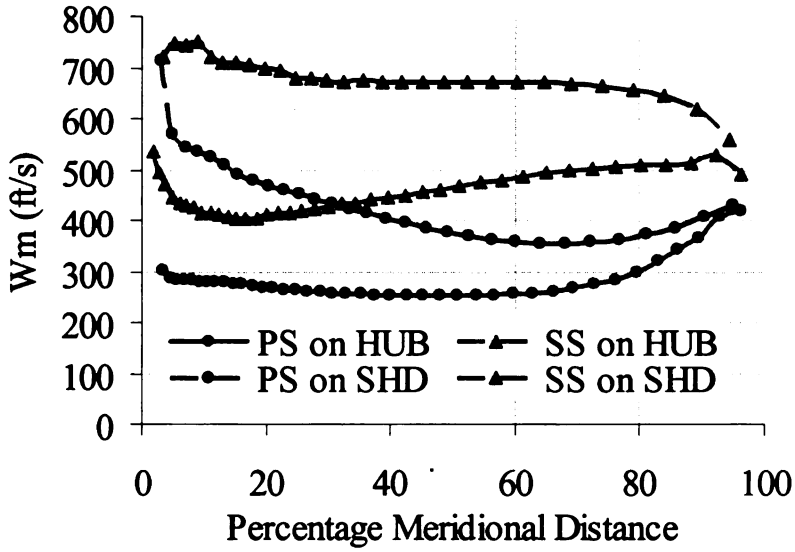

Figure 4-8 Relative velocity distribution based on third meshing method

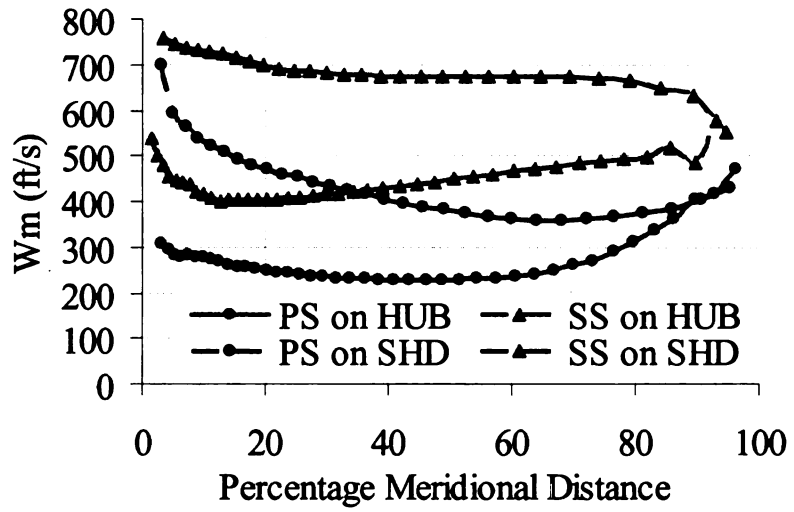

Figure 4-9 Relative velocity distribution based on fourth meshing method

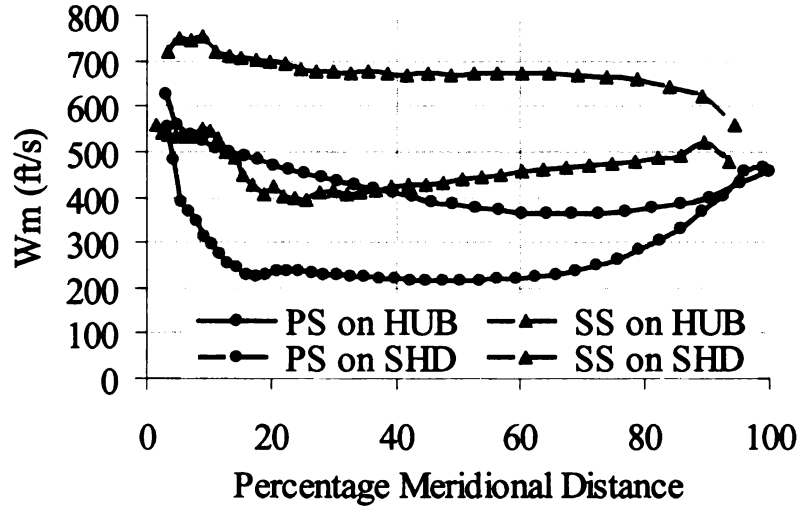

Figure 4-10 Relative velocity distribution based on fifth meshing method

4.2.3 Comparison of Relative Flow Angle

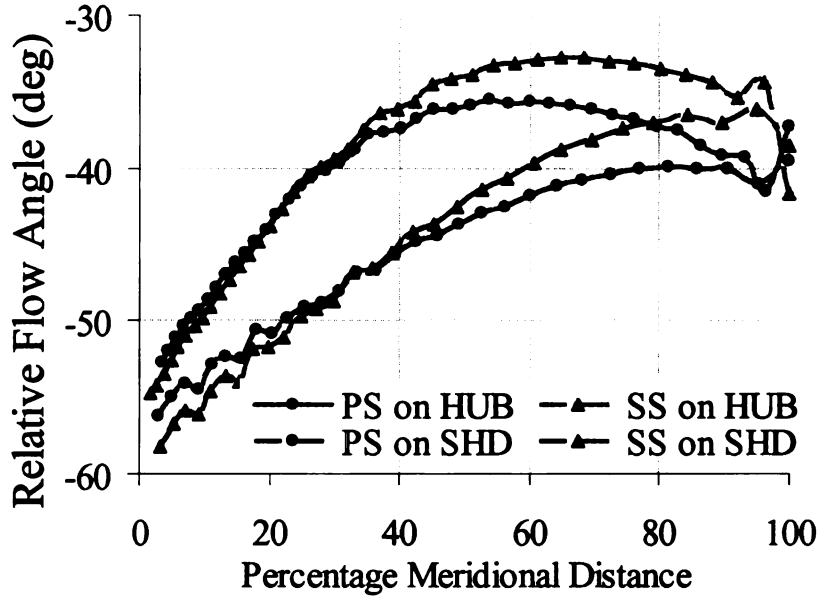

Figure 4-11 Relative flow angle distribution based on first meshing method

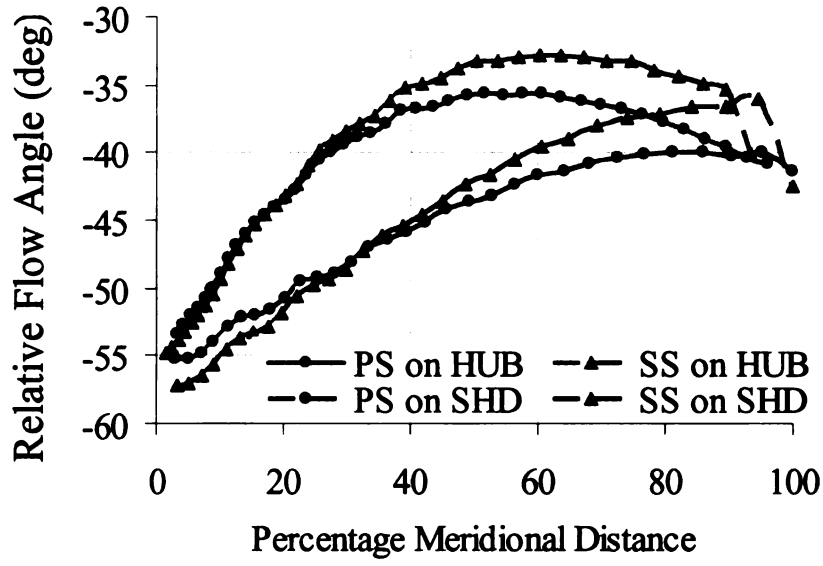

Figure 4-12 Relative flow angle distribution based on second meshing method

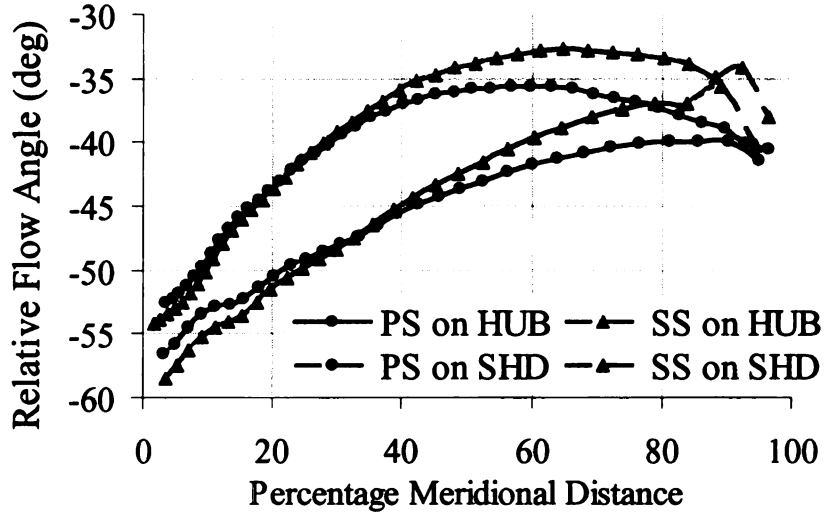

Figure 4-13 Relative flow angle distribution based on third meshing method

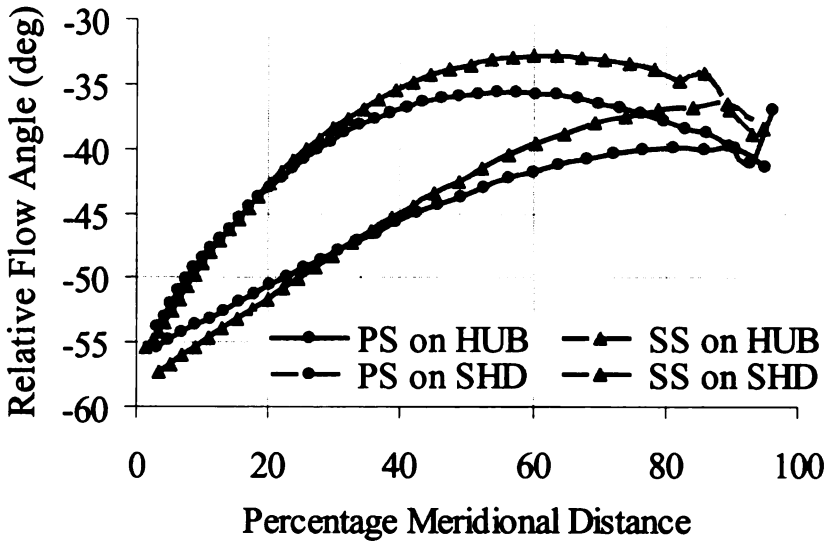

Figure 4-14 Relative flow angle distribution based on fourth meshing method

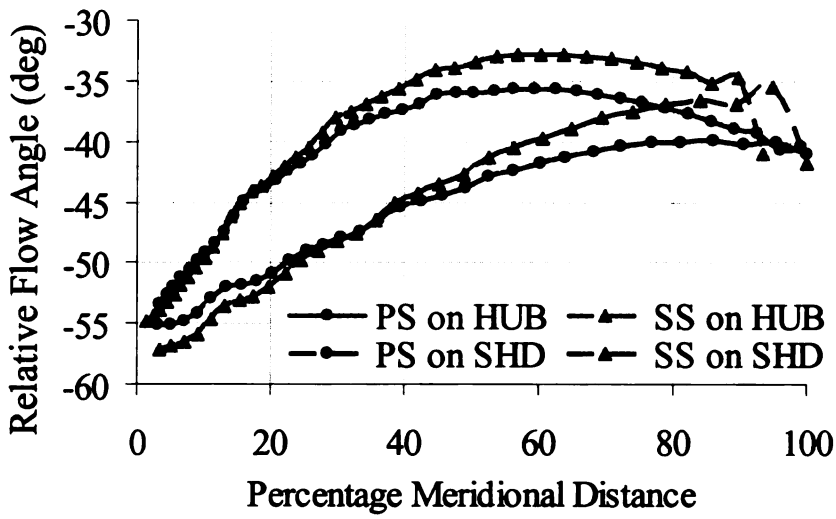

Figure 4-15 Relative flow angle distribution based on fifth meshing method

4.2.4 Comparison of Relative Mach Number

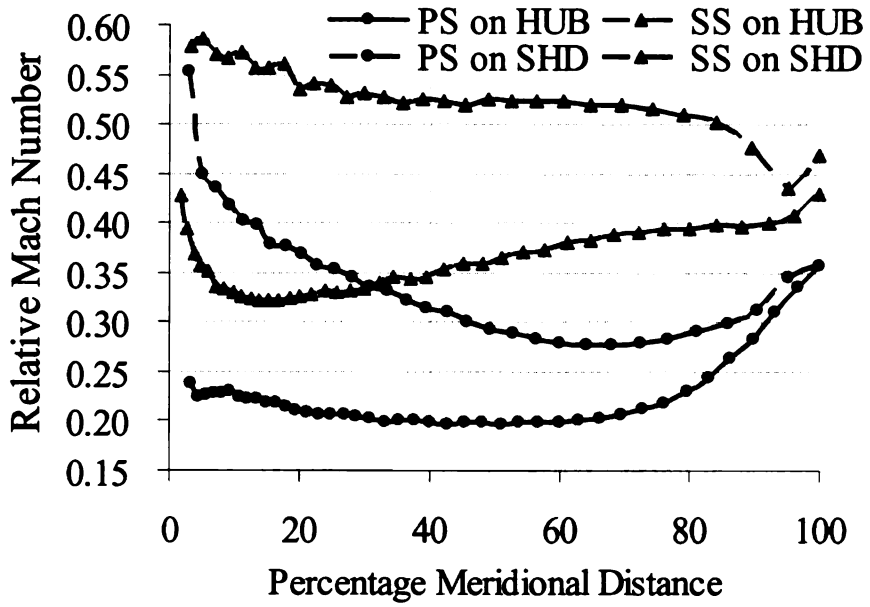

Figure 4-16 Relative Mach number distribution based on first meshing method

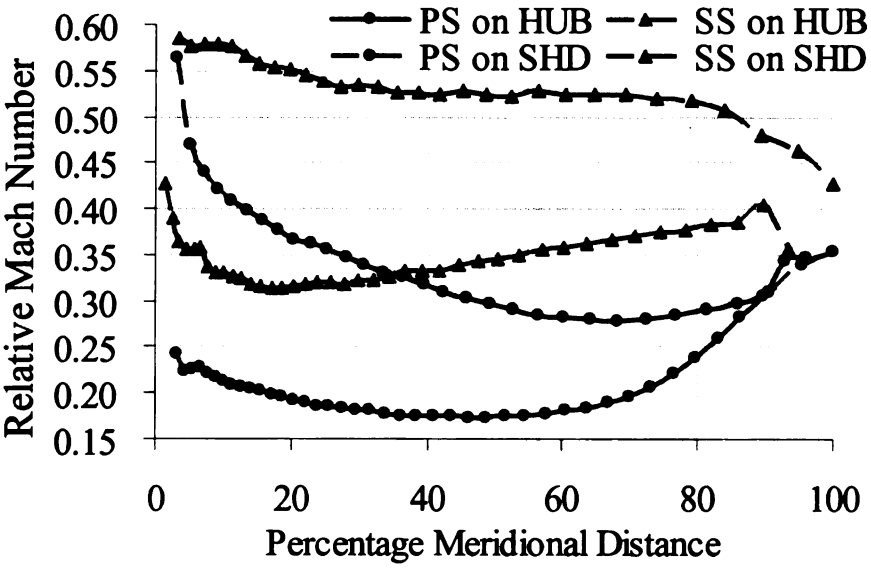

Figure 4-17 Relative Mach number distribution based on second meshing method

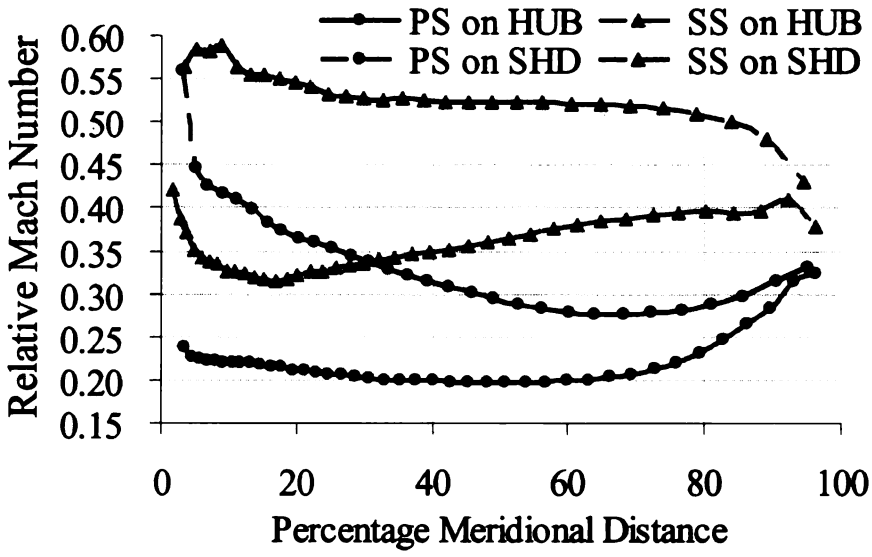

Figure 4-18 Relative Mach number distribution based on third meshing method

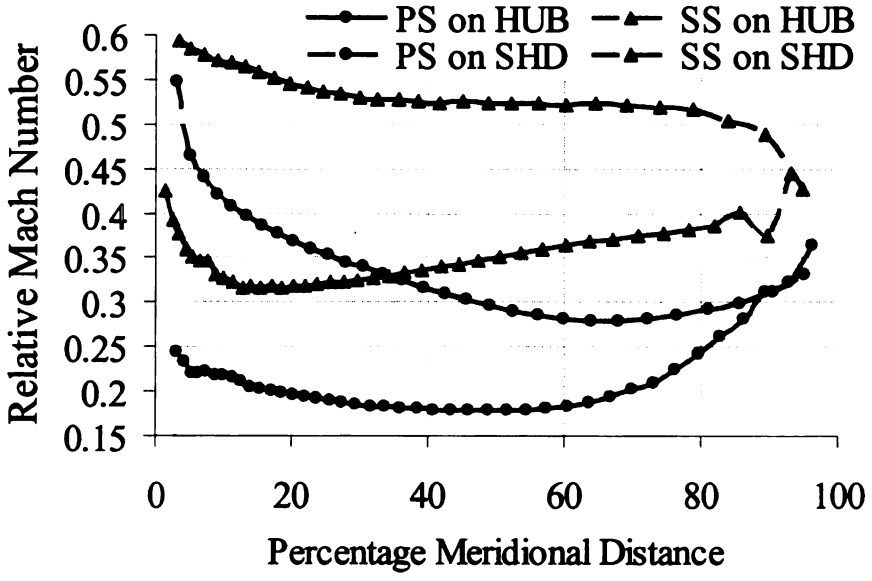

Figure 4-19 Relative Mach number distribution based on fourth meshing method

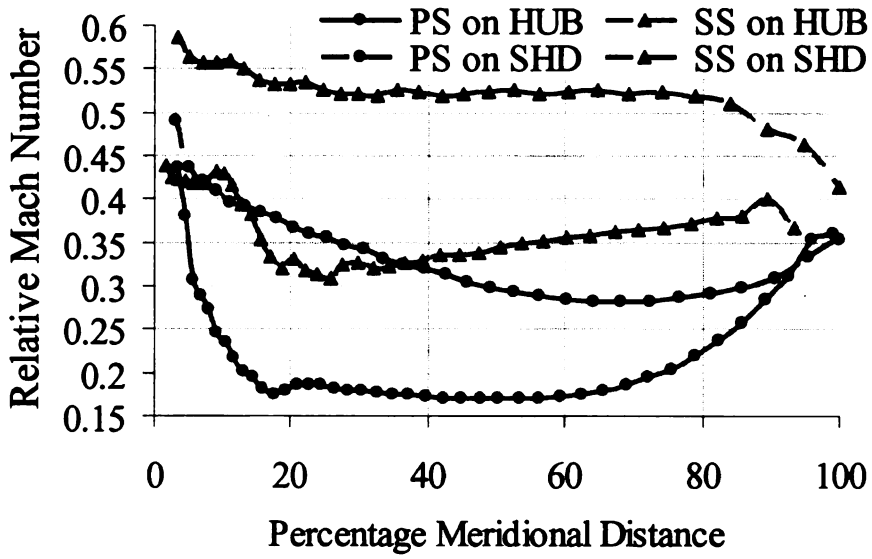

Figure 4-20 Relative Mach number distribution based on fifth meshing method

4.2.5 Comparison of Static Pressure Distribution

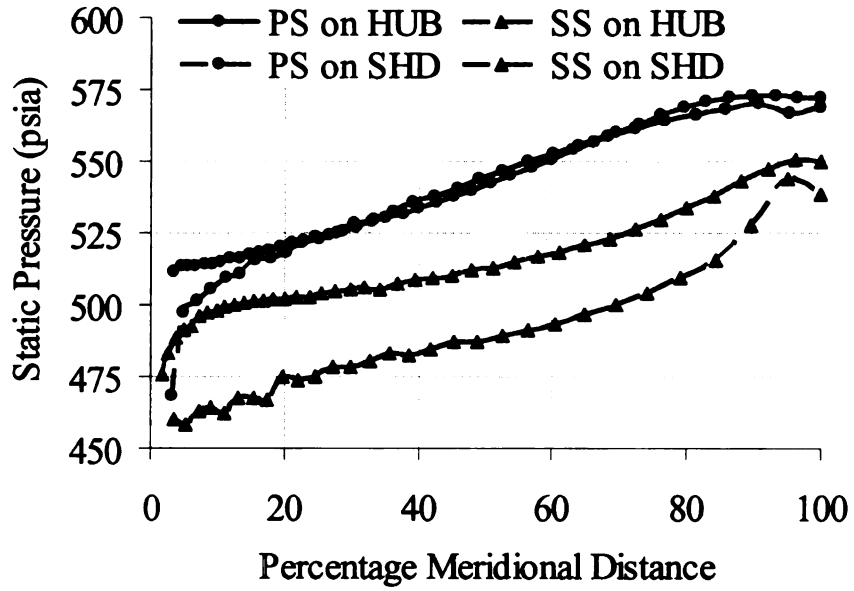

Figure 4-21 Static pressure distribution based on first meshing method

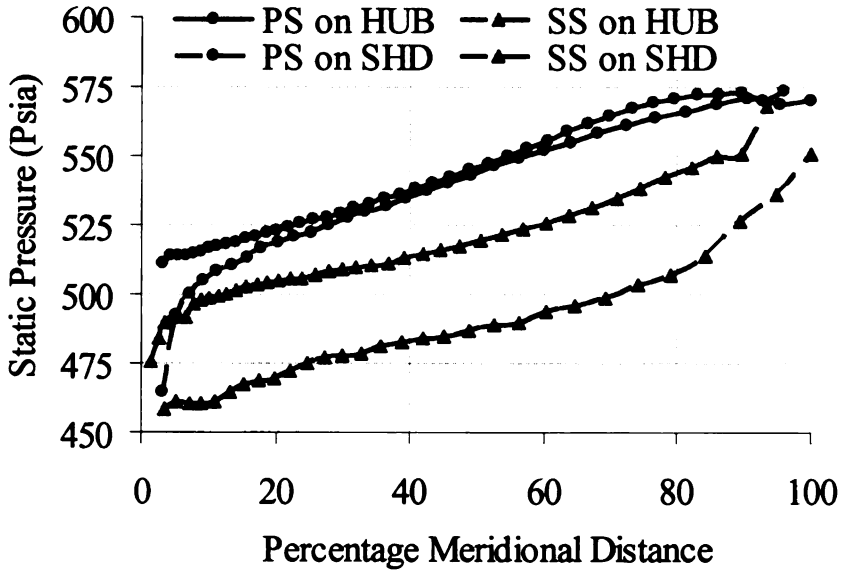

Figure 4-22 Static pressure distribution based on second meshing method

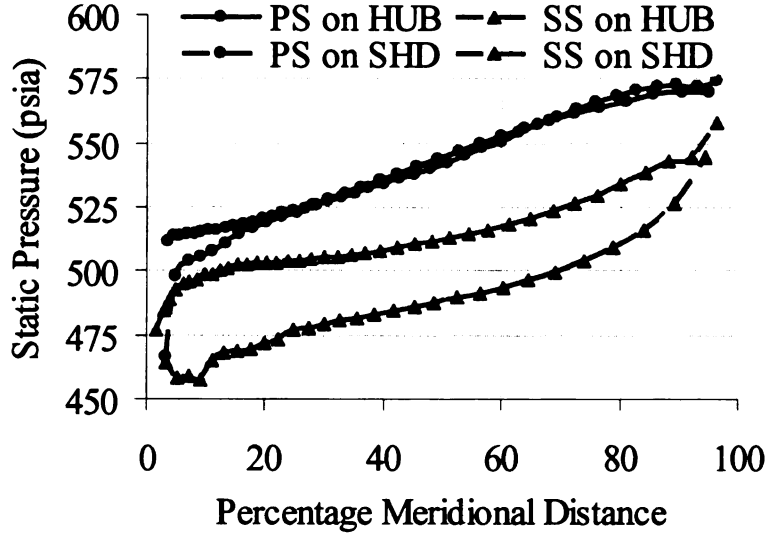

Figure 4-23 Static pressure distribution based on third meshing method

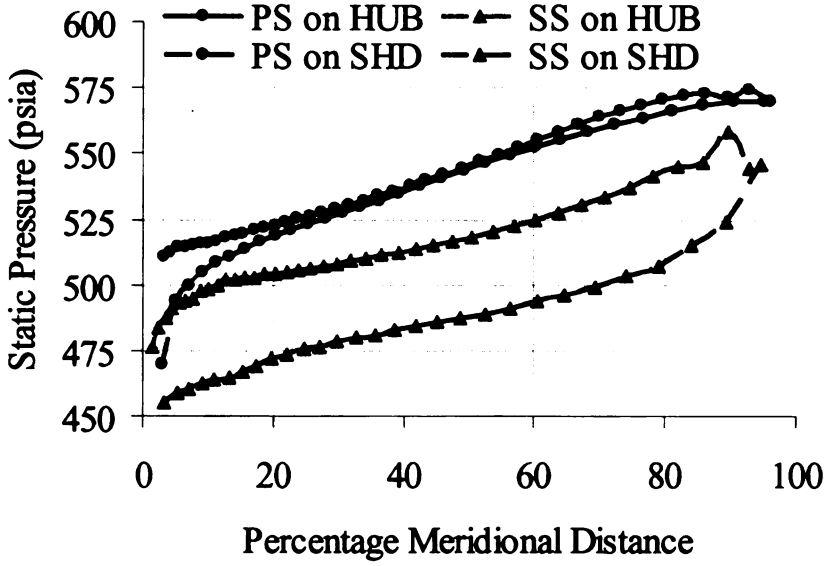

Figure 4-24 Static pressure distribution based on fourth meshing method

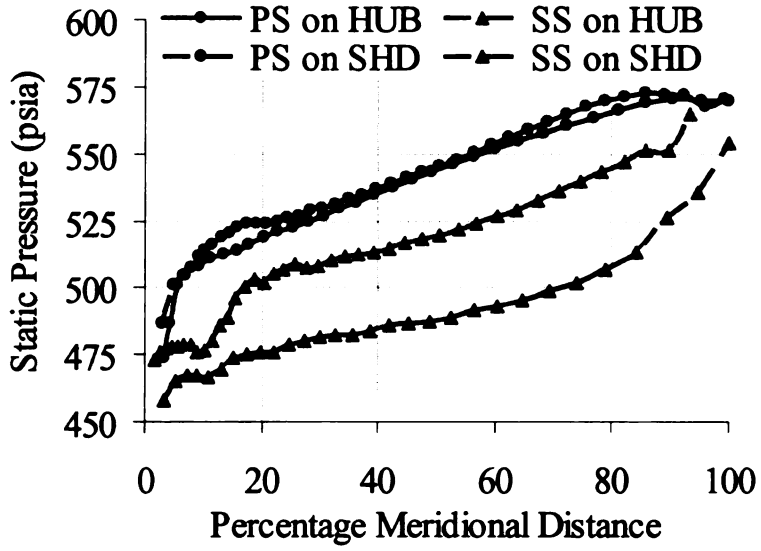

Figure 4-25 Static pressure distribution based on fifth meshing method

4.2.6 Discussion

All results calculated based on these five different types of meshing are similar. However, some of them are smooth while others have waves, which will result in difficulties and bring large errors for the following steps in the optimization procedure. Based on the results of relative meridional velocity, five cases of meshing were sorted from worst to best: Case1=Case5<Case2=Case3 <Case 4.

Based on the results of relative flow angle, five cases of meshing of were sorted from worst to best: Case1<Case2=Case5=Case3<Case 4.

Based on the results of relative Mach number, five cases of meshing were sorted from worst to best: Case1<Case5<Case 2=Case 3<Case 4.

Based on the results of static pressure, five cases of meshing were sorted from worst to best: Case1<Case5<Case 3<Case 2<Case 4.

Based on results of those four variables, the fourth meshing method (Figure 4-4) is the best while the first meshing method (Figure 4-1) is the worst.

It should be mentioned that the influences on only those four variables in the blade to blade direction are considered. The influences on the meridional direction are not considered because almost no waves occur along meridional direction.

4.3 Comparison between TASCFlow and NASA Codes

To evaluate the accuracy of codes of MERIDL and TSONIC, a widely used commercial software TASCflow is applied here. Five cases: Baseline, Case1, Case 2, Case 2b and Case 2c with different geometry are generated. TASCflow and NASA codes are applied to calculate the performances of five compressor impellers. The comparisons of loadings, relative velocity distributions and static pressure distributions are compared.

4.3.1 Geometry Cases

Five cases of compressors with different geometries are compared using TASCflow and NASA codes. The geometries of these inlet casing and diffuser are same. The one dimensional geometries of impellers are same. And the normal thickness distributions of five impellers are the same while blade angle distributions and contours are different. Contours and blade angle distributions of five different cases are shown in Figure 4-26 and Figure 4-27.The meshing used in TASCflow generated by FASTTasc automatically, which is the three dimensional meshing tool. The meshing is

(I,J,K)=(115,25,25). In the NASA codes, there are two parts: MERIDL and TSONIC. Both of them are 2D codes. The meshing in the MERIDL is (I,K)=(50,25), while in the TSONIC, I=50. However, calculation in blade-to-blade surface is based on each streamline, which means the calculation for each streamline is independent. And the value of J is determined by codes automatically based on geometry and varied with the location of streamline. In last section, the fourth meshing method has been proved as the best one. Therefore, that meshing method is used here. For NASA codes, the efficiency is an input instead of output. The input of NASA codes included: 1) upstream Total Temperature: T_{01}; 2) upstream Total Pressure: P_{01} ; 3) upstream Absolute whirl: $U_{01}C_{u1}$ 4) downstream total pressure: P_{02} 5) downstream absolute whirl: U_2C_{u2} 6) gas specific heat ratio: γ 7) gas specific heat measured under constant pressure: C_p. The comparison of results between TASCflow and NASA codes are shown from Figure 4-28 to Figure 4-47.

4.3.2 Comparison of geometries

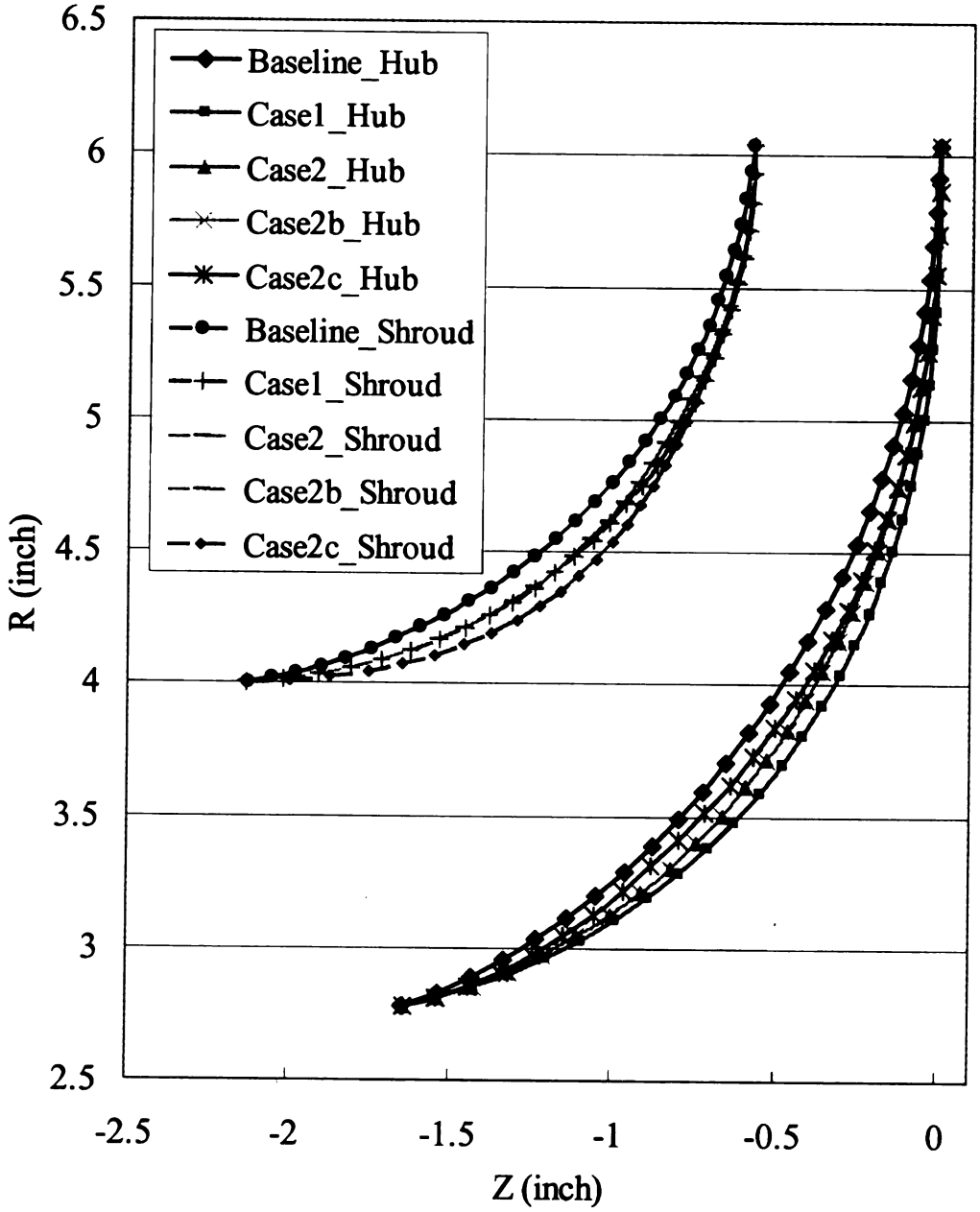

Figure 4-26 Contours of five different cases

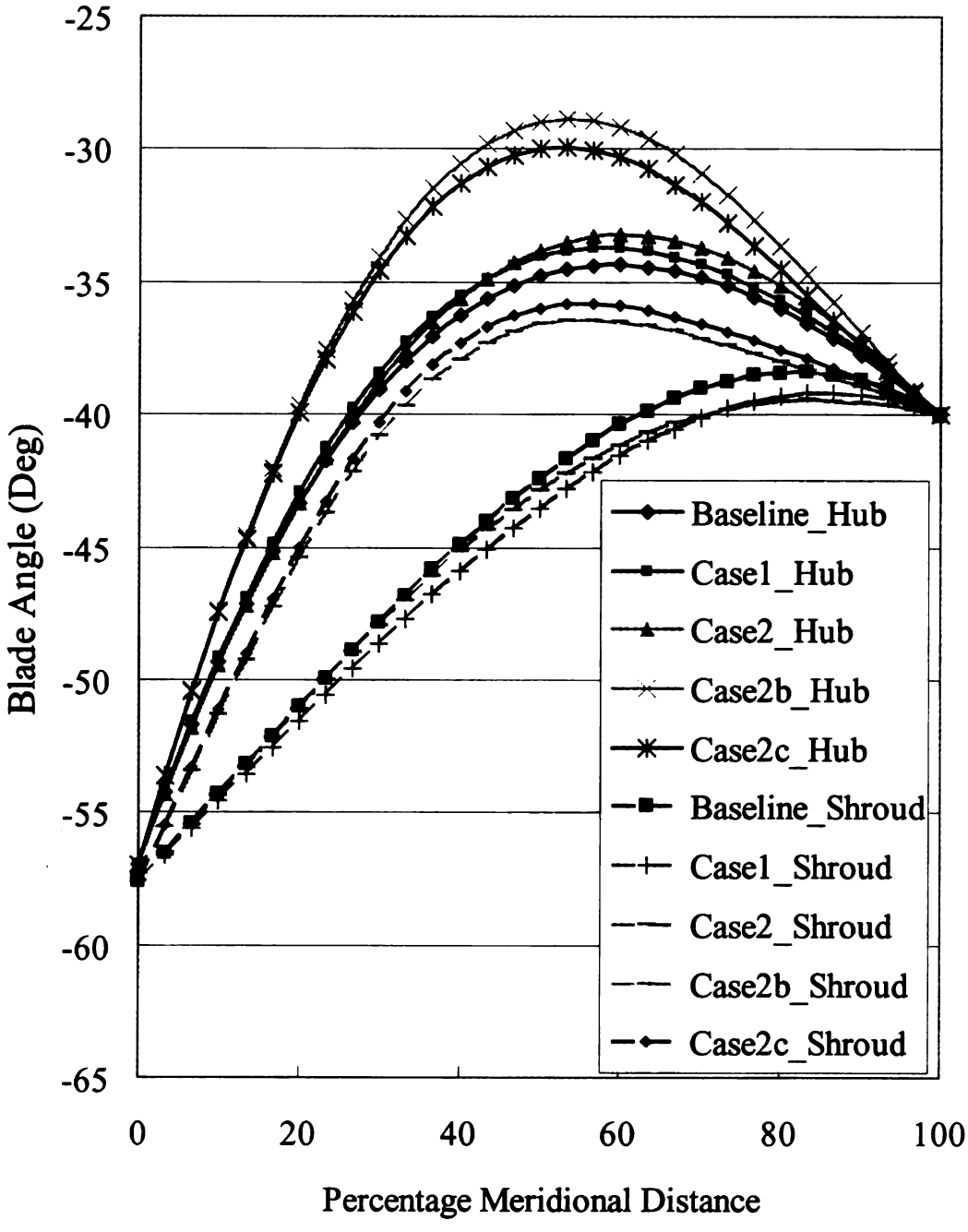

Figure 4-27 Blade angle distributions of five different cases

4.3.3 Comparison of loadings

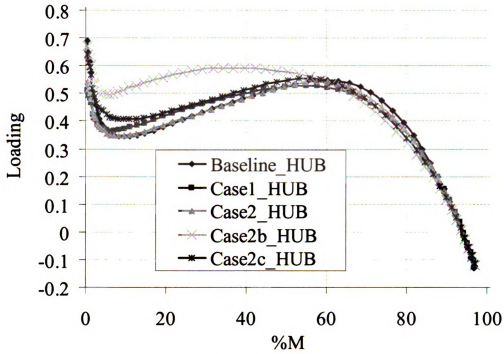

Figure 4-28 Loading on hub calculated by TASCFlow

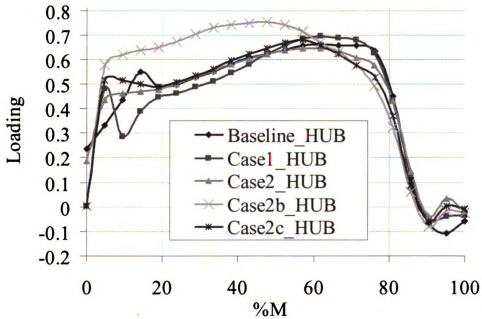

Figure 4-29 Loading on hub calculated by MERIDL and TSONIC

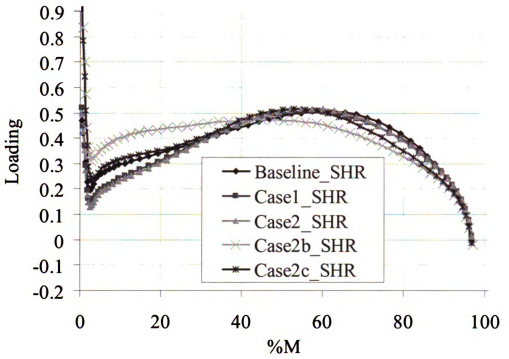

Figure 4-30 Loading on shroud calculated by TASCFlow

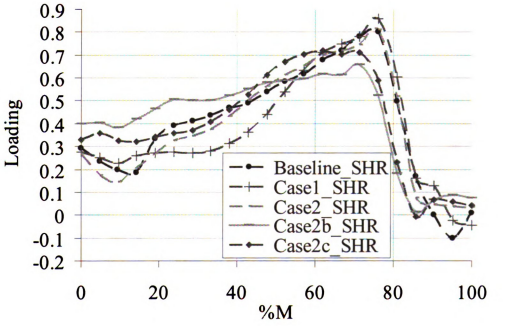

Figure 4-31 Loading on shroud calculated by MERIDL and TSONIC

4.3.4 Comparison of relative velocity distributions

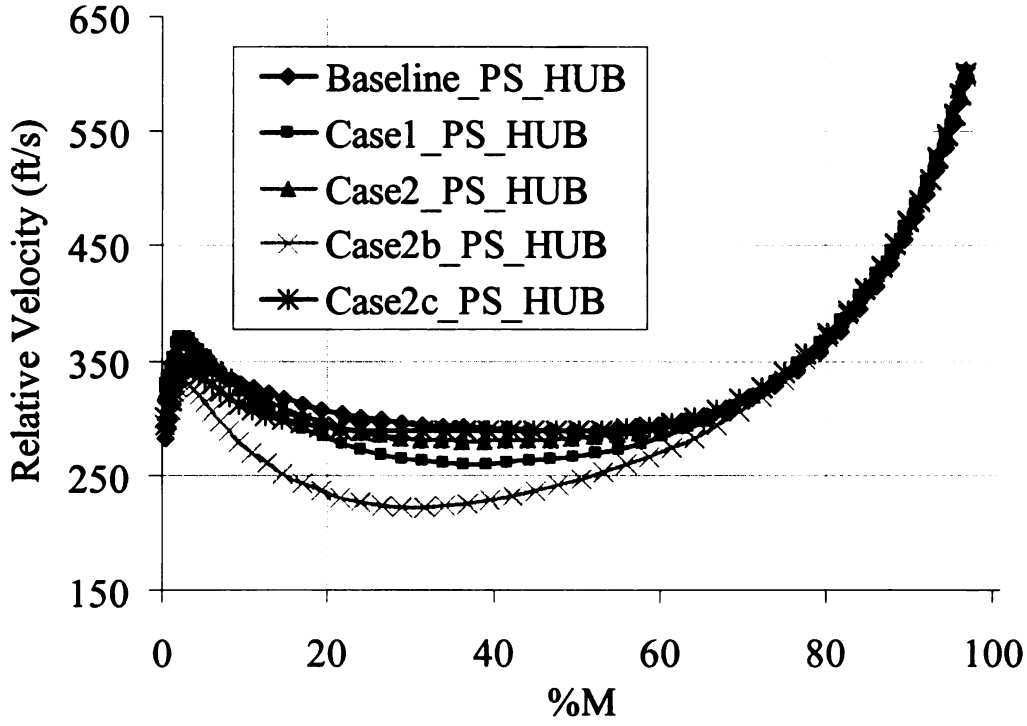

Figure 4-32 Relative velocity distribution on pressure side of hub calculated by TASCFlow

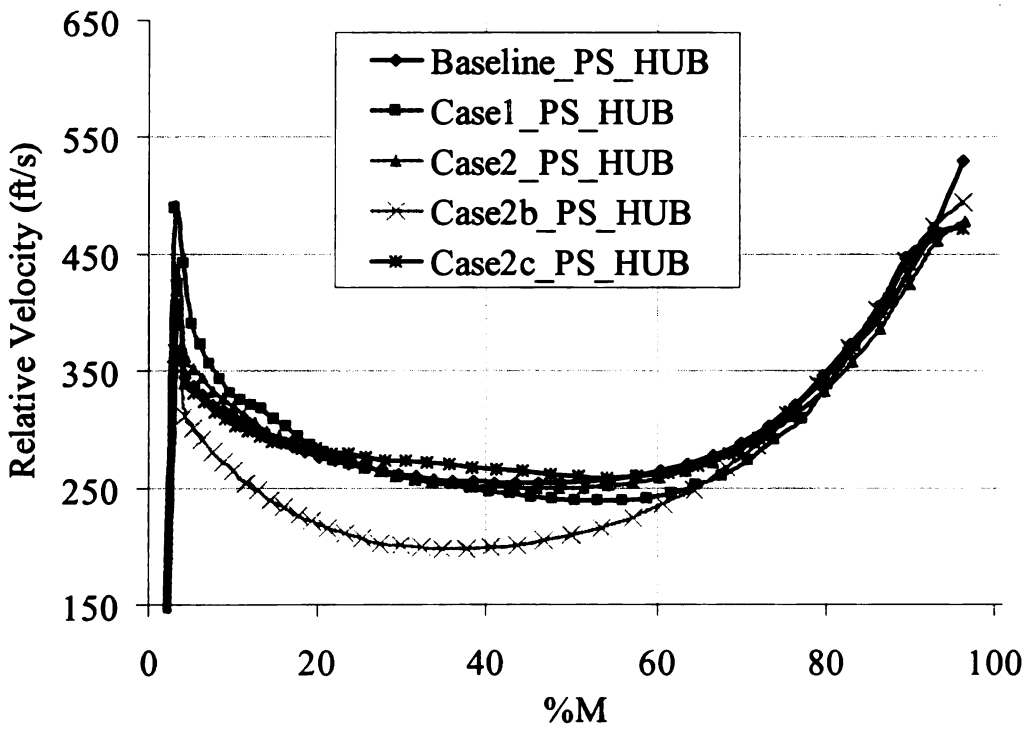

Figure 4-33 Relative velocity distribution on pressure side of hub calculated by MERIDL and TSONIC

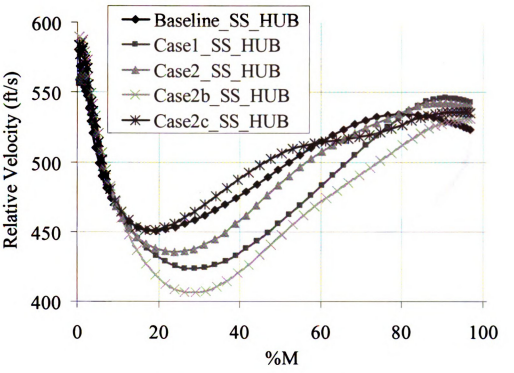

Figure 4-34 Relative velocity distribution on suction side of hub calculated by TASCflow

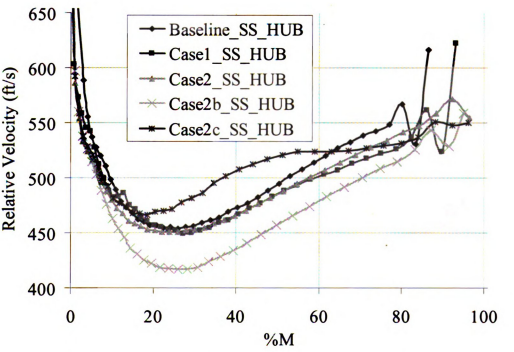

Figure 4-35 Relative velocity distribution on suction side of hub calculated by MERIDL and TSONIC

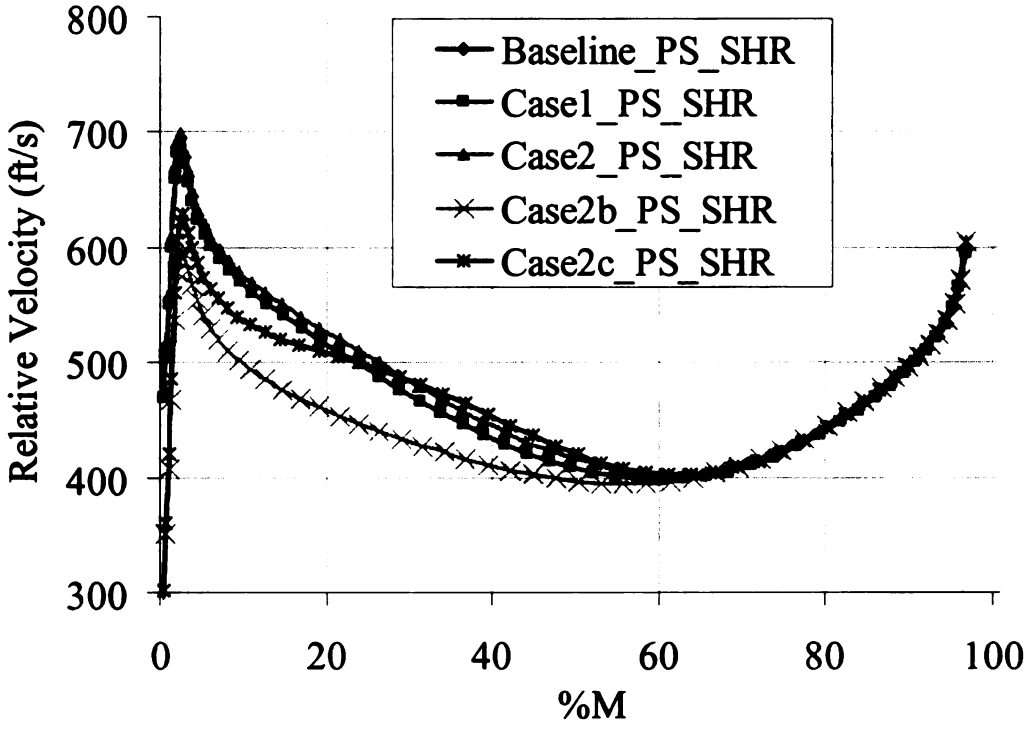

Figure 4-36 Relative velocity distribution on pressure side of shroud calculated by TASCflow

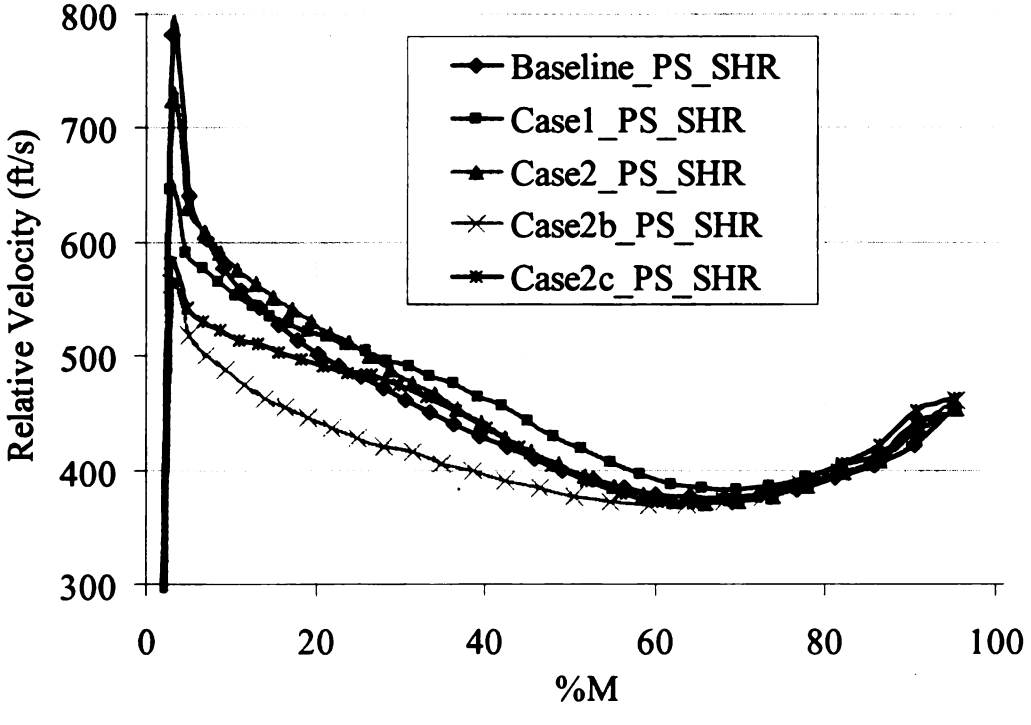

Figure 4-37 Relative velocity distribution on pressure side of shroud calculated by MERIDL and TSONIC

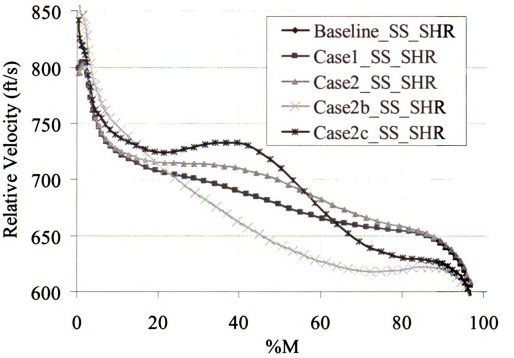

Figure 4-38 Relative velocity distribution on suction side of shroud calculated by TASCflow

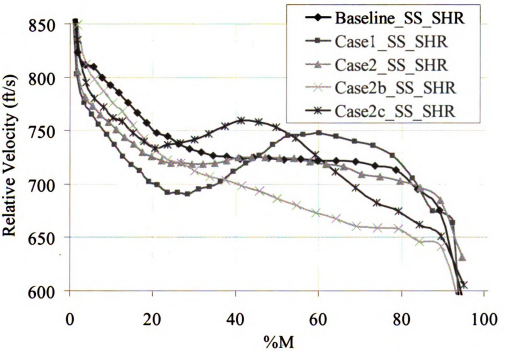

Figure 4-39 Relative velocity distribution on suction side of shroud calculated by MERIDL and TSONIC

4.3.5 Comparison of static pressure distributions

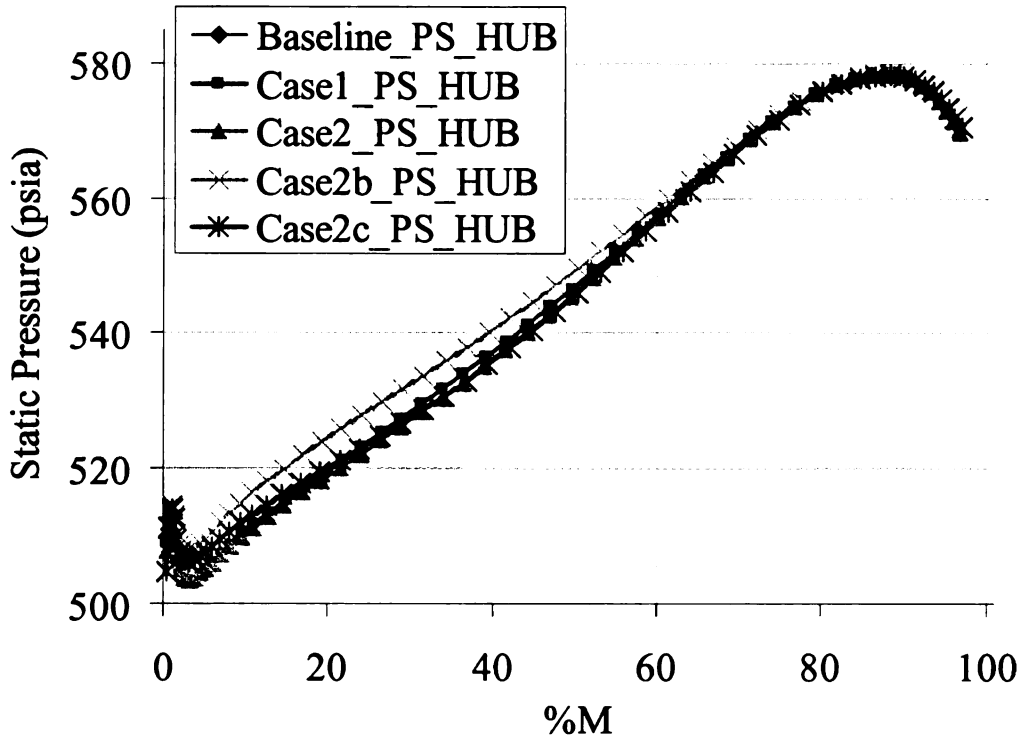

Figure 4-40 Static pressure distribution on pressure side of hub calculated by TASCflow

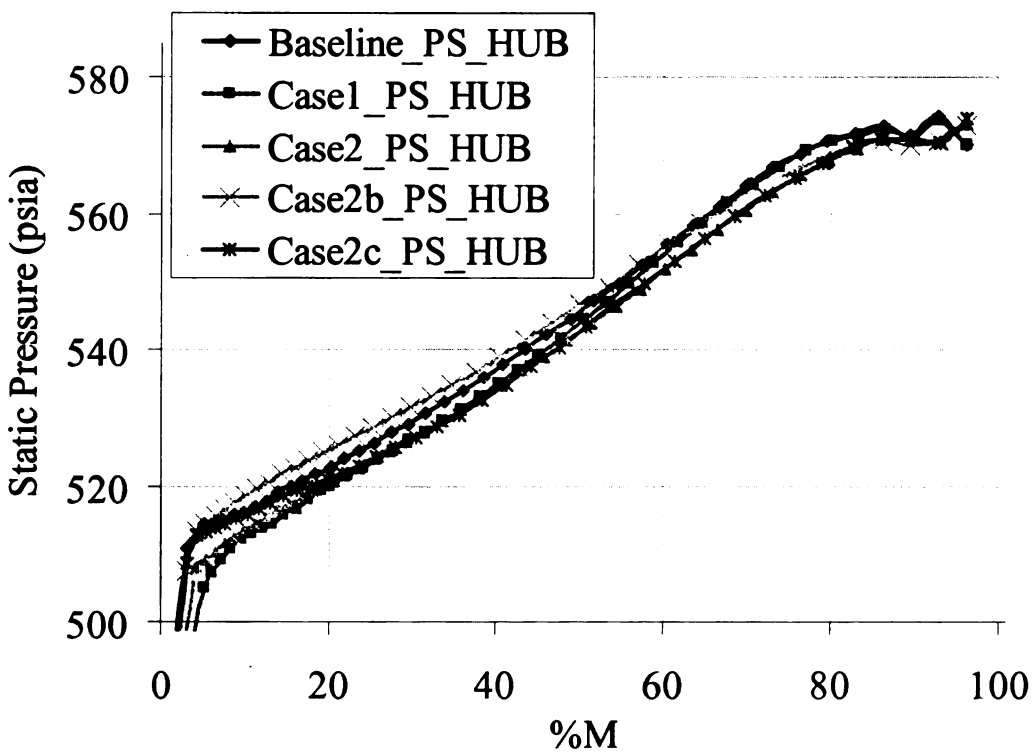

Figure 4-41 Relative velocity distribution on pressure side of hub calculated by MERIDL and TSONIC

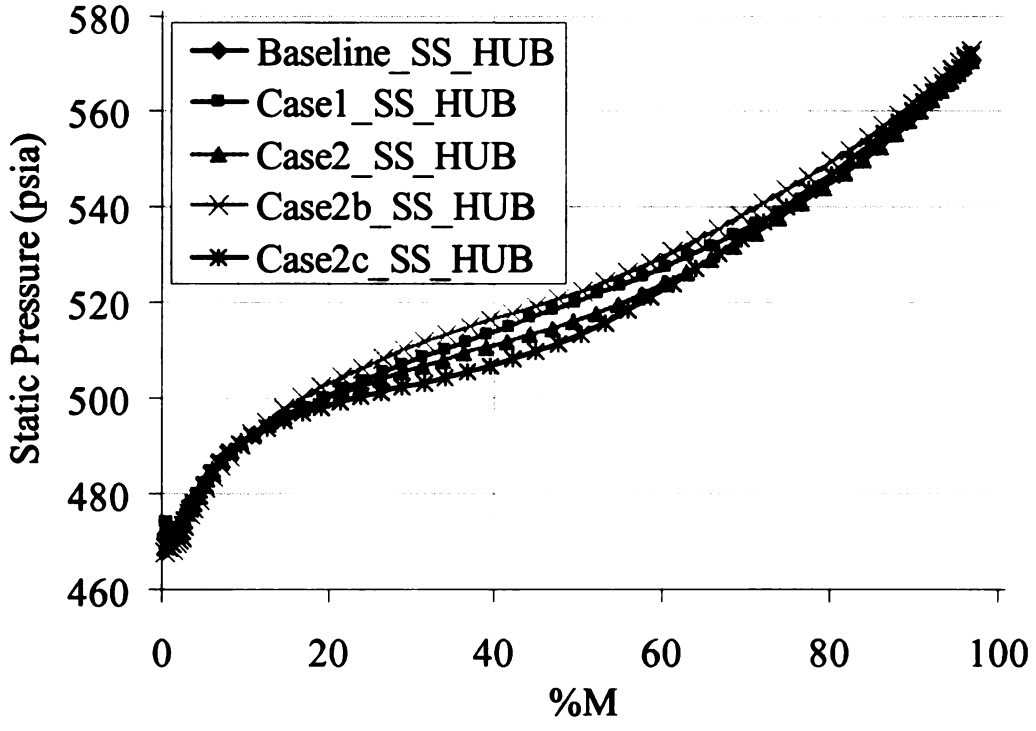

Figure 4-42 Relative velocity distribution on suction side of hub calculated by TASCflow

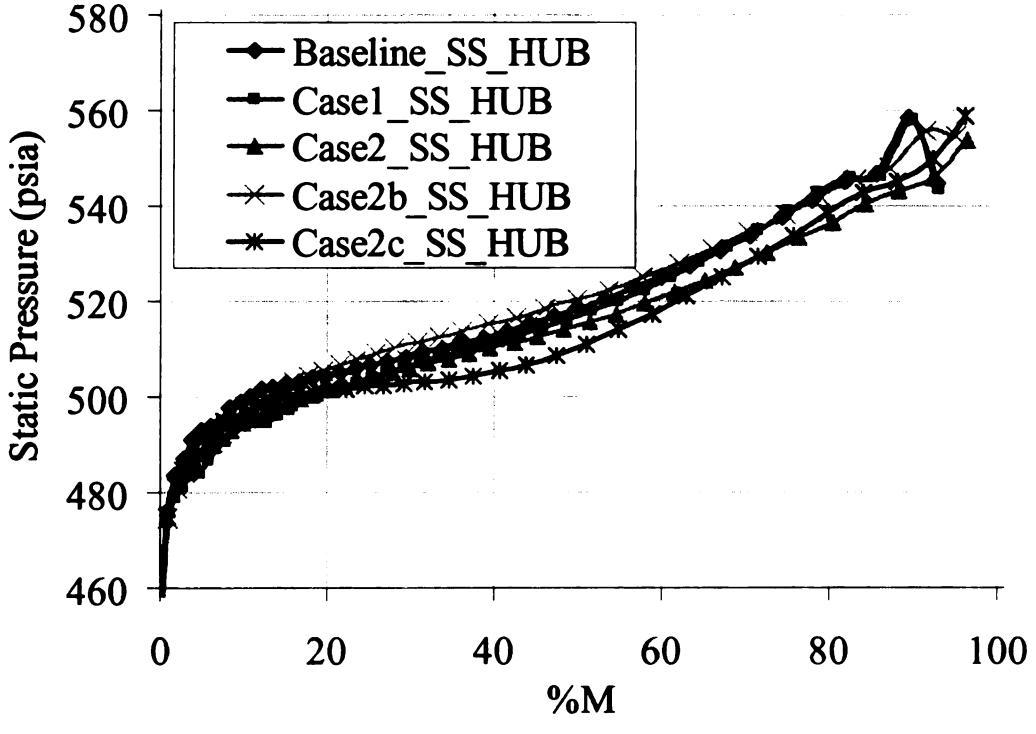

Figure 4-43 Relative velocity distribution on suction side of hub calculated by MERIDL and TSONIC

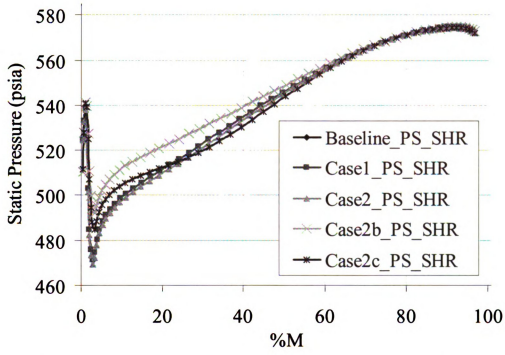

Figure 4-44 Relative velocity distribution on pressure side of shroud calculated by TASCflow

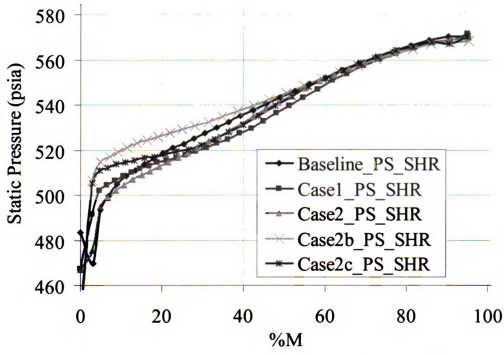

Figure 4-45 Relative velocity distribution on pressure side of shroud calculated by MERIDL and TSONIC

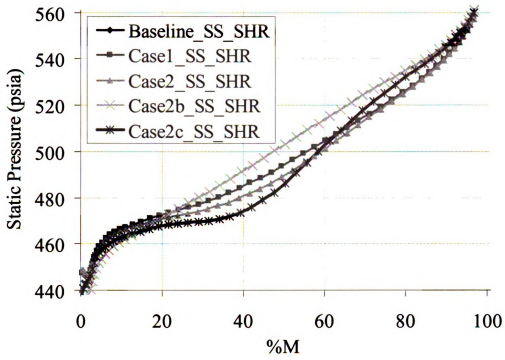

Figure 4-46 Relative velocity distribution on suction side of shroud calculated by TASCflow

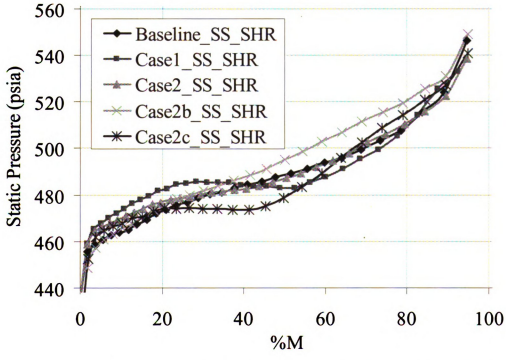

Figure 4-47 Relative velocity distribution on suction side of shroud calculated by MERIDL and TSONIC

4.3.6 Discussions

The differences between TASCflow and NASA codes at the leading and trailing edge are quite different. This is probably because interface between the stators and rotors. Most of comparison results indicate that there are no significant differences of relative velocity distributions and static pressure distributions between TASCflow and NASA codes. NASA codes have the fairly sufficiently accurate for evaluating the compressor performance and therefore are used to evaluate compressor performances in the following optimization procedure.

CHAPTER 5

IMPELLER OPTIMIZATION PROCEDURE WITH ANN & GA

5.1 Introduction

Compared to other components in compressors, such as diffusers[15], return vanes[16], the optimization of impellers is more important and challenging because of its dominant role in compressing flow and relatively complex geometry. Design and optimization techniques can be broadly divided into two categories: inverse method[16, 17] and direct methods[18, 19]. Direct method, which is less efficient but more effective than inverse method, is studied and applied in this study. The general procedure of direct method included five steps and these five optimization steps are interdependent

1) Parameterization

Parameters x are extracted from complex geometry for optimization. There are dozens of parameters required to be considered during the design of centrifugal compressor impeller. However, only parameters with significant effects called as optimization parameters are considered in the optimization because the increase of optimization parameters will result in "the curse of dimensionality", which is introduced by Bellman[20]. Theoretically, the less the number of optimization parameters is, the easier the optimal solution, especially the global one, can be found and the lower the computational cost is. On the other hand, optimization parameters should be sufficient, effective and accurate to represent the geometry of impellers.

2) Proposing objective function

Optimization problem can be subdivided into single-objective[21, 22] and

multiple-objective[23] optimization. The objective function f can be written in the form: $f(y)$

Where f should be a linear or nonlinear function and y is generally the performance of impellers, such as efficiency, entropy, design-point loss, flow range, pressure distribution, or velocity distribution. The chosen objective function greatly depends on the available information from flow solver.

3) Using flow solver to calculate compressor performance

The flow solver used in optimization can be broadly divided into two categories: 2D (Quasi-3D) and 3D flow solver. $k-\omega$ turbulence model is widely used in 3D flow solver for calculating compressor performance.[15, 16] Theoretically, 3D flow solver is much more accurate than 2D codes and can provide much more information such as secondary flow, convex, etc. 2D codes are much lower computational time cost than 3D codes. Performance y can be calculated from a geometry case, which is represented by a set of optimization parameters x. Once we have a set of optimization parameters x, we can calculate performance y by using flow solver. Combined with objective function $f(y)$, we can calculate the value of objective function f and make an evaluation on corresponding geometry.

4) Forming metamodel between optimization parameters and performance.

Considering the high computational cost of flow solver, especially 3D flow solver, a metamodel function between optimization parameters x and performance y is required to form: $y=G(x)$. Once metamodel has been formed, the objective function $f(y)$ can be rewritten in the form with only optimization parameters $f(G(x))$, then the value of objective function can be calculated without using flow solver . The general used mapping methods are Response Surface Methodology (RSM)[24] and an Artificial Neural Network (ANN) [25] while the kriging model is actually an improved

RSM[21]. It seems that RSM is more applicable in forming mapping for axial compressor impeller and centrifugal compressors with low number of optimization parameters because of the relative simplicity in the relationship between geometry and performance. However, low number of optimization seems not to meet the industrial requirements among most of cases. Therefore, many papers used the ANN to form performance map, also called as metamodel.

5) Applying optimization algorithm to find optimal optimization parameters x^*.

Optimization algorithm can be also divided into two categories: Gradient-Based Method (GBM) and Evolutionary Algorithm (EA). In GBM classified as local optimization method and known for its efficiency, steepest descent, conjugate gradient or quasi-Newton techniques can be applied. This method is widely used on optimization of stators, such as inlet vanes, diffuser vanes or airfoil shape, of which the optimization problem is lower dimension, convex or lowly nonlinear. For the optimization of centrifugal compressor impeller, which is a highly nonlinear problem, GBM is not effective and easy to converge into a local minimum. EA, in which biology evolutionary ideas are used to deal with highly dimensional nonlinear problem and find the global optimal solution, is applied in recent years.

5.2 Parameterization

5.2.1 Geometry Parameterization

There is an extensive list of factors, which must be considered in order to reach the most suitable design for a given application in industry.[26] Therefore, it seems it is impossible to optimize all the variables simultaneously limited by the existed optimization algorithm as well as the computation cost. Therefore, the variables are required to be chosen and parameterized carefully to match other components in the optimization algorithms.

Fan[27] use 12 discrete values of blade angle distribution as parametric variables under the assumption that a centrifugal compressor impeller with a smaller exit width and two-dimensional blades of constant thickness.

Oyama[27] parameterized the mean camber line and a thickness distribution by the three order B-spline curves.

Fan[28] assumed that the blades of diffusers have the constant height and thickness, and parameterized the blade profile of diffusers by fourth-order Bezier curve, the blade suction and pressure surfaces with fifth-order polynomials.

Geometry parameters are parameterized from the impeller shape. Chosen geometry parameters should be sufficient to represent impeller geometry. Contour and blade angle distribution of centrifugal impeller are represented by Bezier polynomials. Therefore profiles of contour and blade angle distribution are completely determined by control point nodes and the locations of these control point nodes are chosen as geometry parameters and used as input layer to train ANNs. The geometry parameterization is shown in Figure 5-1 and Figure 5-2. Twelve geometry parameters are chosen from contour shown in Figure 5-1 while eight from blade angle distribution shown in Figure 5-2. Inlet and outlet parameters are not considered in the parameterization because these parameters have already been calculated in one dimensional design and there are extensive studies on one dimensional design of radial gas compressor. Normal thickness distributions have more effects on mechanical performance and lifetime of impellers, and therefore remain conservative in compressor industry. With this consideration, locations of control nodes points of normal thickness distribution are not chosen as optimization parameters.

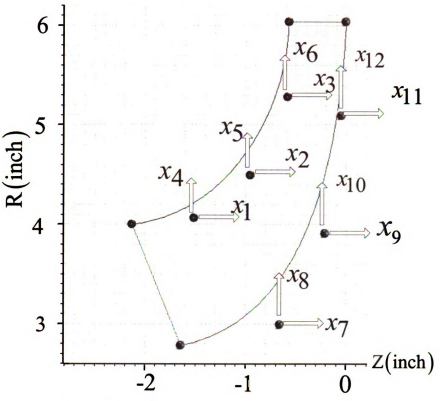

Figure 5-1 Geometry parameterization of contour

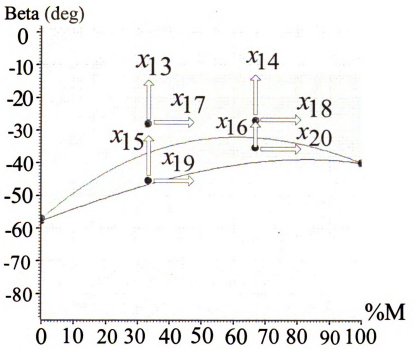

Figure 5-2 Geometry parameterization of blade angle distribution

5.2.2 Performance Parameterization

Performance parameters are parameterized from evaluation results of a flow solver, and should be easily evaluated by designers. The chosen performance parameters can be efficiency[21, 25], total pressure ratio[29], losses[23, 29], velocity distribution[30, 31], pressure distribution[22] and loading[21, 25]. Three dimensional (3D) Computational Fluid Dynamics (CFD) flow solver could be applicable for calculating the compressor performance. However, the application of 3D CFD flow solvers to generate training data cases and test data cases still requires long calculating time. Therefore, Quasi-3D flow solver MERIDL [14] and TSONIC [12], which employ streamline curvature method, are applied instead. The total computational time is approximately one second per case using a CPU Pentium 3.20GHz. Parameters related to relative velocity distribution are chosen as performance parameters because of its importance on analyzing the performance of compressors as well as the limits of streamline curvature method. There are two methods of parameterization for relative velocity distribution: curve fitting and discretization, which are shown in Figure 5-3 and Figure 5-4 respectively.

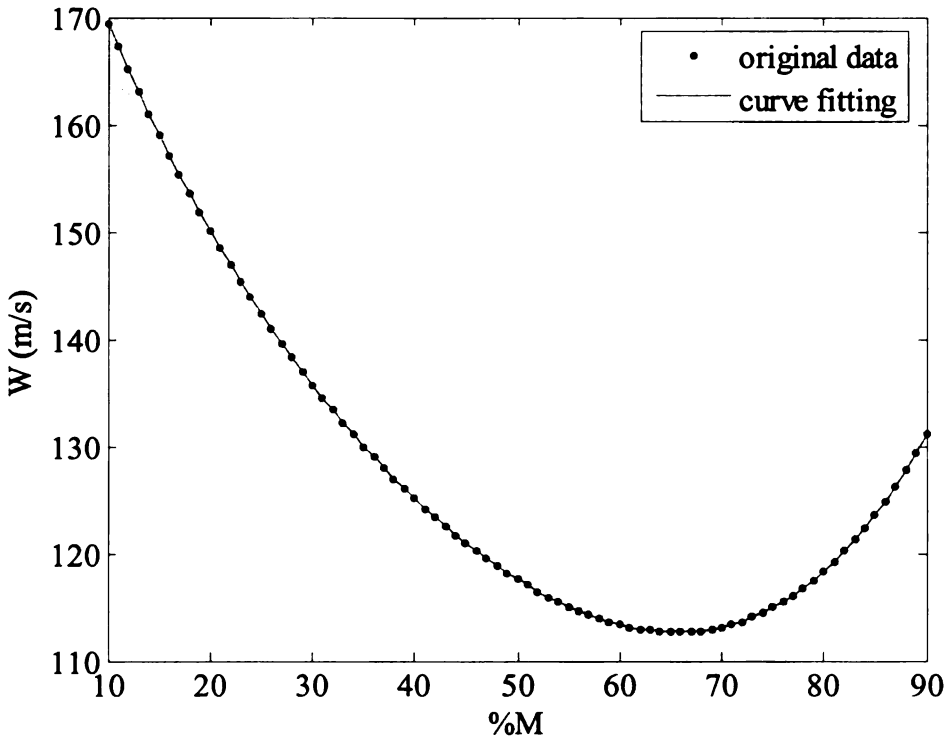

Figure 5-3 Curve fitting of relative velocity distribution

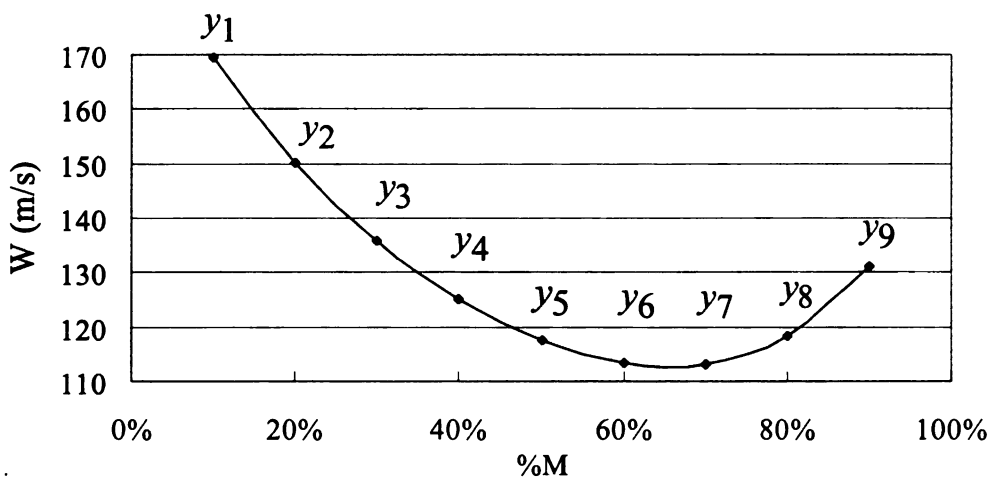

Figure 5-4 Discretization of relative velocity distribution

However, it is found that very small changes on the curve shape can result in a large change on these polynomial coefficients p. Two velocity distributions with very small differences are compared in Figure 5-5. Their corresponding polynomial coefficients p are list in

Table 5-1 by using curve fitting method for relative velocity distribution. The comparison of change of W points between two relative velocity distributions is shown in Table 5-2. We can see that the average change of coefficient polynomials is approximately 6% while the maximum change is 11.67% for curve fitting method. The average change of W points is 0.4% while the maximum change is 1.56%. Therefore the results suggest that the curving fitting brings nonlinear characteristics to the optimization problem and increases the difficulties of the whole optimization problem. Therefore, the discretization is used for parameterization. Nine W points on relative velocity distribution are used as the performance parameters shown in Figure 5-4. The corresponding normalized meridional distance of these nine W points ranges from 10% to 90%.

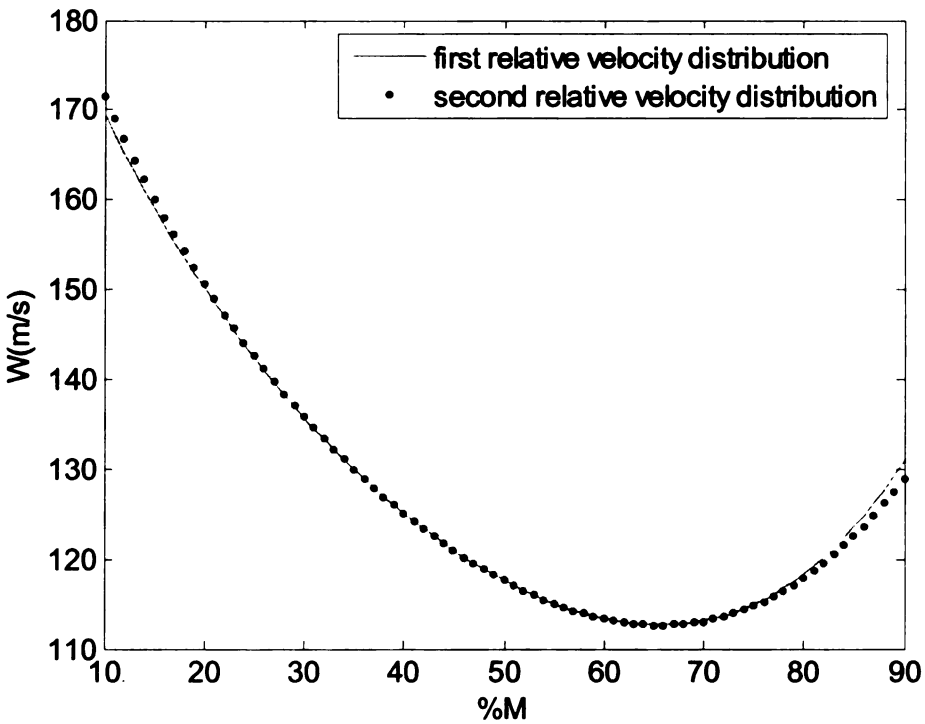

Figure 5-5 Illustration of two relative velocity distributions with small differences

Table 5-1 Comparison of polynomial coefficients p between two W distributions

	P_0	P_1	P_2	P_3	P_4
First relative velocity distribution	2.761e-006	-0.0004815	0.046806	-3.0436	195.68
Second relative velocity distribution	2.761e-006	-0.0005179	0.052267	-3.3039	199.6
Percentage of change	0%	7.56%	11.67%	8.55%	2.0%

Table 5-2 Comparison of W points between two W distributions

	W_0	W_1	W_2	W_3	W_4	W_5	W_6	W_7	W_8
First relative velocity distribution	169.5	150.1	135.7	125.1	117.6	113.4	113.1	118.3	131.1
Second relative velocity distribution	171.5	150.6	135.8	125.1	117.6	113.4	113.1	117.9	129.0
Percentage of change	1.21%	0.32%	0.05%	0.00%	0.00%	0.00%	0.06%	0.41%	1.56%

5.3 Objective Function

The object functions defined in papers are quite different, because it is related to a lot of factors such as parametric variables, flow solver, optimization algorithms, and requirements of product.

Generally, optimization problems can be grouped into two categories: constrained optimization problem and unconstrained problems.

In the unconstrained problems, there are only object functions, such as $f(x)$. The aim is to maximize or minimize $f(x)$. On the other hand, in the constrained problems, both object functions and constrained conditions existed. For example, the constrained conditions in [32] are expressed by:

$$\left|\frac{\dot{m}_{des}-\dot{m}_{actu}}{\dot{m}_{actu}}\right| \le 0.005 \qquad (5\text{-}1)$$

$$\left|\frac{C_{pdes}-C_{pactu}}{C_{pactu}}\right| \le 0.01 \tag{5-2}$$

The objective function and constraints can be transformed into unconstrained type incorporating the exterior penalty function and the mathematical expression can be expressed by Sun[33]:

$$\min P(x,r_k) = \min f(x) + r_k \sum_{i=1}^{n_c} \left|\min\left(g_i(x),0\right)\right| \tag{5-3}$$

Where $r_k = \max\left(1/d, r_{k-1}\right)$, d denotes the mean values of distance from polyhedron centroid to each vertex, while r denotes the penalty factor and k denotes the times of the iteration.

Generally, the object functions can be grouped into two categories: the single and multi object functions[34]. The multi objective functions can be combined into single objective functions by using weight factors:

$$F = \sum_{i=1}^{n} w_n f_n \tag{5-4}$$

where $\sum_{i=1}^{n} w_n = 1$

Jang[34] used the adiabatic efficiency as objective function. The efficiency is widely used in objective function, because a small improvement in efficiency can result in significant saving in annual cost[29]. Oyama[32] used the entropy production as the objective function to be minimized. Brian[35] used maximum principal stress at each node as the objective function within the blade for thermoelastic optimization. Wang[21] used the total pressure losses as the objective function.

For a multi-objective function, Oyama[29] considered one, which involved maximization of efficiency, mass flow rate, total pressure ratio and durability as well as minimization of weight.

Loading and velocity distribution are considered to have influences on the efficiency and flow range. Therefore ten criteria are considered to use in the objective function in this study.

1st Criterion: The deceleration ratio should be larger than 0.65. And deceleration ratio on pressure side should be larger than 0.5. The definition of deceleration ratio is that of outlet velocity at the impeller to maximum velocity.

Table 5-3 Comparison of deceleration ratios of W distribution among five cases

Deceleration Ratio	Base	Case1	Case2	Case2b	Case2c
Pressure side on Hub	0.467	0.444	0.459	0.324	0.469
Suction side on Hub	0.700	0.692	0.694	0.646	0.742
Pressure side on Shroud	0.475	0.589	0.514	0.667	0.655
Pressure side on Shroud	0.706	0.705	0.753	0.706	0.712

Based on the evaluation, we already know that the Base case is the best case while the case 2b is the worst. The deceleration ratio on pressure side on hub shows that the Base and case 2c has the minimum penalty while the case 2b the maximum. It matched our evaluation results. There are no penalty on suction side both on hub and shroud because all the deceleration ratios are larger than 0.65. However, results in Figure 4-37 show that maximum relative velocity at inducer of Base Case is much larger than others, which results the higher deceleration ratio and bring the penalty to Base case. This penalty is not reasonable for Base case because there is no such high inducer relative velocity for Base case.

2nd Criterion: The maximum loading should be reached shortly after the inlet. Based on experiences, if the maximum loading is within the 6% normalized meridional distance, then maximum loading has been reached shortly after the inlet. And all the results meet this criterion. However, it is sensitive to give a criterion range. For instance, the maximum loading of Base case on shroud occurs at 5.5% normalized meridional distance, those of Case1 on hub and of Case 2 on shroud at 5.4% and 5.6% respectively. If a case with maximum loading at 6%-7% normalized meridional distance, it is still quite possible this case is a good design. Therefore, this criterion is not effective to make the judgment, especially for computer-aided optimization.

3rd Criterion: Rapid Deceleration is preferred in the inducer region. The slope of the velocity distribution in the inducer region is calculated. Because the velocity decelerates, the slope should be less than zero. The higher the absolute value of the slope is, the more quickly the deceleration is. Firstly, it is very difficult to give an exact numerical definition of inducer region. Secondly, the slope of the velocity distribution greatly depends on the given inducer region. The slopes of five velocity distribution are compared in Figure 5-6. If the uniform weight factors are given, then Case 2 is considered as the best one based on this criterion.

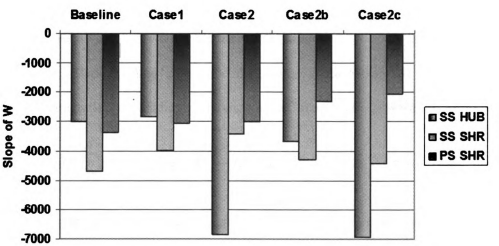

Figure 5-6 Comparison of slope of W in inducer region for 3rd Criterion

4th Criterion: High loading of the inducer compared to the outlet of the impeller. All five cases meet this criterion.

5th Criterion: All unnecessary acceleration or deceleration must be avoided in the overall process. The derivation of velocity is calculated. Times of sign changing are accounted. If sign is positive, it means that the velocity accelerate, while the sign negative, the velocity decelerate. The higher times of sign changes indicate more unnecessary acceleration and deceleration. The times of sign changes for each case are shown in Figure 5-7.

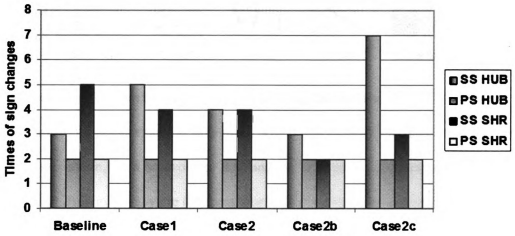

Figure 5-7 Comparison of times of sign changes based on 5th Criterion

6th Criterion: Relative velocity must be kept positive everywhere to avoid reverse flow. No negative relative velocity occurs in these five cases.

7th Criterion: Blade loading should be distributed as uniformly as possible. The numerical integration of loading difference along meridional distance is calculated based on Eqn. $\sum_{i=1}^{n} abs\left(Loading(i) - Loading(i-1)\right)\Delta m$. While $Loading(i)$ is the loading at point i, and $Loading(i-1)$ is the loading at point $i-1$, $Loading(i) - Loading(i-1)$ is loading difference, $\Delta m = m(i) - m(i-1)$. If loading

is perfectly uniformly distributed, the loading difference at any point is zero. Therefore the integral is zero. The results (Figure 5-8) indicate that Case 1 is the worst case based on this criterion while case 2b is the best.

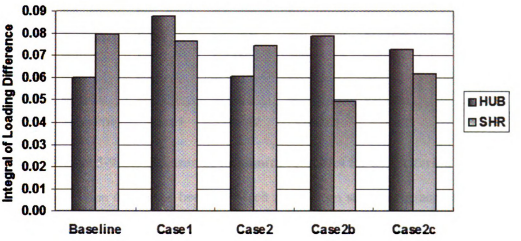

Figure 5-8 Comparison of integral of loading differences for 7th Criterion

8th Criterion: Large deceleration in regions, which will cause thick boundary layers as well as separation, must be avoided. It seems that this criterion is contradictory with Criterion 3. However, they are different. For the Criterion 3, the rapid deceleration is preferred only in the inducer. However, the too much deceleration is not preferred because of the separation. Therefore, the highest minimum velocity is preferred. Therefore, the minimum velocity at the end of deceleration process is used as standard. However, no significant differences can be observed among these five cases (Figure 5-9).

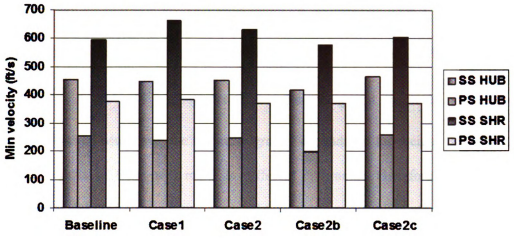

Figure 5-9 Comparison of minimum velocities for 8th Criterion

9th Criterion: The difference between Mach number on suction surface of hub and shroud should be minimized to avoid secondary flow.

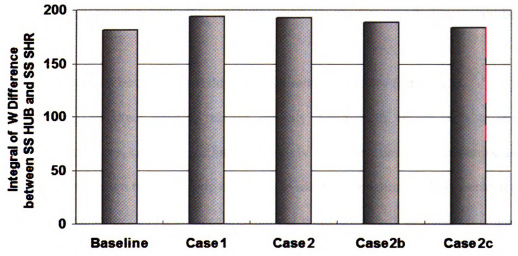

Figure 5-10 Comparison of integrals on relative velocity differences between suction surface on hub and shroud

10th Criterion: Blade loading should have a limit, which is 0.81 based on mechanical stress limit nowadays. However, numerical results at the inducer is very sensitive to the interface between impeller and inlet casing and is not sufficient accurate the make such a judgment.

Cassey[18] also suggests using suction surface peak Mach number, suction surface

average Mach number and etc. However, based on the analysis from 1^{st} Criterion to 10^{th} criterion, we found that some of criteria are not effective to make the judgments such as 2^{nd}, 4^{th}, 6^{th}, 10^{th}. There are some wrong judgment are made because of numerical errors. Moreover, the optimum greatly depends on the weight factors and different values of these will result in different optimums. Therefore, Root mean square error (RMSE) between the predicted relative velocity points of each case and the desired ones is calculated and also defined as objective function in this study. The difference between calculated and target relative velocity distribution is used for objective function for the following reasons:

1) If the designed impeller can reach the relative velocity which results in the least separation and friction loss, the minimum loss or maximum efficiency can be obtained.[36]

2) The loading can be determined directly from relative velocity distribution.

Unfortunately, an exact optimal relative velocity distribution, which leads to the optimal performance, cannot be defined accurately. However, designing expertise as well as general design rules can help designers to identify the optimal relative velocity distribution introduced in [36]. Once the optimal relative velocity distribution called as aerodynamic design criteria is defined, the whole procedure will be degraded into a standard optimization problem.

5.4 Optimization Algorithm

5.4.1 Genetic Algorithm

Genetic algorithm (GA) is categorized as global search heuristics. The Genetic Algorithm uses the genetic evolution and Darwin's theory as a model to simulate the design evolution and to reach the best solution. The core of this theory is "the survival

of the fittest". GA used reproduction, mutation, and genetic recombination to "evolve" a solution to a problem. The terminology of GA applied in optimization methods for centrifugal compressors is presented in Table 5-4.

The main advantages of GA are as Robustness, Intrinsic parallelism, Globality.[28] However, the application of GA is very time consuming.

The goal of GA in this study is to find the optimal set of optimization parameters, which is corresponding to the maximum fitness. There are twenty genes of each individual, which are corresponding to twenty optimization parameters. The optimization parameters have been normalized into range (0,1) based on their given range. The correlation between GA terminology and the parameters used in centrifugal compressor impellers optimization are listed in Table 5-4.

Table 5-4 Terminology of GA applied on centrifugal compressors

Gene	One design Variable
A Chromosome	Impeller geometry parameters
An individual	A geometry case
Population	A group of cases
A Fitness	The objective function value or the evaluation of centrifugal compressor impeller performance

5.4.2 Genetic Algorithm Procedure

The procedure of GA used here is as shown in Figure 5-11. First of all, a new population has been initialized randomly. The fitness of all individuals was calculated by flow solver and the individual with best fitness was saved.

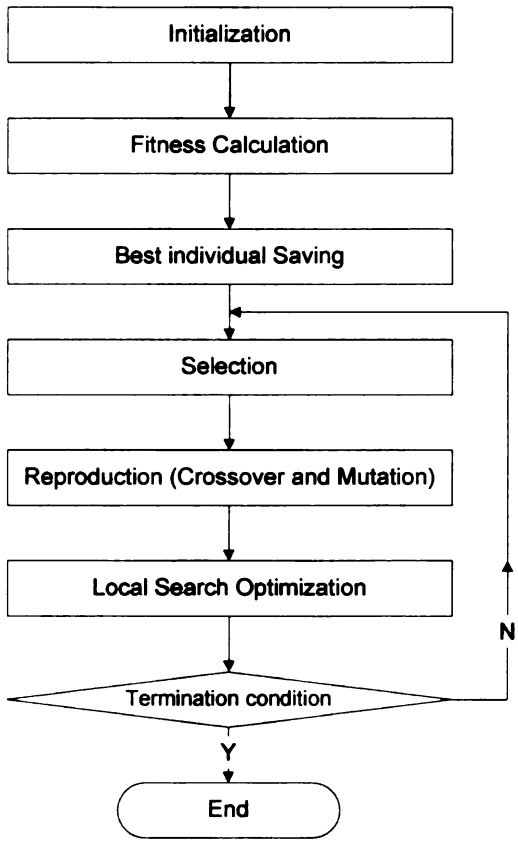

Figure 5-11 Procedure of Genetic Algorithm

In the selection step, a group of current population called as parents was selected to breed next generation. In this study, tournament selection[37] and Stochastic Universal Sampling (SUS)[38] are applied respectively and results were compared. Tournament selection is a selection operator in which a few individuals are chosen randomly from current generation and the winner is selected based on their fitness. In SUS, the probability of being selected from current generation is based on order of fitness. And the results showed that the found optimal solution based on these two selection operators were very similar while the converging was faster based on Tournament Selection and Stochastic Universal Sampling showed better performance on keeping genetic diversity.

In the reproduction step, the next generation of population was generated through genetic operator: crossover (also called as recombination) and mutation.

There are three different crossover operators are applied in sequence: Interpolation

Crossover, Extrapolation Crossover and Two Points Crossover.[39]

The Interpolation Crossover operator is expressed in the equation 5.

$$child_1 = rnd \times parent_1 + (1 - rnd) \times parent_2 \quad (5\text{-}5)$$

$$child_2 = (1 - rnd) \times parent_1 + rnd \times parent_2 \quad (5\text{-}6)$$

The extrapolation crossover operator is expressed in the equation 6.

$$child_1 = (1 + rnd) \times parent_1 - rnd \times parent_2 \quad (5\text{-}7)$$

$$child_2 = -rnd \times parent_1 + (1 + rnd) \times parent_2 \quad (5\text{-}8)$$

where *rnd* is random value between 0 and 1.

$Parent_1$ and $Parent_2$ are two parent individuals while $child_1$ and $child_2$ are children individuals. Values of children individuals should in ranges of those of their parent individuals based on Interpolation Crossover while outside of range based on Extrapolation Crossover. Chromosomes of children individuals don't change but switch between their parents based on two-points crossover operator. Two-Points crossover operator exchanges genes between two randomly generated points from parent individuals.

In mutation operator, analogous to biological mutation, chromosomes changes from their original states. One of the most important function of mutation is to remain genetic diversity and avoid the results converge to local optimum. Four different mutation operators used in this study was given in sequence: Boundary Mutation, Multi-NonUniform Mutation, NonUniform Mutation, Uniform Mutation.[39] In the Boundary Mutation, one of genes is chosen randomly and changed to its upper or bottom boundary. In the Multi-NonUniform Mutation, all genes move toward boundary with a dreasing damping factor based on the equation 7.

$$\begin{cases} child = parent + (1 - parent) \cdot \left(1 - \dfrac{ite_{cur}}{ite_{\max}}\right)^{order}, rnd \in [0, 0.5] \\ child = parent - parent \cdot \left(1 - \dfrac{ite_{cur}}{ite_{\max}}\right)^{order}, rnd \in (0.5, 1] \end{cases} \quad (5\text{-}9)$$

In the NonUniform Mutation, only one chromosome is randomly chosen for mutation based on equation 7. In the Uniform Mutation, one gene is chosen randomly and substituted by a random value. For the details on selection, crossover and mutation operators, please refer to [39].

5.4.3 Local Search Algorithm

Local search algorithm is combined with GA in this study. Because derivative of objective function is not available and the optimization problem is high dimensional, the procedure of local search algorithm is:

1) One or several genes of best individual are chosen randomly.

2) A random value closed to the original value of gene is given and new individual is generated.

3) If the fitness of new individual is better than the original one, then original one is substituted by the new one.

Because of the high computational cost for local research algorithm as well as the importance of best individual, this algorithm was only applied to update the best individual.

There are two termination conditions, which are the global optimum has been found or the maximum iteration number reached.

5.4.4 Test on GA and Local Research Algorithm

Before applying this combined optimization method for centrifugal compressor impellers optimization problem, three test equations are used to test this optimization method as following. In the testing, all testing dimension is 20, which is the same as

that of optimizing centrifugal impellers. However, all equations, which are plotted here, are shown in two-dimensions.

5.4.4.1 De Jong test function

The Eqn of De Jong test function is expressed by:

$$f(x) = 1/n \sum_{i=1}^{n} x_i^2 \qquad -5.12 < x_i < 5.12 \qquad (5\text{-}10)$$

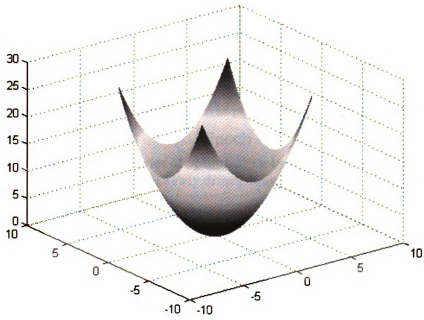

Figure 5-12 Illustration of De Jong test function in two-dimensions

We can see that finding the minimum of De Jong function is a standard convex problem (Figure 5-12). Because there are some random factors in the optimization method, therefore the test runs five times and their corresponding convergence histories are shown in Figure 5-13.

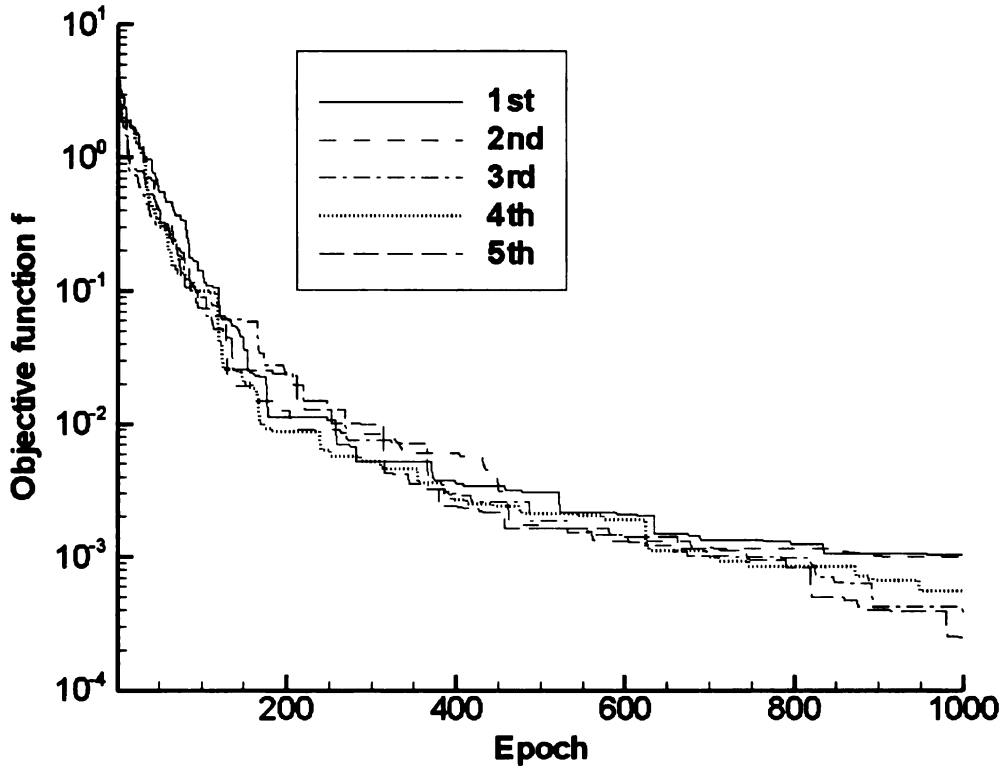

Figure 5-13 Convergence histories of optimization based on De Jong test function in twenty dimensions

5.4.4.2 Rosenbrock Test Function

$$f(x) = 1/n \sum_{i=1}^{n-1} (x_{i+1} - x_i)^2 + (1 - x_i)^2 \qquad -2.048 < x_i < 2.048 \qquad (5\text{-}11)$$

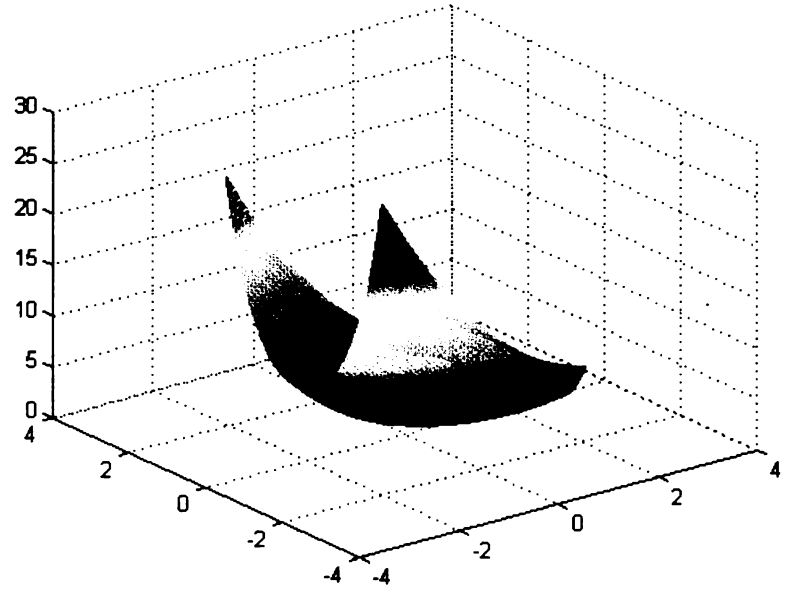

Figure 5-14 Illustration of Rosenbrock test function in two-dimensions

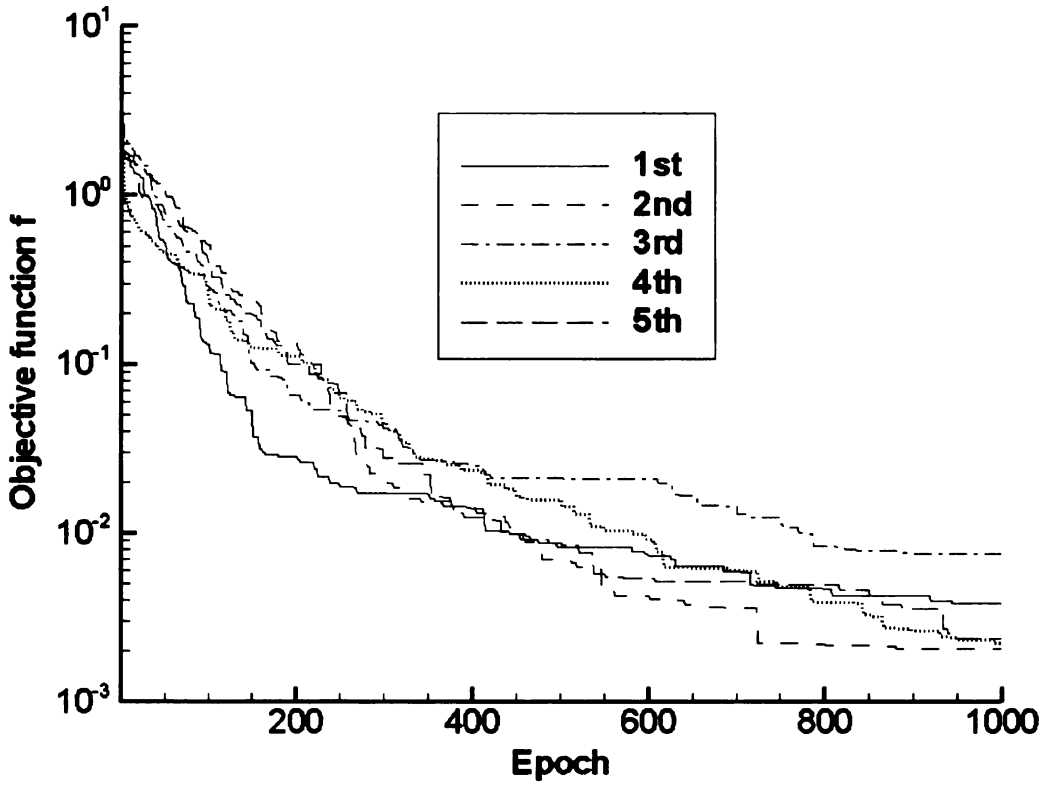

Figure 5-15 Convergence histories of optimization based on Rosenbrock Test Function optimization in twenty dimensions

5.4.4.3 Rastrigin Test Function

$$f(x) = 1/n \sum_{i=1}^{n-1} (x_i)^2 + 10 \cdot (1 - \cos 2\pi x_i) \qquad -5.12 < x_i < 5.12$$

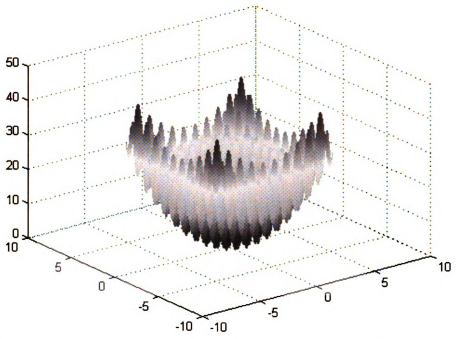

Figure 5-16 Illustration of Rastrigin test function in two-dimensions

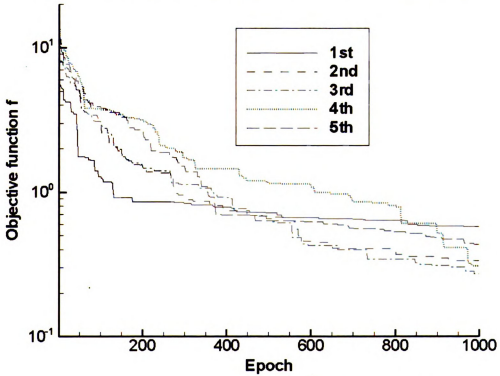

Figure 5-17 Convergence histories of optimization based on Rastrigin test function optimization in twenty dimensions

We can see that the performances of optimization method for Rosenbrock and De

Jong test function are good. However, Rastrigin test function is a high nonlinear and finding a global optimal based on this function is very difficult (Figure 5-16). The results of five times running indicated that the final error is around 0.1 and it is obvious that no global optimal or even close solutions have been found. To the author's knowledge, there is no quite effective optimization method for such as highly nonlinear problem.

5.5 Performance Mapping

An ANN is one type of nonlinear mathematical models, which is used to form a complex relationship between input and output data. The training of the ANN is an adaptive process in which parameters such as weights and bias are changed as internal or external information that flow through the ANN. Moraal et al [40] indicate that ANN can produce better performance compared to other curve fitting techniques if ANN is sufficiently trained. The advantages and drawbacks of ANN is listed in Table 5-5.Feed-Forward Neural Networks (FFNNs) [23, 30, 41]with back-propagation learning algorithm and Radial Basis Function Network (RBFN) [42, 43] are most widely used ANN to train performance map for turbomachinery.

Table 5-5 Cons and Pros of ANN

Pros	Cons
Relative low number of calculation	Searching and applying approximate functions
Efficient if the parameter space if unimodal, convex and continuous	Has no ability for extrapolating
No need for the knowledge of physics	
High mapping capacity	
Suitable for functions with multiple inputs and outputs.	

FFNN, which is one type of ANN, also called as multi-layer perceptrons, consists of one input layer, one or several hidden layers, and one output layer. Information flow

moves only in one direction from the input layer to the output layer without loops in it. Each neuron in one layer has directed connections to all neurons in the subsequent layer. Each neuron performs a weighted summation of the inputs from the previous layer, which then passes an activation function such as sigmoid function. RBFN, another type of ANN, has a less flexible structure compared to FFNN.

RBFN typically has only three layers: an input layer, one hidden layer with nonlinear radial basis function (RBF) used as activation function, and one linear output layer. The most widely used RBF is a Gaussian RBF in the hidden layer while the output is a weighted summation of neurons in the hidden layer. Both FFNN and RBFN are used to create performance maps for centrifugal compressor impellers in this work. Results show that accuracy of FFNN is similar to that of RBFN. However, FFNN provides higher robustness while RBFN provides much lower computational time. The average training time of FFNN varies from 1 to 2 hours depending on its detail structure while that of RBFN takes only 3 to 15 minutes. In this study, a large number of cases including geometry and performance parameters are provided to train neural network because of applications of fast Quasi-3D flow solvers, which help make the trained RBFN more robust and overcome drawbacks of RBFN to some extent. Therefore RBFN is chosen as mapping tool because it has much lower computational time.

There are five cases are generated to train the FFNN or RBFN while other five hundreds cases are generated to evaluate the performance.

The performances of two types of ANNs: FFNN and RBFN are compared. The results show that RBFN can achieve the higher accuracy on the training database than FFNN. However, FFNN shows the better performance on testing database. Therefore, it seems compared with FFNN, RBFN is over-train to some extent. Considering the computation time, that of RBFN is approximately one tenth of that of FFNN.

Table 5-6 Terminology of GA applied on centrifugal compressors

Performance mapping Method	RBFN	FFNN
Average error of training database (ft/s)	3.3007e-014	3.9261
Maximum error of training database (ft/s)	5.1159e-013	27.601
Average error of testing database (ft/s)	19.504	5.607
Maximum error of testing database (ft/s)	106.62	53.512
Computational time (s)	159.54	1446.6

5.6 RESULTS AND DISCUSSIONS

5.6.1 Accuracies of RBFN and FFNN

Five hundred cases in training database are generated randomly to create the ANN while other five hundred cases in testing database to evaluate the created ANN. The number of cases in training database are indicated by X coordinate values in Figure 5-18.

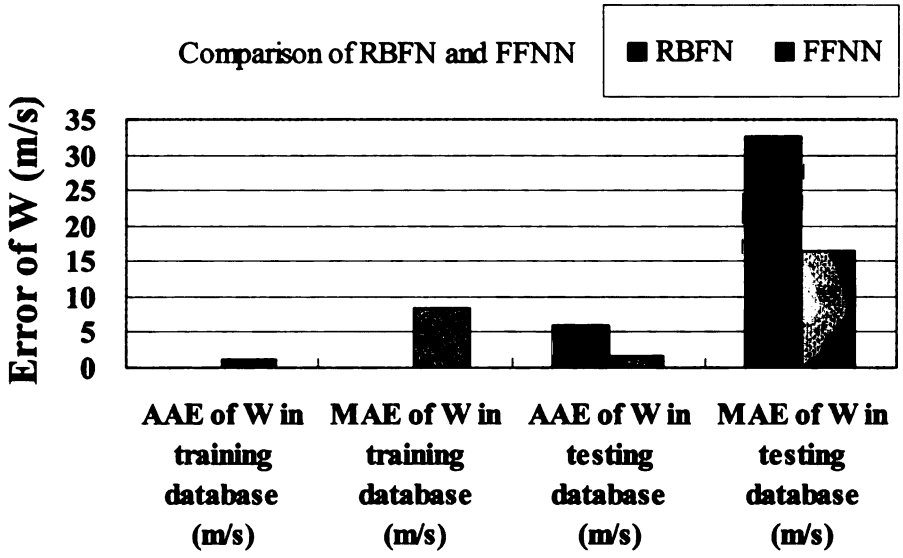

Figure 5-18 Comparisons of accuracies of RBFN and FFNN in training database and testing database

In Figure 5-18, Average Absolute Error (AAE) and Maximum Absolute Error (MAE) between W points in the training database and c W points calculated using RBFN is much smaller than those using FFNN. However, Average Absolute Error (AAE) and

Maximum Absolute Error (MAE) between W points in the testing database and W points calculated using FFNN is larger. Therefore, it seems that compared to FFNN, RBFN is over-trained. However, the training of FFNN is 1446.6 seconds while training of RBFN is 159.54 seconds, approximately one tenth of training time of FFNN.

5.6.2 Performances of Optimization Procedures using RBFN and FFNN

The trained RBFN and FFNN are used in centrifugal compressor impeller optimization procedures. Therefore, the total performances of optimization procedures using RBFN and FFNN are compared. The setting parameters for GA in optimization procedures are the same and the only difference is that two different types of trained ANNs: RBFN and FFNN. In the application of the optimization procedure, desired geometry should be unknown. The desired W points or desired W distribution are given directly by designers. Eventually, optimal geometry can be found. Optimal W points, which are calculated based on the optimal geometry, can then be compared with desired ones. In this study, the desired geometry and its corresponding W distribution are given. Therefore both optimal W points and optimal geometry parameters can be compared with desired ones. This is more effective for comparison between these two optimization procedures. Because of the influences of random factors, each optimization procedure runs for five times under the same setting.

Table 5-7 Comparison of average computational time for centrifugal compressor impeller optimization procedures using RBFN and FFNN

	1st time	2nd time	3rd time	4th time	5th time	average
Computational time of optimization using RBFN (s)	499.6	498.6	473.2	457.5	471.9	480.2
Computational time of optimization using FFNN (s)	408.5	535.1	542.1	545.8	546.7	515.6

In

Table 5-7, results show each computational time and average computational time. It can be seen that there is almost no differences between using RBFN and FFNN. This is because FFNN or RBFN is applied in the training procedure, and there is no extra computational time for using them to evaluate geometries in optimization procedures. The computational time differences are because of the different structures between RBFN and FFNN, which results in the different application time. The results show that it takes more time to call performance map trained by FFNN than that by RBFN. Centrifugal compressor impeller optimization procedures, which employ RBFN and FFNN, are used to calculate optimal geometries based on a given desired W distribution. Their corresponding optimal W distributions calculated from optimal geometries are compared with the desired W distribution in Figure 5-19.

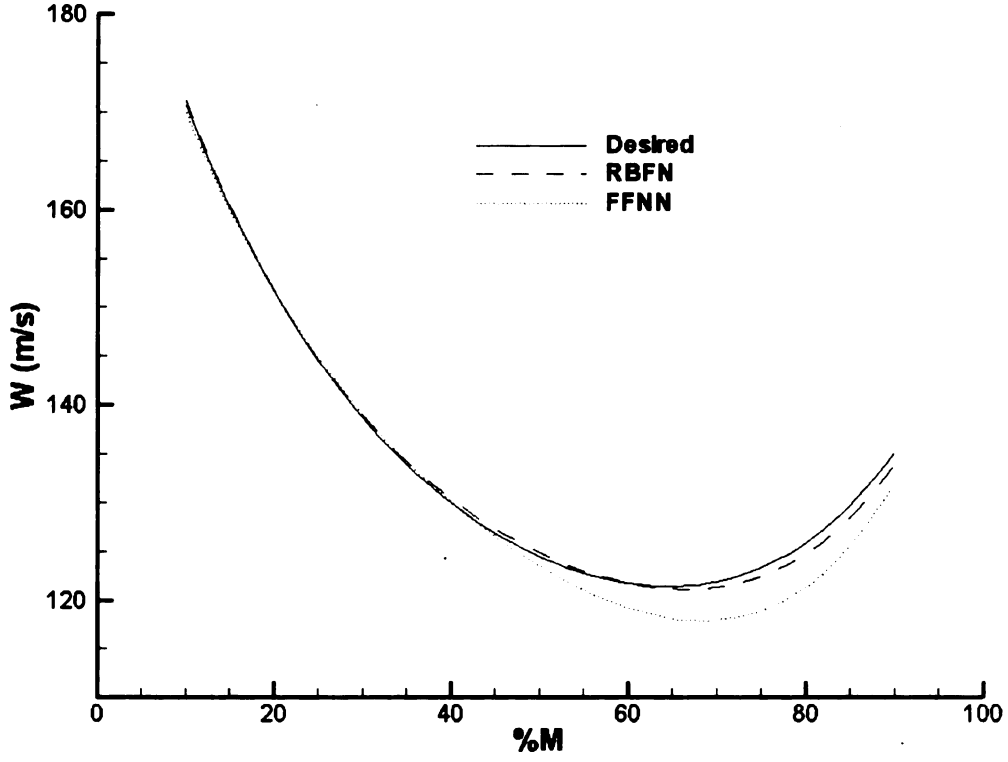

Figure 5-19 Comparison of optimal W distributions calculated by employing RBFN and FFNN

It is observed that the optimization procedure can find an optimal W distribution

much closer to the desired one by using RBFN than FFNN. In order to comprehensively evaluate RBFN, statistical results: AAE and MAE between optimal W points and desired ones are shown in Figure 5-20, respectively. In GA, the initial populations are required to give randomly, which leads that different optimal geometries are found even under the exactly same given desired W points, optimization algorithm and RBFN. Therefore, optimization procedure has been run five times under the same algorithm specification. All AAE and MAE in Figure 5-20 are illustrated in the form of mean±SD (Standard Derivative).

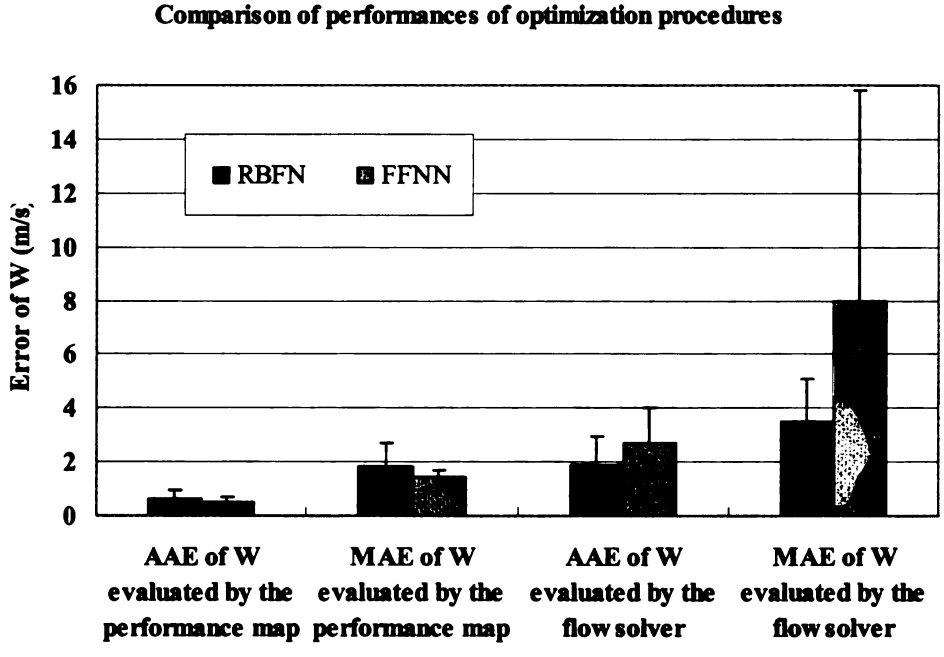

Figure 5-20 Statistical results of Average Absolute Error (AAE) and Maximum Absolute Error (MAE) between optimal W points & desired ones between using RBFN and FFNN

All results show that AAE and MAE between optimal W points and desired ones based on performance maps using FFNN has higher values compared to FFNN. However, AAE and MAE of W evaluated by flow solver show that RBFN has lower values. This demonstrates that the optimization procedure using RBFN is able to find optimal W points much closer to the desired ones compared to FFNN although the

accuracy of RBFN is lower than that of FFNN (Figure 5-18). Therefore, the RBFN is used for the following chapters because of its much lower computational time and slight better performance than those of FFNN.

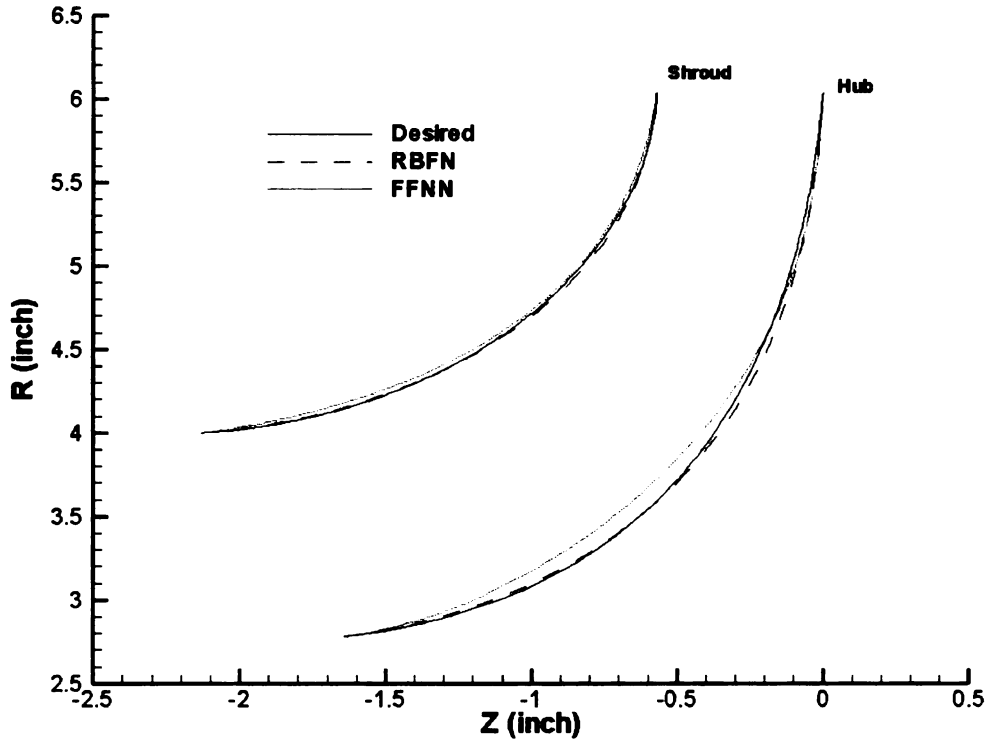

Figure 5-21 Comparison of optimal contours between using RBFN and FFNN

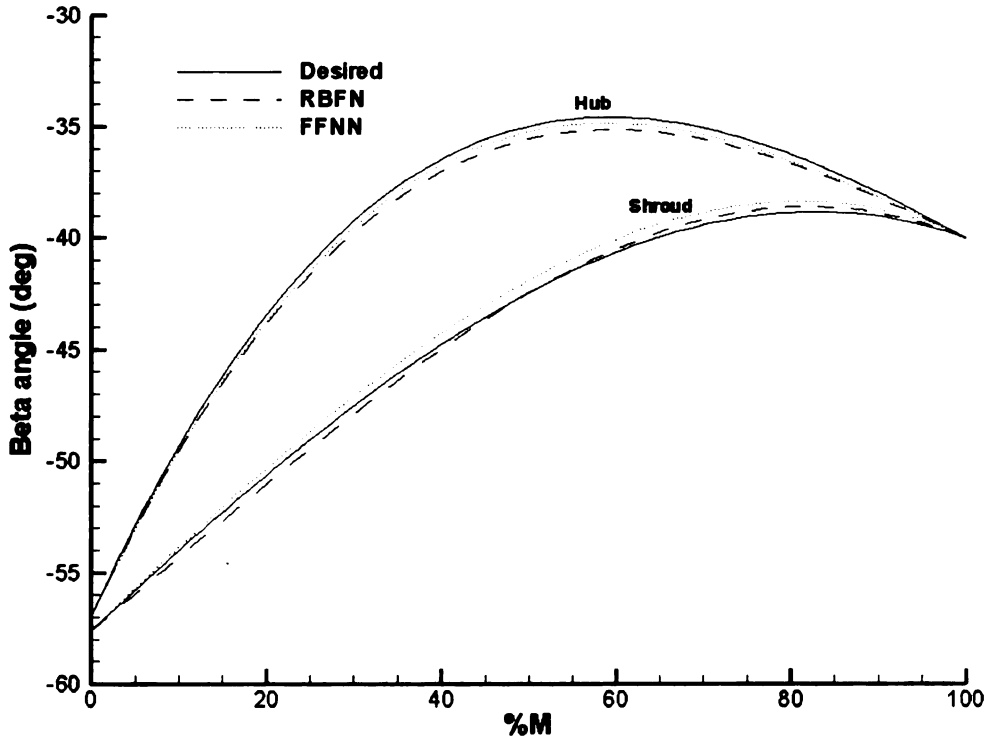

Figure 5-22 Comparison of optimal beta distributions between using RBFN and FFNN

In Figure 5-21 and Figure 5-22, optimal contour and blade angle distribution, also called beta distribution, are compared with desired ones, respectively. The optimization procedure, which employs RBFN, finds closer hub profiles, beta angle distribution on shroud than that using FFNN. However, the optimization procedure using FFNN finds the closer beta angle distribution on hub. There is no guarantee that all geometry parameters can be found closer to the desired one because this optimization problem is highly nonlinear problem. Figure 5-23 show statistical results: AAE and MAE between optimal geometry parameters and desired ones. Units of geometry parameters are diverse, e.g. inch for contour, degree for blade angle and dimensionless for normalized meridional distance. Therefore, all geometry parameters are normalized to dimensionless quantity in the range (0, 1).

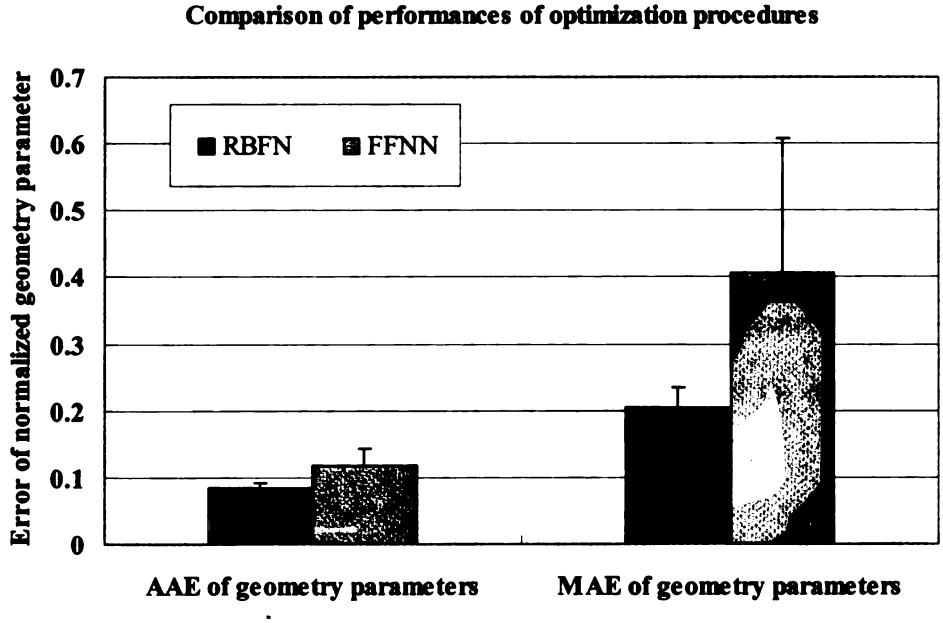

Figure 5-23 Average Absolute Error (AAE) between optimal geometry & desired ones

Results in Figure 5-23 suggest that the optimization procedure employing RBFN is able to find optimal geometry closer to the desired ones compared to FFNN in

average.

5.7 Summary

In this chapter, the centrifugal impeller optimization procedure using artificial neural network and genetic algorithm is established, which concludes the following steps:

1) Impeller geometry contour and blade angle distribution are used for parameterization, from which twenty geometry parameters are chosen. Two methods: curve fitting and discretization are compared. The discretization is used to parameterize the relative velocity distribution because the results show that parameters from discretization are more stable as change of curve.

2) The limits of Quasi-3D flow solver MERIDL and TSONIC are discussed. The reasons of the use of relative velocity distribution are also discussed.

3) The possible criteria in objective function are proposed and applied on existed cases. The calculation results of objective functions are compared with judgments of engineering designer. It is found that these criteria is not effective because either these are too loose for design cases or too difficult to express in exact numerical equation. Eventually, the differences between relative velocity distribution and desired the calculated and tried to apply on existed cases. Finally, root mean square error (RMSE) between the predicted relative velocity points of each case and the desired ones is defined as objective function.

4) Feed-forward Neural Network (FFNN) and Radial Basis Function Network (RBFN) are used to create performance maps respectively. These two performance maps are further used in the optimization procedure in which the Genetic Algorithm (GA) is used as optimization method. Created performance maps as well as the total optimization procedures between using RBFN and FFNN are evaluated and

compared.

5) The results show that the RBFN has higher accuracy on training database while lower accuracy on the testing database than FFNN, which indicates the RBFN is over-trained. However, the optimal results show that optimization procedure using RBFN is able to find the better optimal based on the evaluating results of flow solvers.

6) Although the application of modeling tools greatly decreases the computational time, it also brings errors to the optimization procedure due to the application of approximate performance map. Because the dimension of created performance map equals to the number of geometry parameter, which is a high number. To the authors' knowledge, it is very difficult to create an exact performance map for such a high nonlinear problem. Based on our calculating results, the errors of the approximate map is much larger than those caused by an optimization method. The errors of approximate performance maps diminish the effects of high fidelity flow solvers and highlight that the increase on modeling is more important than searching a better and more effective optimization method for this centrifugal compressor impeller optimization problem. Therefore, an improved offline flow solver optimization procedure and an online flow solver optimization procedure are presented in Chapter 6 and Chapter7 respectively.

CHAPTER 6

IMPROVED IMPELLERS OPTIMIZATION PROCEDURE

6.1 Introduction

In last chapter, Artificial Neural Networks (ANNs) is used to create an approximate performance map. However, it is found that although the introduction of ANN greatly decreases the computational time, it also brings errors to the optimization procedure because of the application of approximate performance map. Wang et al. [21] consider only blade angle distribution for parameterization, which helps reduce geometry parameters, the dimension of input layer as well as the whole dimensions of this optimization problem. This makes training of ANN and searching of global optimum become much easier. Verstraete et al. [25] propose to use the online-trained ANN, which uses the new calculated results to update the existed ANN, and increases the accuracy of performance gradually as the iteration proceeds. Ghorbanian .et al. [42] use rotated general regression neural network (RBRNN). Its basic theory is that rotation can reduce the nonlinear characteristics of relationship between geometry parameters and performance parameters in new rotated coordinate system. In our research it is found that the chosen geometry parameters and performance parameters are of importance because ANNs are trained to represent the relationship between geometry parameters and performance parameters. The simpler the relationship between geometry parameters and performance ones is, the more easily ANNs can be trained and the higher accuracies of ANNs will be. In our study, RBFN, a type of ANN, is applied to create a performance map for centrifugal compressor impellers. Instead of applying training database to train RBFN directly, Principle Component Analysis (PCA) or Independent Component Analysis (ICA) is applied to transform

training database into new transformed coordinate system, in which RBFN is trained. Accuracies of three different trained ANNs: RBFN, RBFN with PCA and RBFN with ICA are compared. Performances of centrifugal compressor impeller optimization procedures employing three different trained Artificial Neural Networks (ANNs): RBFN, RBFN with PCA, and RBFN with ICA are also compared.

6.2 Application of ICA and PCA

We use PCA and ICA to improve the accuracy of RBFN. Generally, PCA is a mathematical technique to transform a high-dimensional space into a few orthogonal axes called principle components, along which the variances of data are maximized. In our study, PCA is used as an orthogonal transformation, which preserves the dimension of data and only transforms data into a new coordinate system on which maximum variances of data are projected. ICA is superficially related to principle component analysis. ICA involves a computational procedure for separating multivariate data, which are assumed to be linear mixtures of unknown latent variables, into non-gaussian and mutually independent components called the independent component of the observed data.

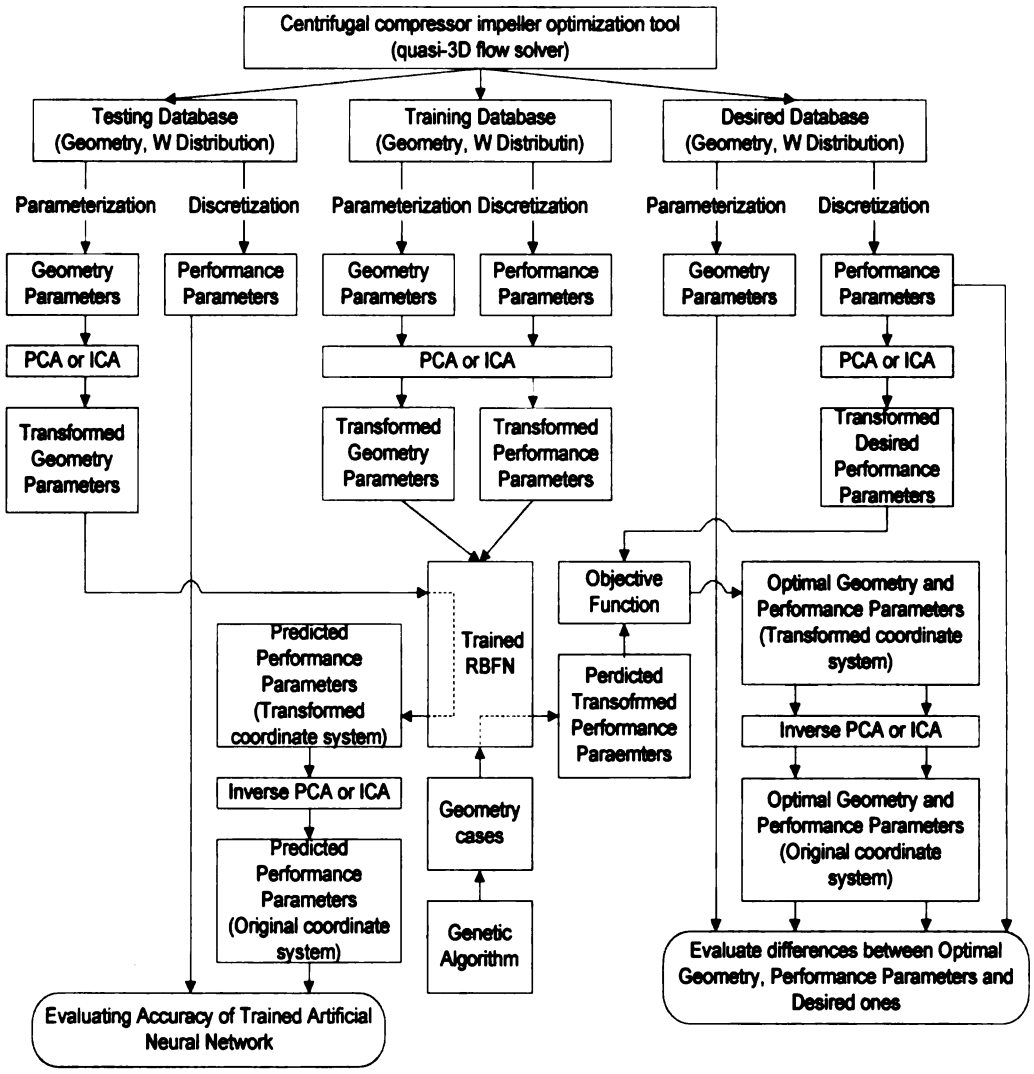

Figure 6-1 Centrifugal compressor impeller optimization procedure with PCA or ICA

The flowchart of centrifugal compressor impeller optimization procedure using PCA or ICA is shown in Figure 6-1. It consists of three steps: generation of three databases, training and evaluation of RBFN, searching and evaluation of optimum based on Genetic algorithm (GA) and desired W points. Firstly, geometry generation tool with a quasi-three dimensional flow solver is used to generate three groups of database: training, testing and desired database. Training and testing database are generated randomly while desired database is given by designers. Each database can be divided into two parts: geometry parameters and performance parameters. As for each case,

there are twenty geometry parameters and nine performance parameters. Secondly, if PCA or ICA is not used, geometry parameters and performance parameters in training database are used respectively as input layer X and output layer Y to train RBFN. Otherwise, PCA or ICA is used to transform training database to those in a new coordinate system which is used to train RBFN in this new coordinate system. Then twenty geometry parameters in testing database are also transformed into those in a new coordinate system by PCA or ICA, and then transformed geometry parameters in the new coordinate system are input into trained RBFN, followed by the prediction of corresponding performance parameters using RBFN. These predicted performance parameters are represented in the new coordinate system because RBFN is trained in new one. Therefore, by using inverse PCA or ICA, these predicted performance parameters in the new coordinate system are transformed back to those in the original coordinate system, which are used to compare with performance parameters in testing database. The differences between predicted performance parameters in the original coordinate system and performance parameters in the testing database are used to evaluate the accuracy of trained RBFN. Because there is no transformation using RBFN without PCA or ICA, therefore accuracies of RBFN between with and without using PCA or ICA can only be compared in the original coordinate. This is the reason why inverse PCA or ICA is used to transform predicted performance parameters back to the original coordinates. The smaller errors between predicted performance parameters and performance parameters in the testing database means higher accuracy of trained ANN. Thirdly, nine W points calculated from desired geometry is used as the desired W points or desired performance parameters. GA is used to generate the first generation: a group of geometry cases and their corresponding performance parameters are predicted using RBFN. Root mean square error (RMSE) between the

predicted performance parameters of each case and the desired ones is calculated and also defined as objective function in this study. GA is then used to generate the next generation based on genes and finesses of first generation using selection, crossover and mutation. This process continues until it meets these requirements: the exact desired performance parameters are found or maximum generation number reaches. Optimal geometry and performance parameters are transformed into the original coordinates and compared with desired ones to evaluate the total performance of optimization procedure.

6.3 Results and Discussion

6.3.1 Accuracy of RBFN

In this optimization procedure, cases in training and testing databases are generated randomly. It seems that one group of results is not sufficiently strong to evaluate the effects of PCA or ICA on the accuracies of trained RBFN and the performance of centrifugal compressor impeller optimization procedure due to influences of random factors. Therefore, four independent groups with different numbers of cases in training database are generated to better evaluate the application of PCA and ICA. The number of cases in training database are indicated by X coordinate values in Figure 6-2 and Figure 6-3.

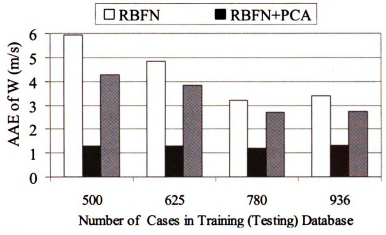

Figure 6-2 Comparisons of accuracies of trained RBFN, RBFN with PCA, and RBFN with ICA on Average Absolute Error (AAE) between predicted W points & those in testing database

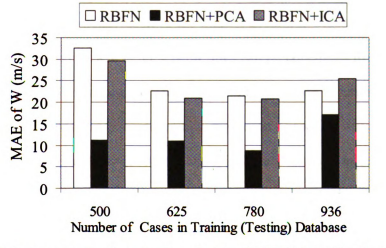

Figure 6-3 Comparisons of accuracies of trained RBFN, RBFN with PCA, and RBFN with ICA on Maximum Absolute Error (MAE) between predicted W points & those in testing database

As mentioned above, each training database and testing database in these four groups is used to train and evaluate three different ANNs: RBFN, RBFN with PCA and RBFN with ICA. Accuracies of RBFN, RBFN with PCA, and RBFN with ICA are compared and results are shown in Figure 6-2 and Figure 6-3. Results in Figure 6-2 and Figure 6-3 show Average Absolute Error (AAE) and Maximum Absolute Error (MAE) between W points in the testing database and predicted W points based on three different ANNs: RBFN, RBFN with PCA, and RBFN with ICA for four different testing databases. The unit of AAE and MAE is m/s. In our study, numbers

of cases in the training database are equal to those of the testing database. The comparison of three different ANNs: RBFN, RBFN with PCA, RBFN with ICA on both AAE and MAE are shown in different colors. In Figure 6-2 and Figure 6-3, results of these four groups uniformly show that AAE and MAE of RBFN with PCA is approximately 50% of those of RBFN with ICA or RBFN. AAE and MAE of RBFN with ICA are slightly lower than those of RBFN. As the increase of case numbers in the training database, the AAE of RBFN or RBFN+ICA gradually decrease while AAE of RBFN+PCA remain the same. This is probably because RBFN or RBFN+ICA can create more accurate ANN as the increase of training cases while RBFN+PCA has already achieve the highest accuracy, which is limited by its characteristics. However, there is no general rules can be concluded from MAE. The MAE with 936 cases in training database and testing database is larger than others. This is because the possibility of generating a geometry case, on which the created performance map does not has good prediction, is increased as the increase of testing database. However, the increase of the number of cases results in unfavorable exponential increase on the training time for ANN shown in Table 6-1. Therefore, increase of the number of cases is not reasonable when it is sufficient to create a fairly accurate RBFN. The comparison of computational time for training RBFN, RBFN with PCA and RBFN with ICA are shown in in Table 6-1. Results of four groups of database show that there is a slight increase, approximately 5-6%, on the training RBFN caused by the introduction of PCA or ICA. In summary, trained RBFN with PCA has a much higher accuracy than RBFN or RBFN with ICA because it shows lower value of AAE and MAE with only a slight increase on the training time.

Table 6-1 Comparison of computational time for training three different ANNs: RBFN, RBFN with PCA and RBFN with ICA

	Number of Cases in a training Database			
	500	625	780	936
Computational Time of RBFN (s)	110.73	199.46	480.97	875.38
Computational Time of RBFN with PCA(s)	115.87	231.22	474.69	881.08
Computational Time of RBFN with ICA(s)	111.05	239.06	483.96	887.30

6.3.2 Performance of Optimization Procedure

It has been approved that RBFN with PCA has better performance than RBFN and RBFN with ICA. However, this does not guarantee that RBFN with PCA can bring benefits to total optimization procedure. Because training of ANN is only one part of optimization procedure. It is possible that RBFN with the increased accuracy does not play an important role in the total optimization procedure. Moreover, introduction of PCA may lead to some drawbacks and diminish the effects of higher accuracy of RBFN with PCA. Therefore, the total performances of optimization procedures using three different ANNs should be compared. The setting parameters for GA in optimization procedures are the same and the only difference is that three different trained ANNs: RBFN, RBFN with PCA, and RBFN with ICA are applied in these optimization procedures.

In the application of the optimization procedure, desired geometry should be unknown. The desired W points or desired W distribution are given directly by designers. Eventually, optimal geometry can be found. Optimal W points, which are calculated based on the optimal geometry, can then be compared with desired ones. In this study, the desired geometry and its corresponding W distribution are given. Therefore both optimal W points and optimal geometry parameters can be compared with desired ones. This is more effective for comparison among three ANNs as well as the evaluation of application of PCA or ICA.

Table 6-2 Comparison of average computational time for centrifugal compressor impeller optimization procedures using three different ANNs: RBFN, RBFN with PCA and RBFN with ICA

	Number of Cases in a training Database			
	500	625	780	936
Computational time of optimization using RBFN (s)	56.95	67.11	75.45	80.69
Computational time of optimization using RBFN with PCA(s)	56.32	70.33	75.34	78.86
Computational time of optimization using RBFN with ICA(s)	56.72	71.86	74.81	79.54

In Table 6-2, results show average computational time of three optimization procedures. It can be seen that there is almost no difference among using RBFN, RBFN with PCA, or RBFN with ICA in the optimization procedure. This is because PCA or ICA is applied in the training procedure, and there is no extra computational time for using them to evaluate geometries in optimization procedures. Also, structures of RBFN, RBFN with PCA and RBFN with ICA trained by same databases are identical although they are trained in different coordinate systems. However, results in Table 6-2 reveal that it takes more time to use RBFN trained with higher number of cases because there are more neurons in the hidden layer and therefore prediction by using such a RBFN requires more calculations. Centrifugal compressor impeller optimization procedures, which employ RBFN, RBFN with PCA and RBFN with ICA, are used to calculate optimal geometries based on a given desired W distribution. Their corresponding optimal W distributions calculated from optimal geometries are compared with the desired W distribution in Figure 6-4.

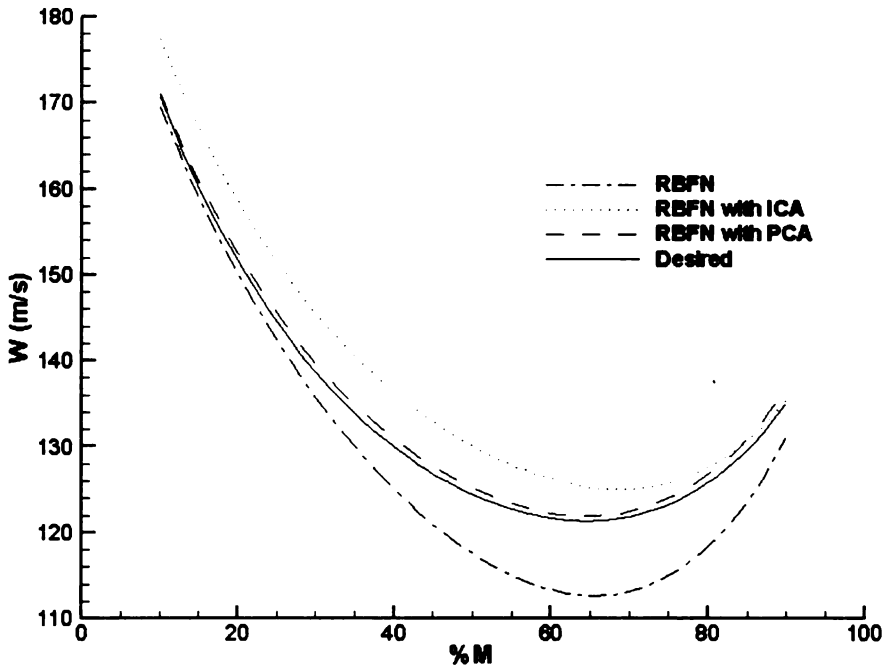

Figure 6-4 Comparison of optimal W distributions calculated by employing RBFN, RBFN with PCA, RBFN with ICA

It is observed that the optimization procedure can find an optimal W distribution much closer to the desired one by using RBFN with PCA. In order to comprehensively evaluate RBFN with PCA, the optimization procedure uses RBFNs trained with four different numbers of cases indicated by X coordinate and statistical results: AAE and MAE between optimal W points and desired ones are shown in Figure 6-5 and Figure 6-6, respectively. In GA, the initial populations are required to give randomly, which leads that different optimal geometries are found even under the exactly same given desired W points, optimization algorithm and RBFN. Therefore, optimization procedure has been run five times under the same algorithm specification. All AAE and MAE in Figure 6-5 and Figure 6-6 are illustrated in the form of mean±SD (Standard Derivative).

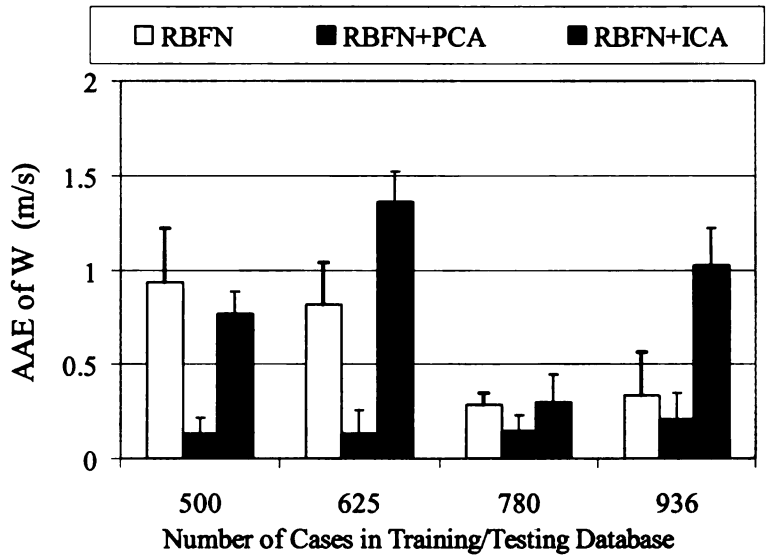

Figure 6-5 Comparison of Average Absolute Error (AAE) between optimal W points & desired ones among three different ANNs: RBFN, RBFN with PCA, RBFN with ICA

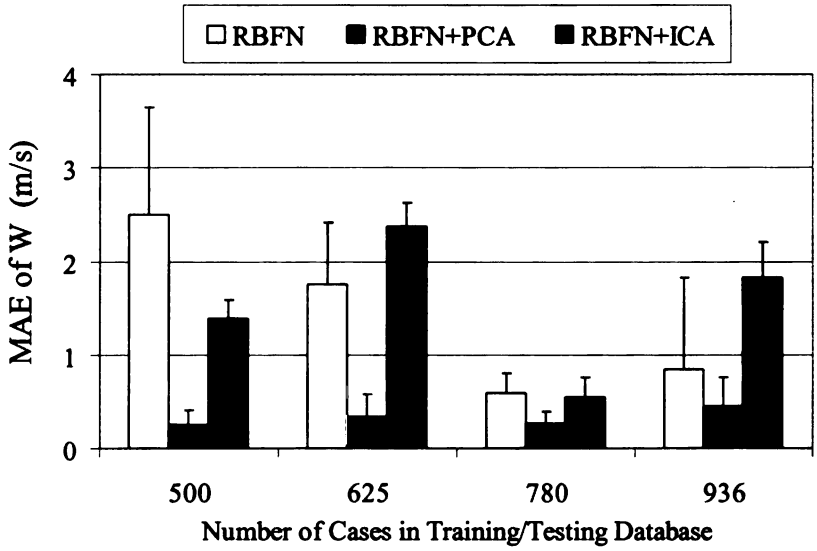

Figure 6-6 Comparison of Maximum Absolute Error (MAE) between optimal W points & desired ones among centrifugal compressor impeller optimization procedures using three different ANNs: RBFN, RBFN with PCA, RBFN with ICA

All results of four different groups of databases show that AAE and MAE between optimal W points and desired ones using RBFN with PCA has lower values compared to RBFN or RBFN with ICA. This demonstrate that the optimization procedure using RBFN with PCA is able to find optimal W points much closer to the desired ones

compared to other two different ANNs. However, optimization procedure which employs RBFN with ICA does not show better performance although RBFN with ICA has a slightly higher accuracy.

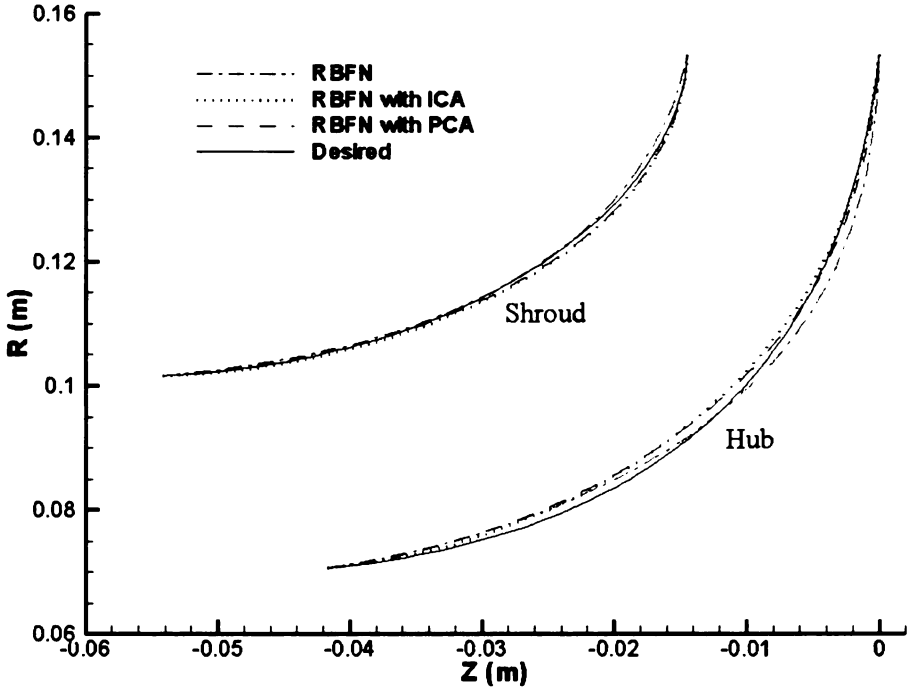

Figure 6-7 Comparison of optimal profiles calculated by employing RBFN, RBFN with PCA, RBFN with ICA

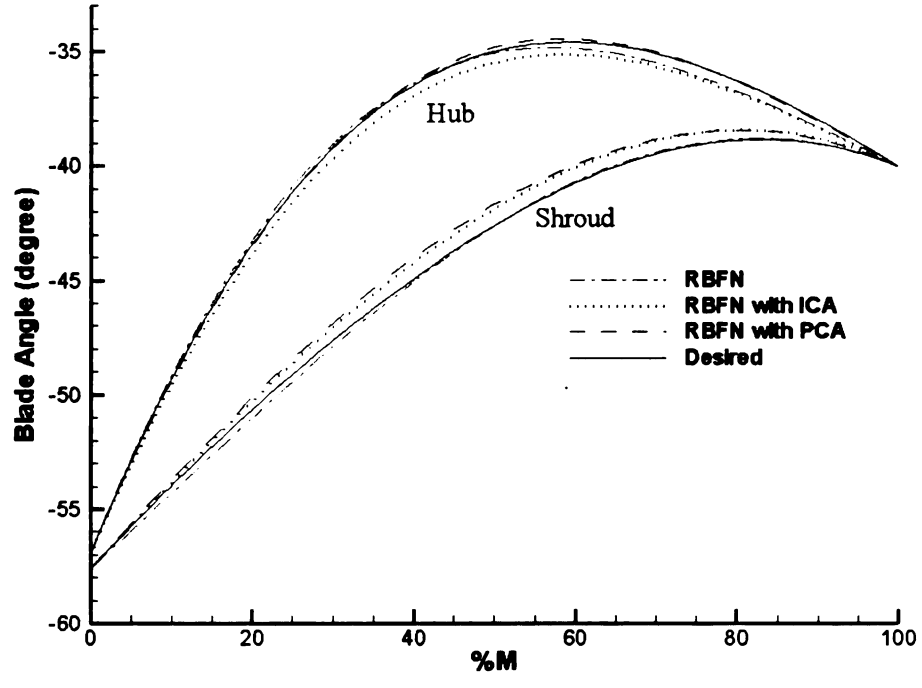

Figure 6-8 Comparison of optimal beta distributions calculated by employing RBFN, RBFN with PCA, RBFN with IC

In Figure 6-7 and Figure 6-8, optimal contour and blade angle distribution, also called beta distribution, are compared with desired ones, respectively. The optimization procedure, which employs RBFN with PCA, finds closer profiles on the second half part of impeller and beta distribution on hub. However, there is no guarantee that all geometry parameters can be found closer to the desired one because this optimization problem is 20 dimensions, which is also the number of geometry parameters. It is possible that the application of PCA can improve performances on some of dimensions while it may decrease those on other dimensions. This problem is also highly nonlinear and has many local optimums, which makes a group of geometry parameters provide a high value of objective function although these geometry parameters are not close to the desired ones. Figure 6-9 and Figure 6-10 show statistical results: AAE and MAE between optimal geometry parameters and desired ones. Units of geometry parameters are diverse, e.g. inch for contour, degree for blade angle and dimensionless for normalized meridional distance. Therefore, all geometry parameters are normalized to dimensionless quantity in the range (-1, 1).

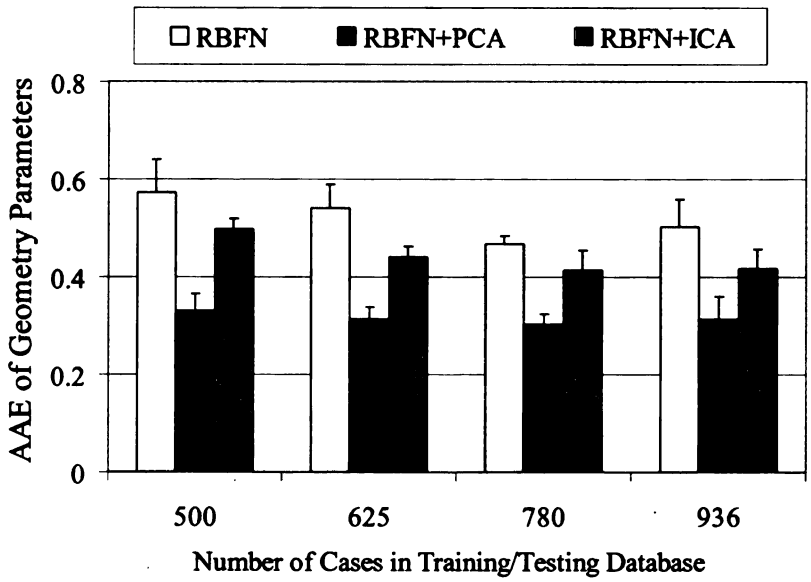

Figure 6-9 Average Absolute Error (AAE) between optimal geometry & desired ones

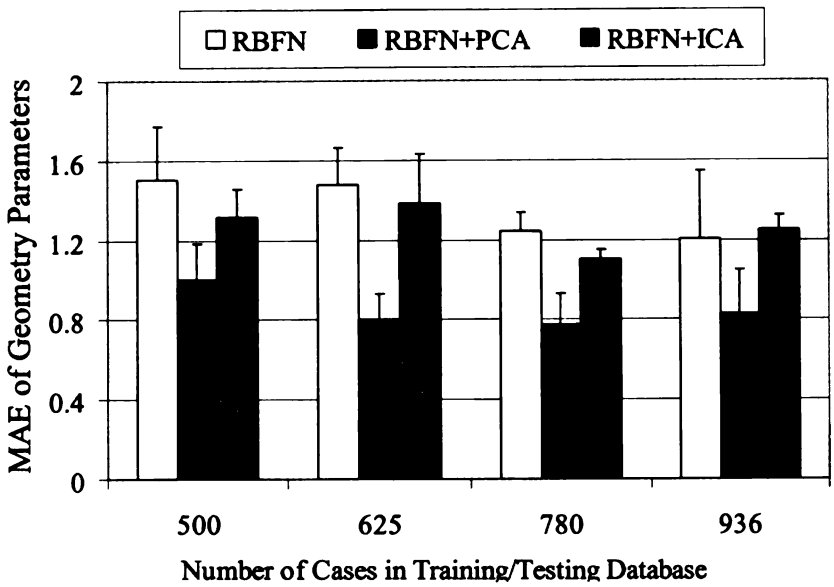

Figure 6-10 Maximum Absolute Error (MAE) between optimal geometry & desired one

The form of Figure 6-9 and Figure 6-10 is exactly the same as that of Figure 6-5 and Figure 6-6 because W points in Figure 6-4 are correlated to the geometry parameters in Figure 6-7 and Figure 6-8. Results of four different groups of databases in Figure 6-7 and Figure 6-8 suggest that the optimization procedure employing RBFN with PCA is able to find optimal geometry closer to the desired ones compared to other two ANNs in average; AAE and MAE between RBFN with ICA and RBFN can hardly be discriminated.

6.3.3 Sensitivity Analysis of GA Parameters

In addition to trained ANNs and initial populations, there are some other parameters, e.g. GA parameters which also influence optimums. Population size is set as 100, maximum generation number 100, crossover rate is 6 and mutation rate is 18 for all the above calculations shown above. Crossover rate represents the number of pairs of chromosomes for crossover while mutation rate means the number of chromosomes for mutation in each generation. In this section, one of these four GA parameters varies while three others remain the same to study the influences of the variation of

these parameters. The influences of population size, maximum generation number, crossover rate and mutation rate on whole optimization procedure are shown in Figure 6-11, Figure 6-12, Figure 6-13 and Figure 6-14 respectively.

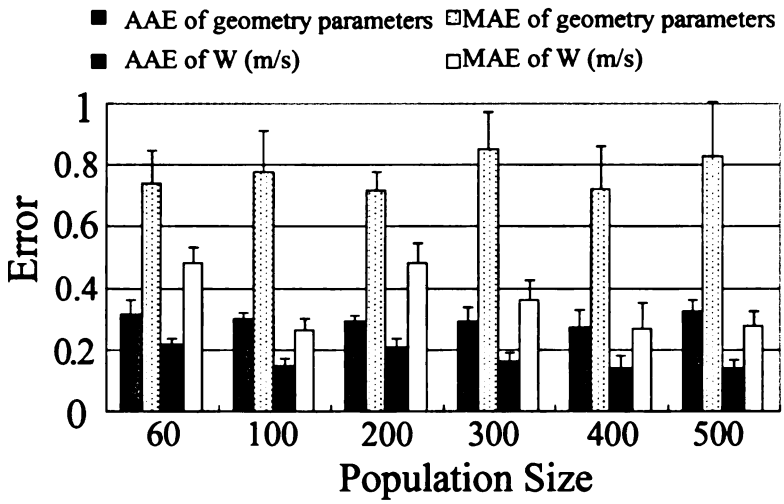

Figure 6-11 Influence of population size

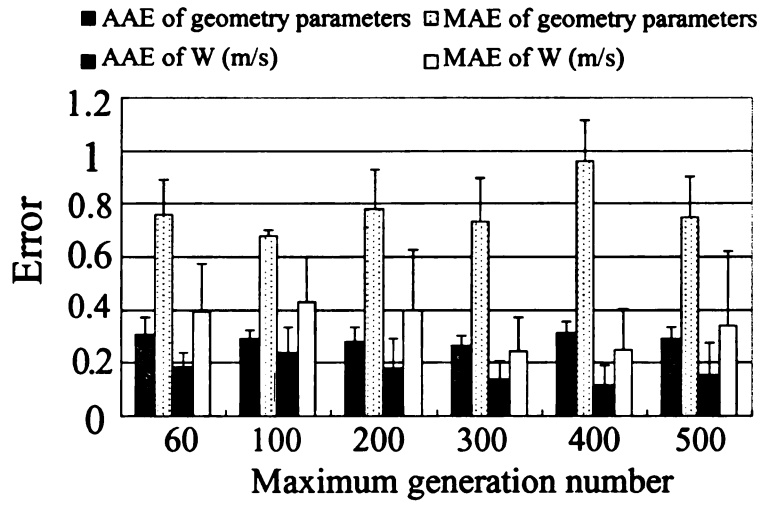

Figure 6-12 Influence of maximum generation number

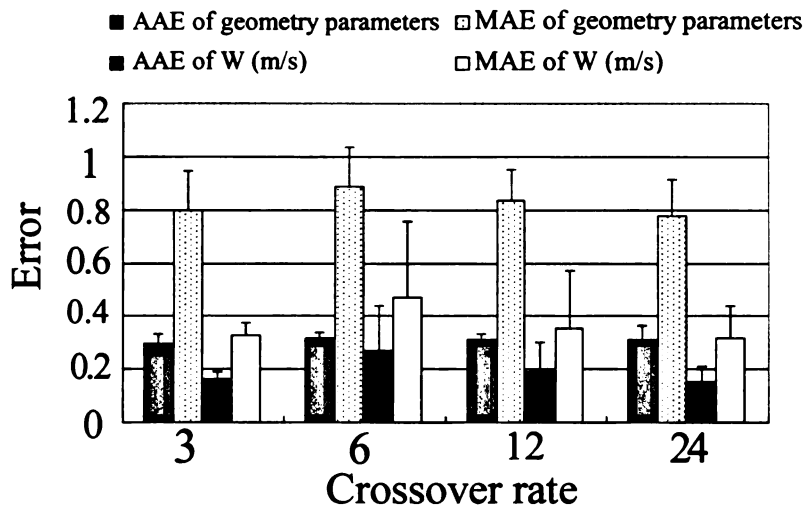

Figure 6-13 Influence of crossover rate

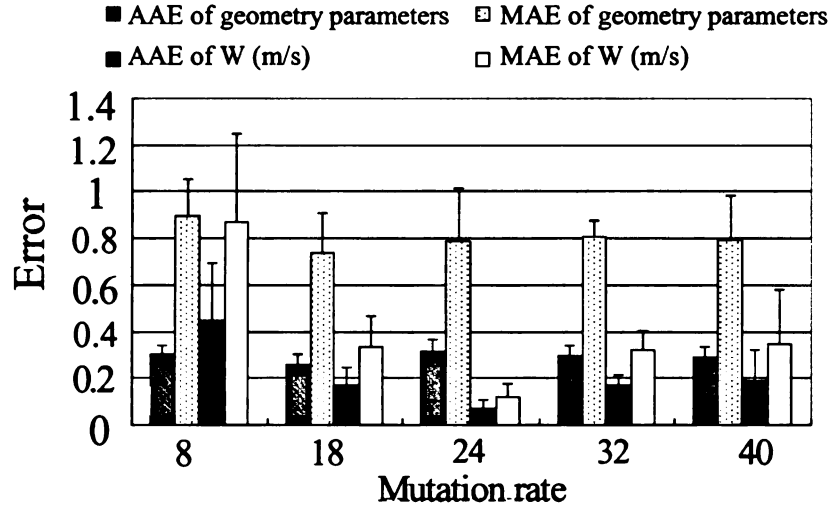

Figure 6-14 Influence of mutation rate

For each parameter, changes of AAE and MAE between desired W points and optimal W points as well as AAE and MAE between desired geometry parameters and optimal geometry parameters are compared. AAE between optimal W points and desired W points is considered as the most important factor because its value is directly related to that of objective function here. In Figure 6-11, Figure 6-12, Figure 6-13, the results show the possibility of finding a better optimum, which is represented by a lower value of AAE between optimal W points and desired W points, is increased as the value of population size, maximum generation number or crossover rate increase.

However, the results in Figure 6-14 show that the mutation rate at 24 provides better performance on finding optimum for this optimization problem compared with higher values.

6.4 Conclusions

ANN, a nonlinear statistical data modeling tools, is widely used to create a performance map to substitute the direct application of flow solvers during optimization procedure, especially the application of GA. Because the ANN is used to create an approximate map, the accuracy of the trained ANN is of critical importance and greatly influences its applications and final optimal results.

PCA and ICA are also applied to transformed training database and make RBFN trained in a new coordinate system. The accuracies of these three trained ANNs: RBFN, RBFN with PCA, RBFN with ICA have been compared. Then these different ANNs are used in the optimization procedure. The influences of PCA or ICA on total performances of optimization procedure are also studied by comparing the performances of optimization procedures employing different ANNs. Also, the influences of other GA parameters on the performances of centrifugal compressor optimization procedure have also been studied.

These results suggest that PCA can significantly decrease evaluation error and improve the accuracy of trained RBFN with slightly increased computational time. Using RBFN with PCA in the optimization procedure can increase total performance and help find better optimum without increasing computational time. ICA can slightly improve the accuracy of the trained ANN while no subsequent benefits on the total optimization procedure. Large number of population size, maximum generation number and crossover rate as well as mutation rate at 24 result in a better optimum based on statistical results.

CHAPTER 7

ONLINE IMPELLERS OPTIMIZATION PROCEDURE

7.1 Introduction

In last chapter, Principle Component Analysis (PCA) is applied to improve the performance of existed centrifugal compressor impeller optimization procedure. Many papers on this optimization problem have been published and different optimization procedures have been proposed. A flow solver is directly used as performance evaluation tool in optimization method, which is called as an online flow solver optimization here. If the flow solver is only used to create a performance map in the optimization procedure, then this optimization procedure is called as offline flow solver optimization procedure in this study. This is because the flow solver in this optimization procedure is not directly used for evaluating geometry in the optimization method. In order to evaluate the performances of online flow solver optimization procedure, firstly, the optimal results calculated by optimization procedure using online flow solver and Genetic algorithm (GA) are compared to those calculated by offline flow solver optimization procedure with the same GA parameter setting. These comparisons both on performances and geometry are used to estimate the influences of different applications of the flow solver. Furthermore, the influences of GA parameters and local research algorithm combined with GA on the performance of online flow solver optimization procedure are also investigated.

7.2 Optimization Procedure

Comparison of flowcharts between online flow solver optimization procedure and offline flow solver optimization procedure is as shown in Figure 7-1 and Figure 7-2.

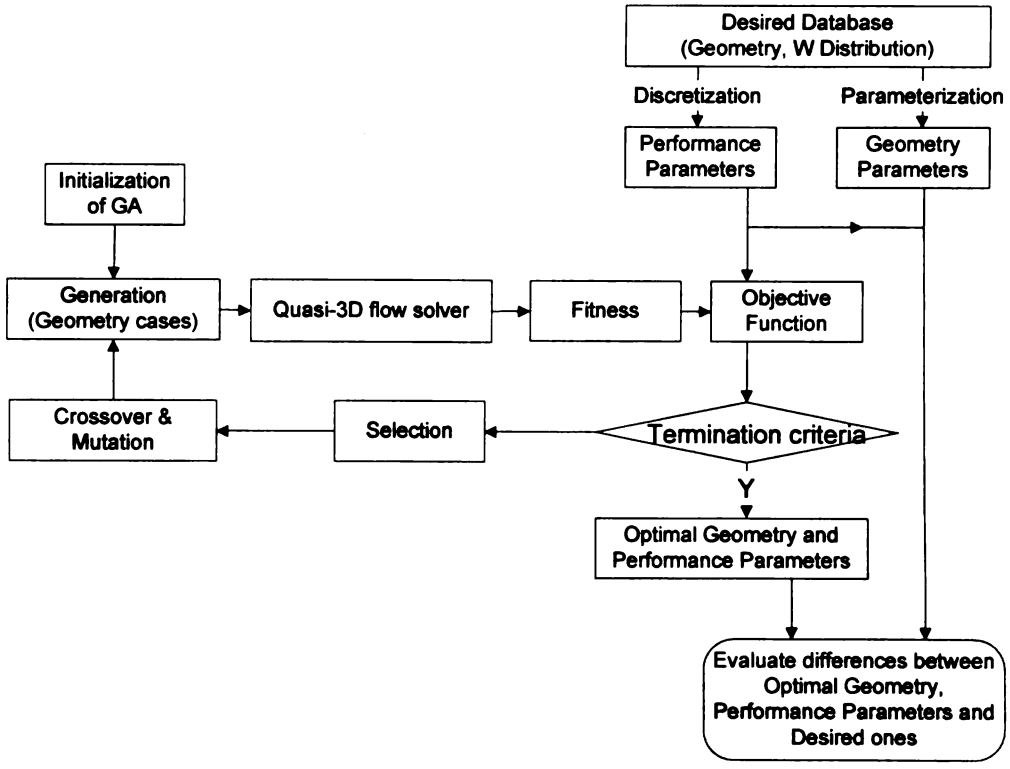

Figure 7-1 Online flow solver optimization procedure

In online flow solver optimization procedure (Figure 7-1), GA parameters are firstly set in the initialization. A group of geometry cases are generated randomly and represented by the first generation of individuals in GA. Each individual consists of twenty chromosomes, which indicate twenty geometry parameters of each geometry case. Mathematically, each individual is a vector and each chromosome is a float number. This generation of individuals, or this group of geometry cases is input into quasi-three dimensional (3D) flow solver MERIDL and TSONIC, and their corresponding performances, especially relative velocity distributions are calculated. Nine W points are discretized from each relative velocity distribution. RMSE between these nine W points and desired ones, which is the objective function and also called the fitness in GA, is calculated. If the global optimum is found or maximum generation reaches, which are termination criteria in this study, then this generational process and the total procedure stops. Otherwise, selection operator is applied to the

first generation of individuals. Two different selection operators: tournament selection[44] and Stochastic Universal Sampling (SUS)[45] are applied respectively and comparison results are shown in next section. Tournament selection is a selection operator in which a few individuals are chosen randomly from current generation and the winner with best fitness among these individuals is selected. In SUS, all the individuals are arranged in a order of fitness from high to low, and then are mapped to contiguous segments of a line, such that each individual's segment on the line decrease exponentially and represents probability of being selected. Followed by selection step, these selected individuals are used to generate new individuals for next generation via genetic operators: crossover and mutation. In the crossover step, three different crossover operators are applied in sequence: arithmetic crossover, heuristic crossover and two points crossover operators[46, 47]. In the mutation step, four different mutation operators: boundary mutation, multi-nonuniform mutation, nonuniform Mutation, Uniform Mutation are used in sequence [46, 47] in this study. After new generation of individuals are created, quasi-3D flow solvers are used again to calculate their performances and their corresponding finesses. Genetic algorithm continues until termination criteria mentioned above reach.

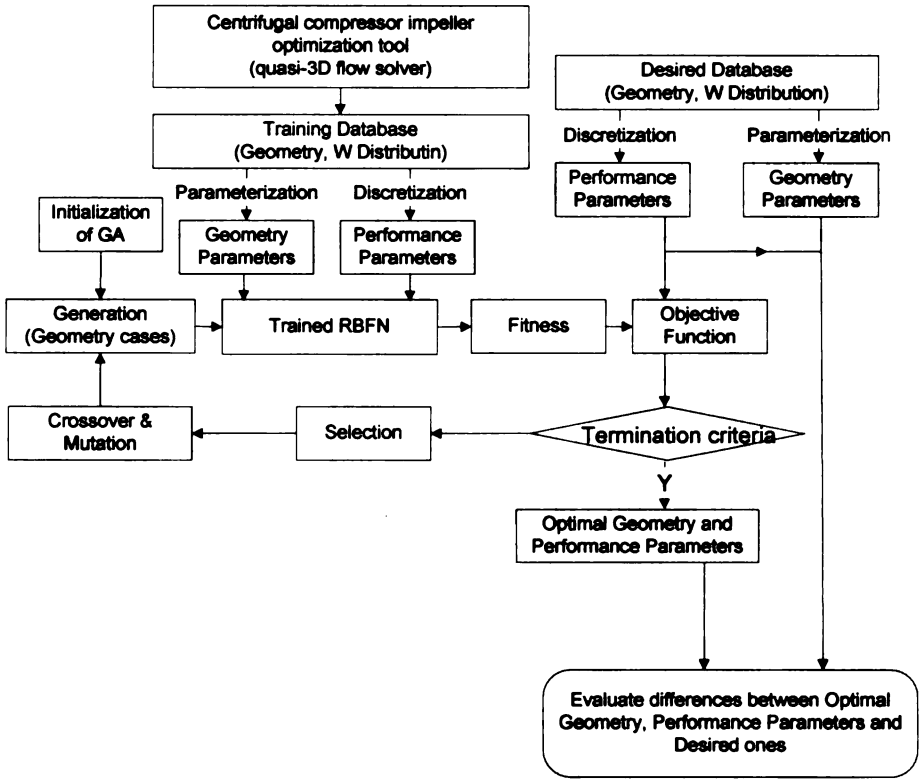

Figure 7-2 Offline flow solver optimization procedure

The offline flow solver optimization procedure is very similar to the online flow solver optimization procedure with the exception of evaluation tool for impeller performance, which is shown in Figure 7-2. A group of geometry cases are generated and their corresponding performances, especially relative velocity distributions, are calculated by the quasi-3D flow solver MERIDL and TSONIC. Geometry parameters are parameterized from their contours and blade angle distributions. Performance parameters W points are discretized from their relative velocity distributions. Both geometry parameters and performance parameters are used as input and output layers respectively to train Artificial Neural Network (ANN) in this procedure. Actually, the most widely used Artificial Neural Networks (ANNs) include: Radial Basis Function Network (RBFN) and Feed-forward Neural Network (FFNN). Both FFNN and RBFN, two types of ANNs are used to create performance maps for centrifugal compressor impellers in this work. It is found that the accuracy of FFNN is similar to that of

RBFN. However, FFNN provides higher robustness while RBFN provides much lower computational time. The average training time of FFNN varies from 1 to 2 hours depending on its specific structure while that of RBFN takes only 3 to 15 minutes. In this study, a large number of cases are provided to train neural network because of applications of fast quasi-3D flow solvers, which helps to make the trained RBFN more robust and overcome drawbacks of RBFN to some extent. Therefore RBFN is chosen as mapping tool in offline solver flow optimization procedure. The performance map is trained by RBFN and used to calculate W points and evaluate fitnesses of individuals in GA.

7.3 Flow Solver

Flow solvers are used to calculate impeller performance based on its geometry and can be generally categorized into three groups: flow solvers using Navier-Stokes equations, e.g. Fluent[48], EURANUS/TURBO[21], TRAF code[17] and CFX-Tascflow[16], those using two-dimensional Euler equations without considering viscosity[49], and those with streamline curvature throughflow method[13, 50, 51], e.g. MERIDL[14] and TSONIC[12]. Flow solvers using Navier-Strokes equations are the most accurate but very time consuming while those using streamline curvature methods are most efficient. As mentioned above, flow solvers are directly used in online flow solver optimization procedure to evaluate impeller performances. Obviously, three dimensional flow solvers using Naiver-Strokes equations are not feasible due to its high computational time and high times of its application in optimization procedure. Hence MERIDL and TSONIC using streamline curvature method are used in optimization procedure here, which is the same as flow solvers used in references [28] and [18]. MERIDL is used to calculate the flow conditions in meridional plane while TSONIC in blade-to-blade plane. In the original codes of

MERIDL and TSONIC, arbitrary quasi-orthogonals are used for meshing. However, it is found that there are some waves in the results, which are caused by numerical errors due to the application of the arbitrary quasi-orthogonals. Therefore, uniform quasi-orthogonals are used to substitute of arbitrary quasi-orthogonals for meshingn, which has been mentioned in Chapter 5. New relative velocity distribution calculated based on uniform-orthogonals is very close to the original one based on arbitrary-orthogonals but most of waves of original results are eliminated.

7.4 Results and Discussion

7.4.1 Comparison of Online and Offline Flow Solver Optimization procedures

In the application of the optimization procedure, desired geometry is unknown. The desired W points or desired W distribution are given directly by designers and optimal geometry can be found eventually. Optimal W points, which are calculated based on the optimal geometry, can be compared with desired ones.

Table 7-1 Running Conditions and Gas Properties

Mass flow rate	37 (kg/s)
Rotating speed	1685.15 (rad/s)
Inlet Total Temperature	287.78 (K)
Inlet Total Pressure	3447378.65 (Pa)
Blade Number	17
Specific Heat Capacity Cp	1969.53 (J/kg.K)
Specific Heat Capacity Cv	1515.01 (J/kg.K)
Viscosity	1.006×10^{-5} (kg/m.s)

However, in order to better evaluate the performance of online flow solver optimization procedure, both the desired geometry and its corresponding relative velocity (W) distribution are given in this study. Hence both optimal W points and optimal geometry parameters can be compared with desired ones. The running

conditions of centrifugal compressor and gas property are given in Table 7-1. Optimal contour, blade angle distribution and relative velocity distribution calculated by online flow optimization procedure are compared with optimal ones by offline flow solver optimization procedures in Figure 7-3, Figure 7-4 and Figure 7-5.

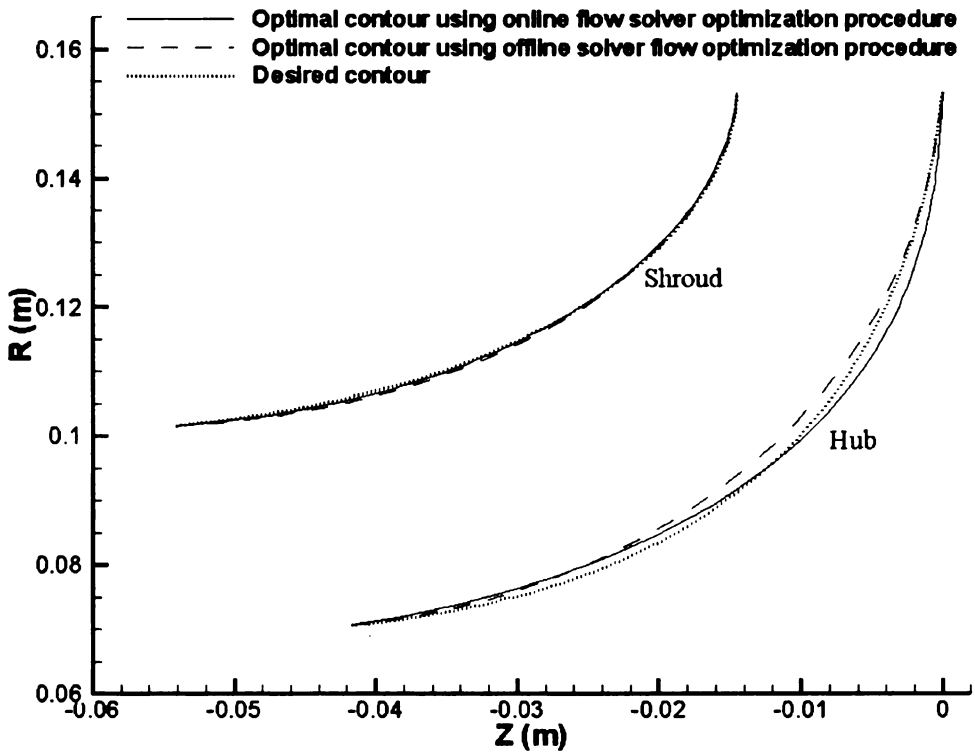

Figure 7-3 Comparison of optima contour calculated using online flow solver and offline flow solver optimization procedure

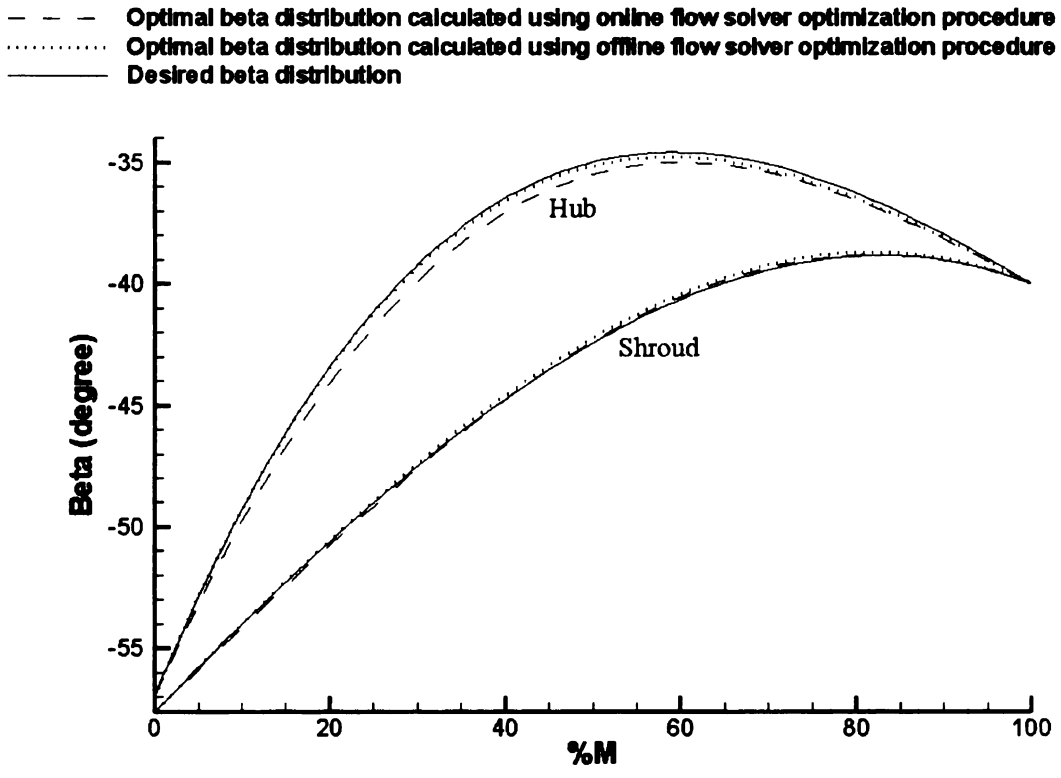

Figure 7-4 Comparison of Blade angle distribution calculated using online flow solver and offline flow solver optimization procedure

Typically 100 generations containing 50 individuals are used in GA. Average computational time of online flow solver optimization procedure is 1400s while that of flow solver flow varies from 800 to 2000s, which depends on the number of cases in the training database and the specific structure of RBFN. Results in Figure 7-3 show that there are no significant differences between two optimal shroud profiles and both to them match desire shroud profiles very well. Also, there are no significant differences between these two optimal shroud profiles and desired shroud profile. However, the optimal hub profile calculated by online flow solver optimization procedure is closer to the desired one compared with that by offline flow solver optimization procedure.

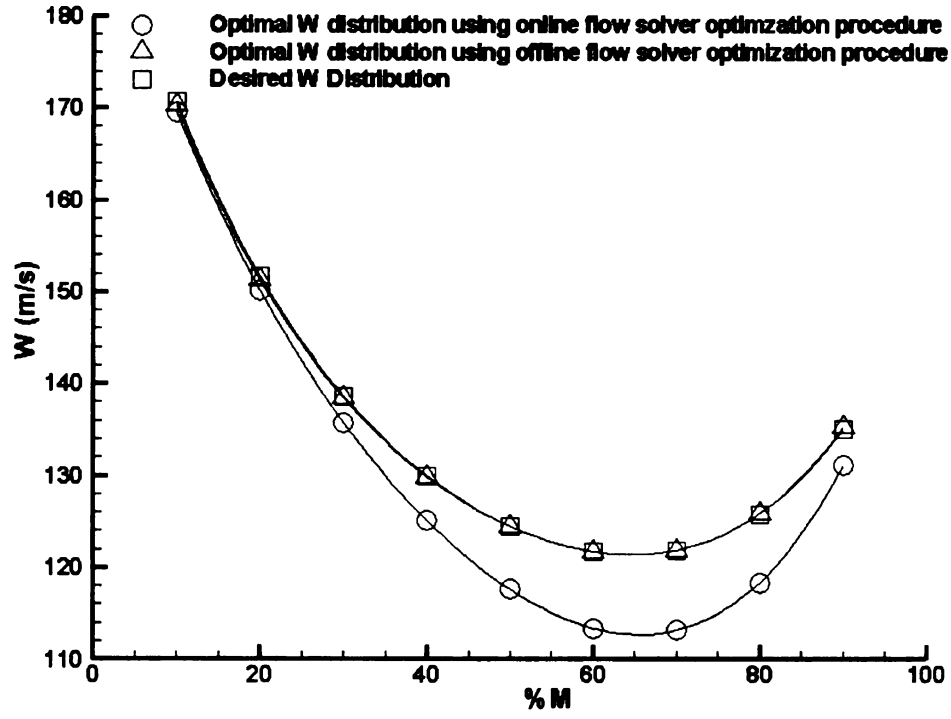

Figure 7-5 Comparison of relative velocity distribution (W) calculated using online flow solver and offline flow solver optimization procedure

Results in Figure 5-3 show the similar phenomena as those in Figure 7-4. Optimal blade angle distributions on shroud calculated by these two optimization procedures are very similar while optimal blade angle distribution on hub calculated using online flow solver optimization procedure is closer to desired one. In Figure 7-5, differences between desired relative velocity distribution and optimal one calculated by online flow solver optimization procedure are much smaller. Due to the effects of random factors in GA, e.g. randomly generated initial individuals, this centrifugal compressor impeller optimization problem is calculated for five times using online and offline flow solver optimization procedures respectively. Five converge histories of online flow solver and offline flow solver optimization procedures are shown in Figure 7-6 and Figure 7-7. It can be seen the significant differences among five converge histories due to the influences of random factors in optimization method (Genetic Algorithm and local research algorithm). It should be reminded that the best fitness is

calculated by flow solvers in online flow solver optimization procedure while that calculated by approximate performance map in offline flow solver optimization procedure. Statistical results of these five optimal solutions are represented in the form of mean±SD (Standard Derivative) shown in Figure 7-8. These results are reevaluated using MERIDL and TSONIC eventually. It can be seen that mean value of root mean square error (RMSE) between optimal W points and desired ones using online flow solver optimization procedure is only 50% of that using offline flow solver optimization procedure. As for RMSE between optimal geometry parameters and desired ones, there are no significant differences. RMSE between optimal W points and desired ones is much more important than RMSE between optimal geometry parameters and desired ones in evaluating performance of optimization procedure because RMSE between optimal W points and desired ones is the definition of fitness in GA and smaller RSME reveal that the better solution is found by optimization procedure. However, optimal geometry parameters closer to desired ones do not guarantee a better fitness because this optimization problem is high nonlinear and there are many local optima.

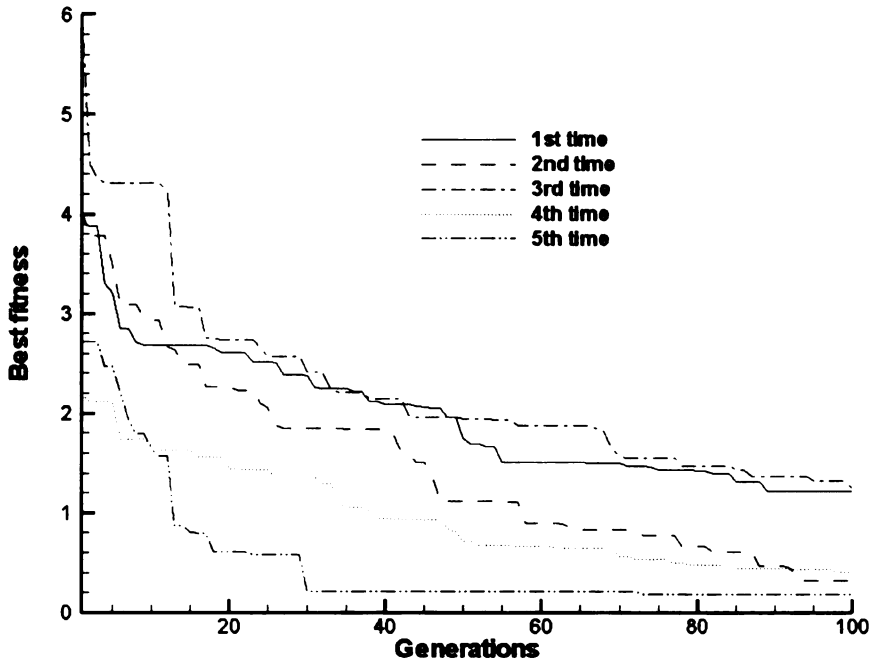

Figure 7-6 Converge history of online flow solver optimization procedure

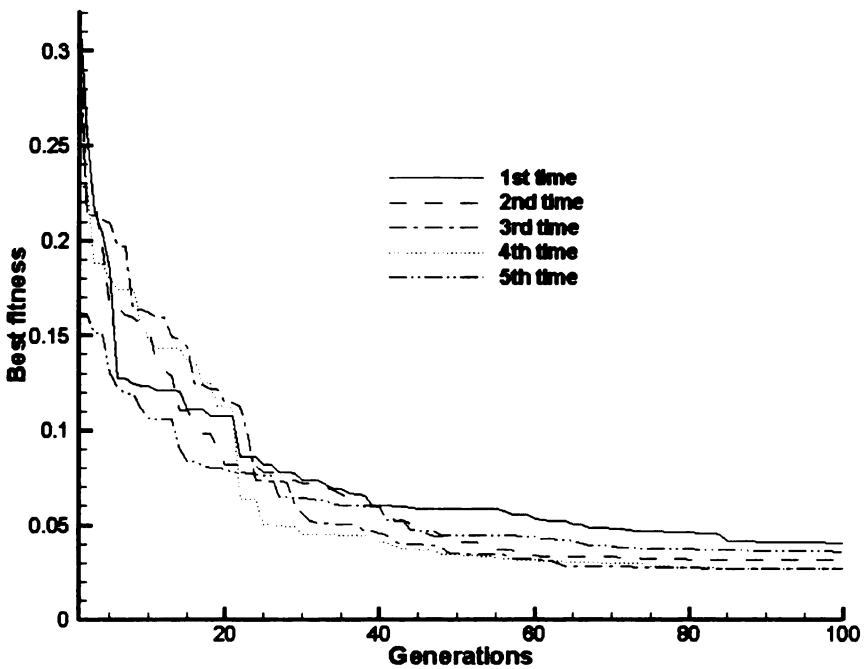

Figure 7-7 Converge history of offline flow solver optimization procedure

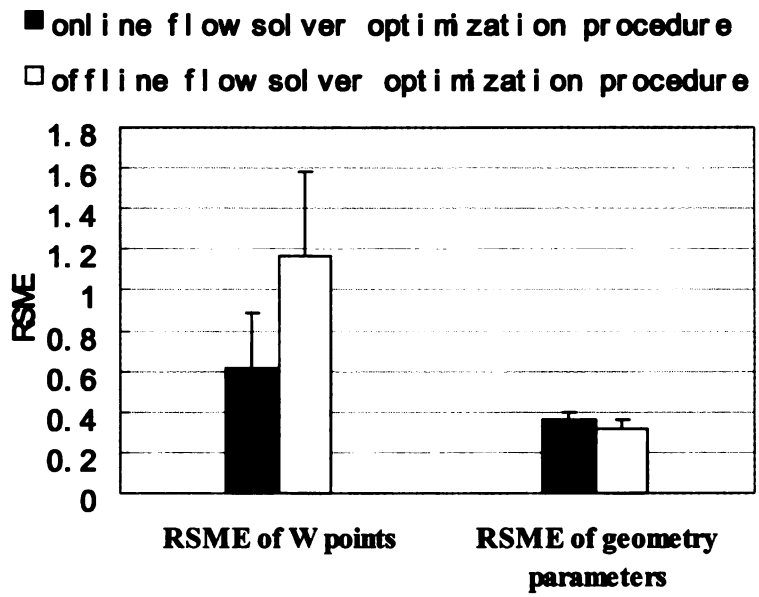

Figure 7-8 Comparison of statistical results on optima calculated between using online flow solver optimization procedure and using offline flow solver optimization procedure

Although the values in objective function (RSME of relative velocity points) is less than 0.1 m/s (Figure 7-8), these values are calculated based on approximate performance map. RMSE of relative velocity points using flow solver is about 1.17 m/s (Figure 7-8). This is proved that errors of approximate performance map play an important factor on the optimal results: these errors can diminish the effects of high fidelity flow solvers. Resolution of optimization method is less than 0.1 m/s while the average errors of approximate performance map, however, is larger than 1 m/s. Therefore, the increase on modeling is much more important than searching a better and more effective optimization method. This is the reason why online flow solver method is employed in this study. All results from Figure 5-3 to Figure 7-8 suggest the better performance of online flow solver optimization procedure compared to offline flow solver optimization procedure.

7.4.2 Influences of Optimization Method

Influences of GA parameters, GA operators and local research algorithm on the optimization procedure performances are studied and results are shown in Figure 7-9 to Figure 7-15.

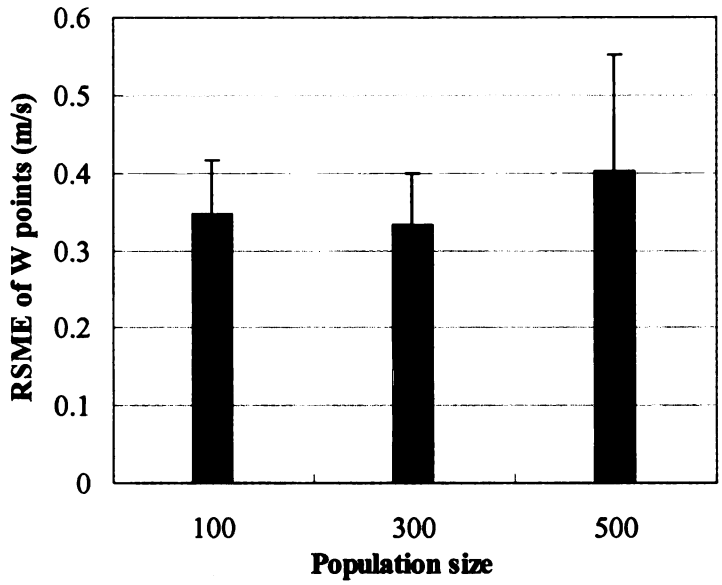

Figure 7-9 Influences of population size in GA

Centrifugal impeller online flow solver optimization procedure runs five times under each set of parameters due to the influences of random factors. Mean and standard derivatives (SD) of these five objective function values, which are RMSE between optimal W points and desired ones, are calculated. No relationships between population size and optimization performance can be concluded from results in Figure 7-9. Results in Figure 7-10 suggest that possibility of finding a better optimum represented by a lower objective function value increase as maximum generation increases. However, computational time also linearly increase with maximum generation shown in Table 7-2.

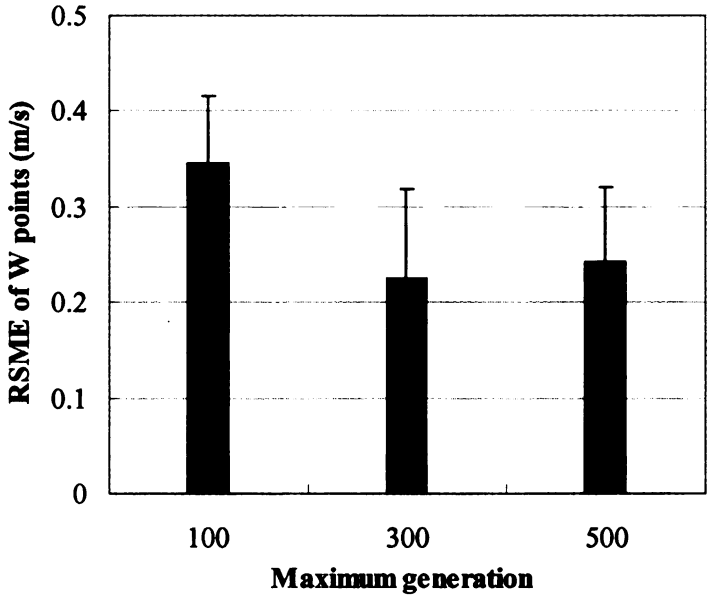

Figure 7-10 Influences of maximum generation in GA

Table 7-2 Computational time with different GA parameters

Population size	3	6	9
Average computational time (s)	1342	1437	1533
Maximum generation	8	18	26
Average computational time (s)	1342	3910	6475
Crossover rate	3	6	9
Average computational time (s)	1114	1342	1574
Mutation rate	8	18	26
Average computational time (s)	957	1342	1714
Using Local search algorithm	Yes	No	
Average computational time (s)	1431	1342	
Selection operators	Tournament	SUS	
Average computational time (s)	1331	1342	

Crossover rate (Figure 7-11) presents the number of pairs used for crossover and

generating new individuals in each generation. Statistical results reveal that crossover rate at 6 leads to better found optimum compared to other values.

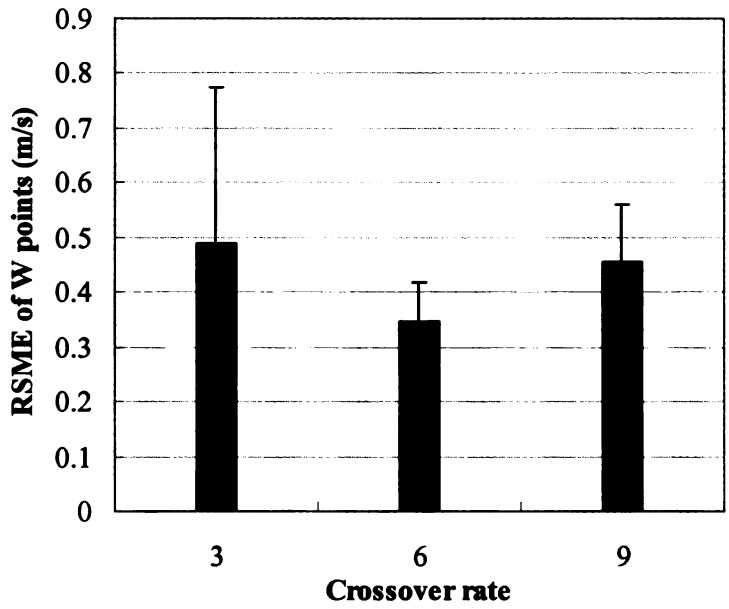

Figure 7-11 Influences of crossover rate in GA

In Figure 7-12, mutation rate indicated by X coordinate denotes the number of individuals used for mutation in GA in each generation. Results reveal that mean value of RMSE of W points decrease gradually as mutation rate increases. However, computational time of whole optimization procedure almost become double when mutation rate increases from 10 to 26 shown in Table 2.

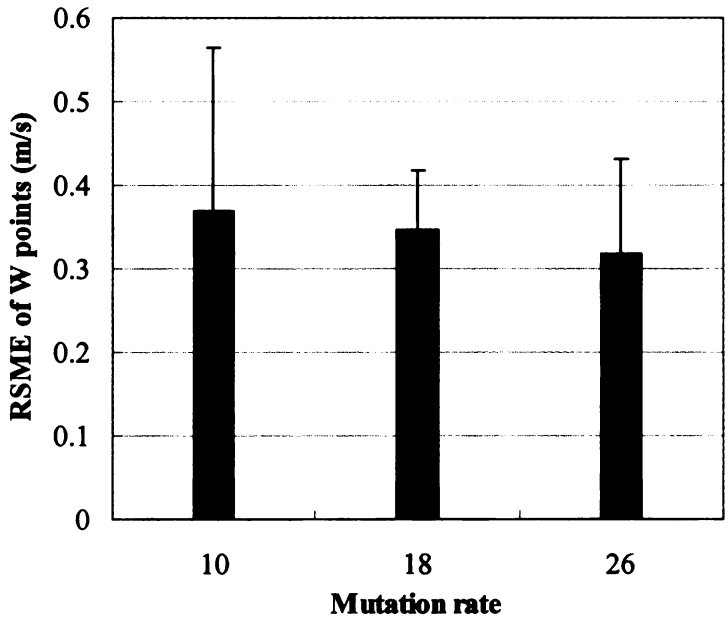

Figure 7-12 Influences of mutation rate in GA

Optima calculated using only GA as optimization method and those using combined GA and local search algorithm are compared in Figure 7-13. The mean of RMSE of W points greatly decreases approximately 40% by using local search algorithm. The use of local research algorithm averagely increases the computational time from 1342 to 1431 seconds, approximately 6.5%. Results in Figure 7-13 and comparison of computation time in Table 2 suggest that with slight increase in computational time.

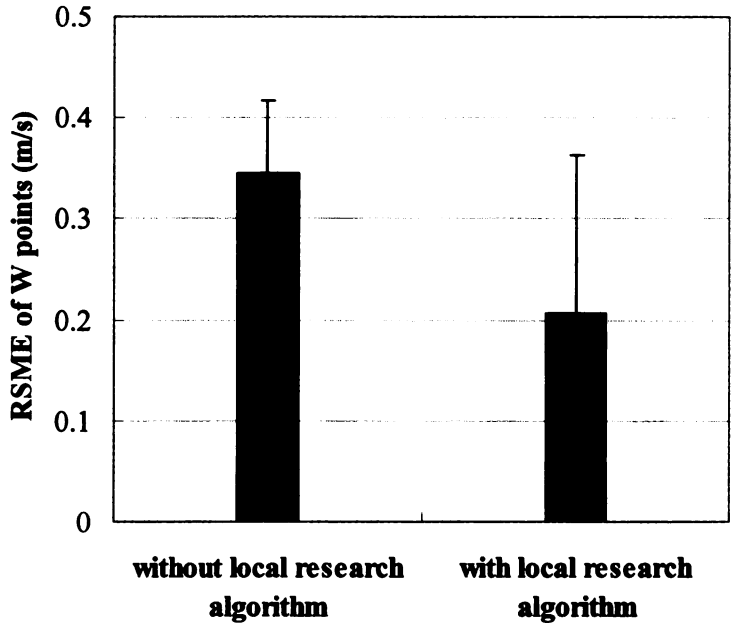

Figure 7-13 Comparison of optima with and without using local search algorithm

The performance of two selection operators: Tournament selection and stochastic universal sampling (SUS) are compared and results (Figure 7-14) indicate SUS has better performance than Tournament selection on this centrifugal impeller optimization problem.

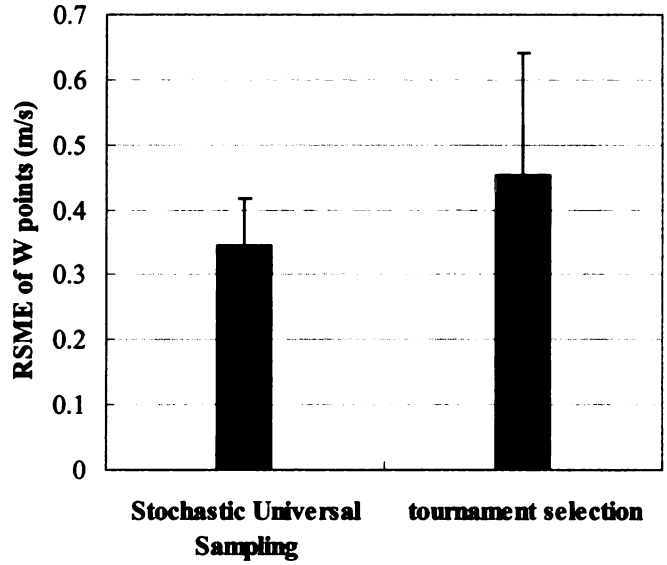

Figure 7-14 Comparison of two selection operators: Stochastic Universal Sampling (SUS) and Tournament selection in GA

During the reproduction step, seven reproduction operators (three crossover operators and four mutation operators) are used in sequence. In order to evaluate the performance of each operator, effective times and effective ratio of each reproduction operator are shown (Figure 7-15). The definition of effective ratio of each operator is the ratio between its effective times and sum of all effective times of these seven operators. Therefore, effective times and effective ratio are in accordance with each other. Statistical results in Figure 7-15 is based on the 55 times of impeller optimizations. The average crossover rate is 2 while average mutation crossover rate is 4. However, each crossover operator can generate two individuals while one for mutation operator. Therefore, each operator generates the same amount of new individuals in these 55 times of optimizations totally. Theoretically, the higher effective times or ratio an operator obtains, the better performance the operator has. Results (Figure 7-15) show that the mutation operator averagely works better for this centrifugal compressor impeller optimization problem. Nonuniform mutation seems the most effective mutation operator while arithmetic crossover has best performance among these three crossover operators.

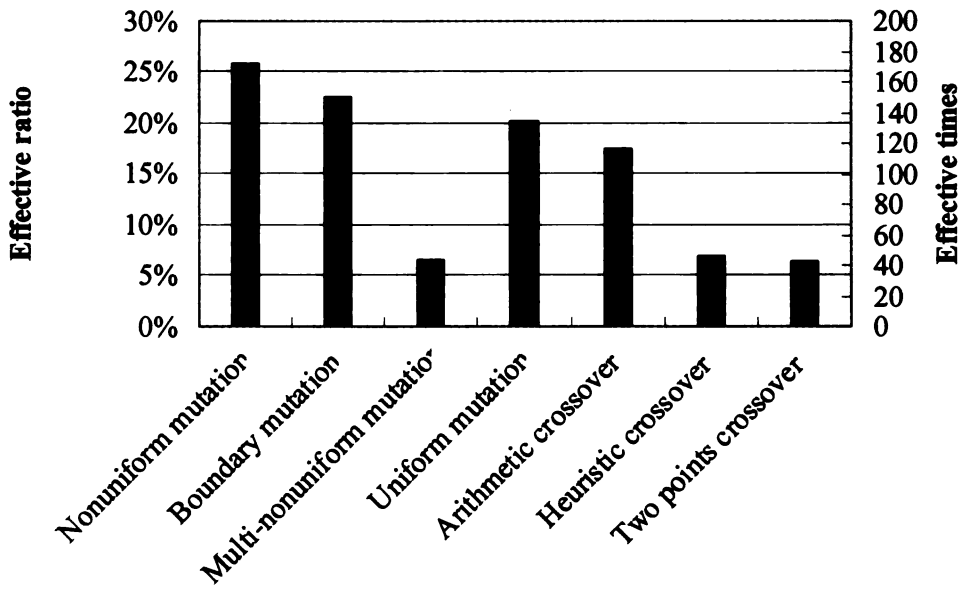

Figure 7-15 Comparison of performances of reproduction operators

7.5 Conclusion

In this chapter, the online flow solver optimization procedure method are presented and optimal parameters of optimization method are analyzed in order to diminish the influences of the errors of created performance maps and improve the performance of centrifugal compressor impeller optimization procedure. Quasi-three dimensional flow solvers MERIDL and TSONIC, which use streamline curvature method and have low computational time, are directly used to evaluate impeller performance in Genetic Algorithm (GA). This is called as online flow solver optimization procedure here. Optima calculated by online flow solver optimization procedure are compared with those by offline flow solver optimization procedure under same GA parameters. In offline flow solver optimization procedure, same flow solvers are only used to calculate impeller performances in the training database, which are then used to create a performance map. This performance map is used to evaluate impeller performances in GA and substitute the direct application of the flow solvers. Statistical results of

RSME between optimal relative velocity (W) points and desired ones, which is the definition of objective function, reveal that online flow solver optimization procedure can find better the impeller geometry with closer relative velocity distribution to desired one comparing to offline flow solver optimization procedure.

Influences of optimization method on the performances of optimization procedure are also evaluated. Results suggests that increases of mutation rate and maximum generation in Genetic Algorithm can result in the higher possibilities of finding a better solution besides the use of online flow solver. However, the increases of these two parameters greatly increase the computational time. The alternative method is to increase the mutation rate and decrease crossover rate simultaneously, especially the increase of the mutation rate on uniform mutation and the decrease of the crossover rates on two points crossover and heuristic crossover. Moreover, the use of local search algorithm combined with GA as optimization method seems the most effective way to increase optimization procedure performance with only slight increase on computational time.

CHAPTER 8

APPLICATION OF IMPELLER OPTIMIZATION PROCEDURES

8.1 Optimization Conditions

In this chapter, the different types of developed centrifugal compressor impeller optimization procedures, which are introduced in Chapter 5, 6 and 7 respectively, are applied on an industrial gas centrifugal compressor impeller made by Solar Turbine Inc, Caterpillar Company. The running condition and gas properties for this compressor have been introduced in the preliminary design parameters are listed in Table 8-1.

Table 8-1 Parameters of preliminary design

R_{1S} (inch)	4	R_{1H} (inch)	2.78
Z_{1S} (inch)	-2.13	Z_{1H} (inch)	-1.64
R_{2S} (inch)	6.04	R_{2H} (inch)	6.04
Z_{2S} (inch)	-0.57	Z_{2H} (inch)	0
β_{1S} (deg)	-57.62	β_{1H} (deg)	-57
β_{2S} (deg)	-40	β_{2H} (deg)	-40
Z	17		

There are no vanes in the inlet casing and diffuser. The contour profiles of the inlet casing and diffuser as shown in Figure 8-1.

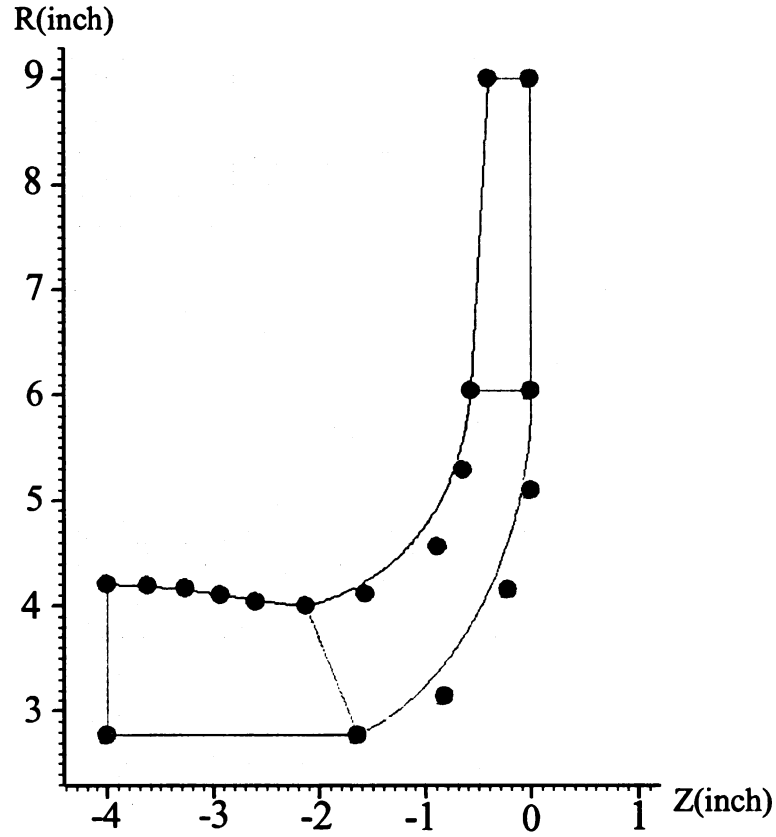

Figure 8-1 Illustration of inlet casing and diffuser contours

The desired relative velocity distribution is given and shown in Figure 8-2.

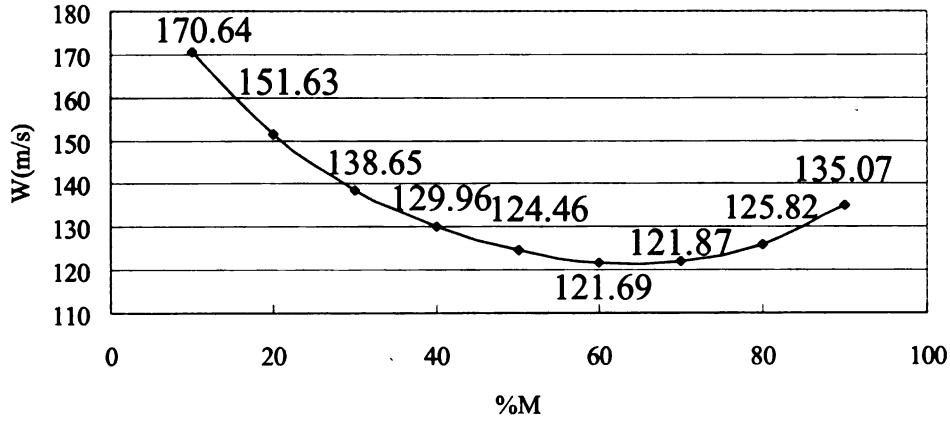

Figure 8-2 Illustration of desired relative velocity distribution

8.2 Optimization Using Impeller Optimization Procedures

Five different types of centrifugal compressor impeller optimization procedures are applied here and represented by RBFN+GA, FFNN+GA, RBFN+PCA+GA, RBFN+ICA+GA, and Online+GA. The similarities of these five optimization procedures are introduced as following:

1) The parameterizations of impeller geometries are same. Twelve parameters are chosen from contour between leading and trailing edge while eight from blade angle distribution for each case.

2) The discretizations of relative velocity distributions are the same. The definitions of objective functions are same and based on the RMSE between the calculated relative velocity points and desired ones.

3) The flow solvers: Quasi-3D codes MERIDL and TSONIC, used in these five optimization procedures are same and meshing methods in flow solver are under same setting. The flow solvers are used to evaluate the compressor performance and also create the training and testing database.

4) The Genetic Algorithms used in these optimization procedures are same, which means the selection, crossover, and mutation operators and parameters in GA are same.

5) The training database and testing database for RBFN+GA, FFNN+GA, RBFN+PCA+GA and RBFN+ICA+GA are same though the cases in these databases are generated randomly.

The differences between these five optimization procedures are mainly focus on the application of performance map and the optimization methods:

1) RBFN+GA employ the Radial Basis Function Network (RBFN) to train the performance map

2) FFNN+GA use the feed-forward Neural Network (FFNN) to train the performance map

3) RBFN+ICA+GA use Independent Component Analysis (ICA) to transfer the training database into the new coordinate system, in which the coordinates are independent from each other, and make the training finished in this new coordinate system.

4) RBFN+PCA+GA use Principle Component Analysis (PCA) to transfer the training database into the new coordinate system, in which the maximum variances of data are projected in the coordinates and make the training done in this new coordinate system.

5) Online+GA directly uses the flow solvers instead of performance maps to evaluate the compressor performance.

The optimal impeller geometries (contours and blade angle distributions) found by these five types of optimization procedures are shown and compared with desired ones in Figure 8-4 and Figure 8-5. The corresponding optimal relative velocity distributions are shown and compared with desired one in Figure 8-3.

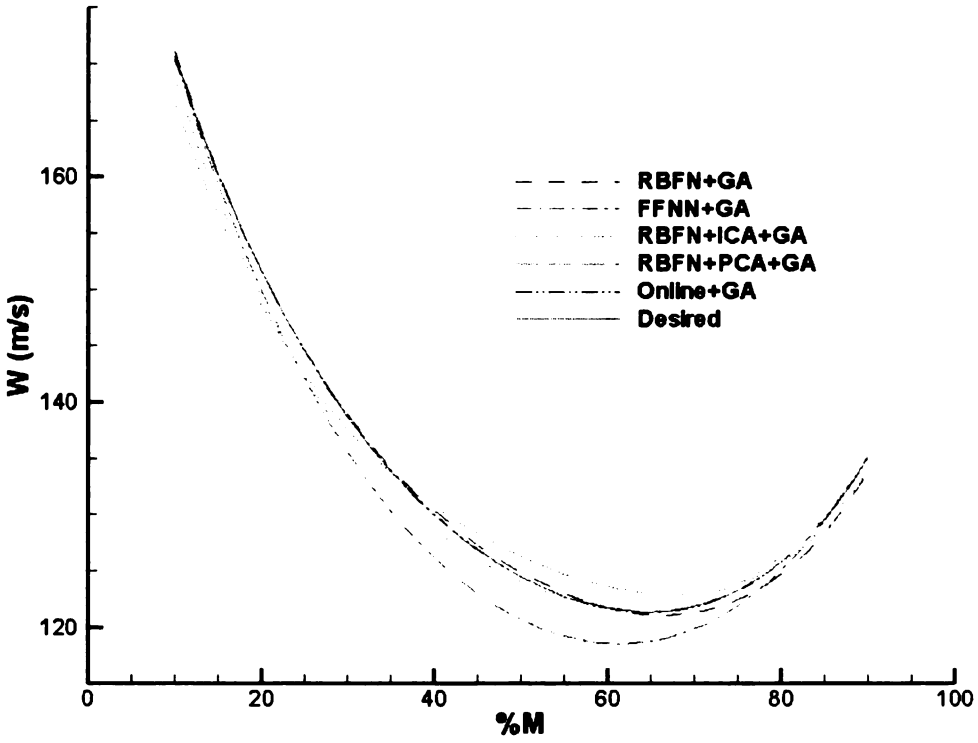

Figure 8-3 Comparison of optimal relative velocity distributions

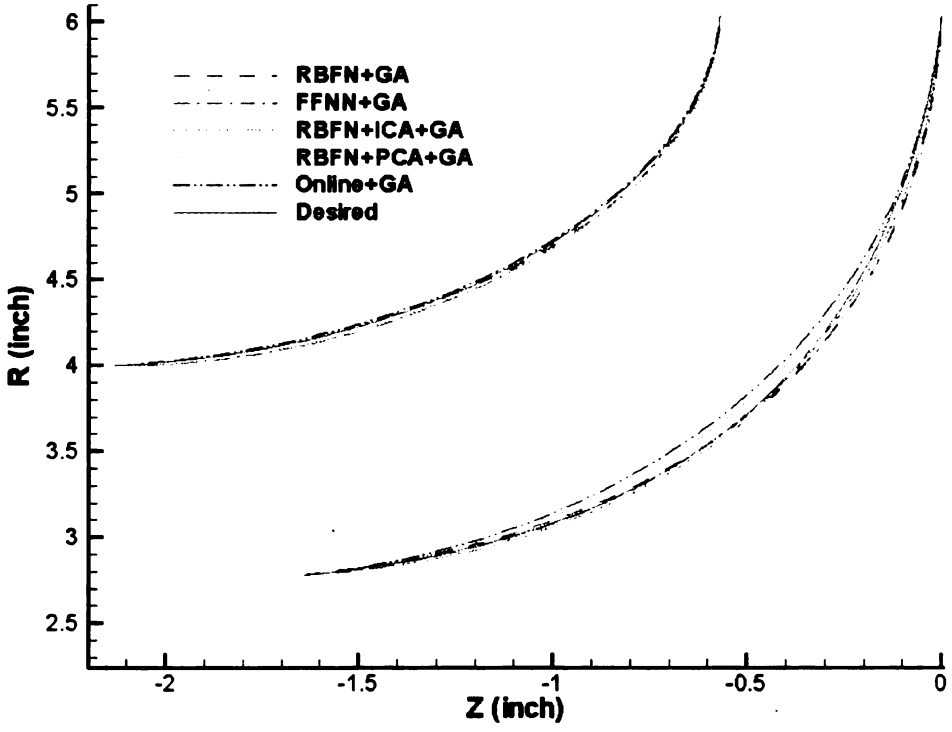

Figure 8-4 Comparison of optimal contours

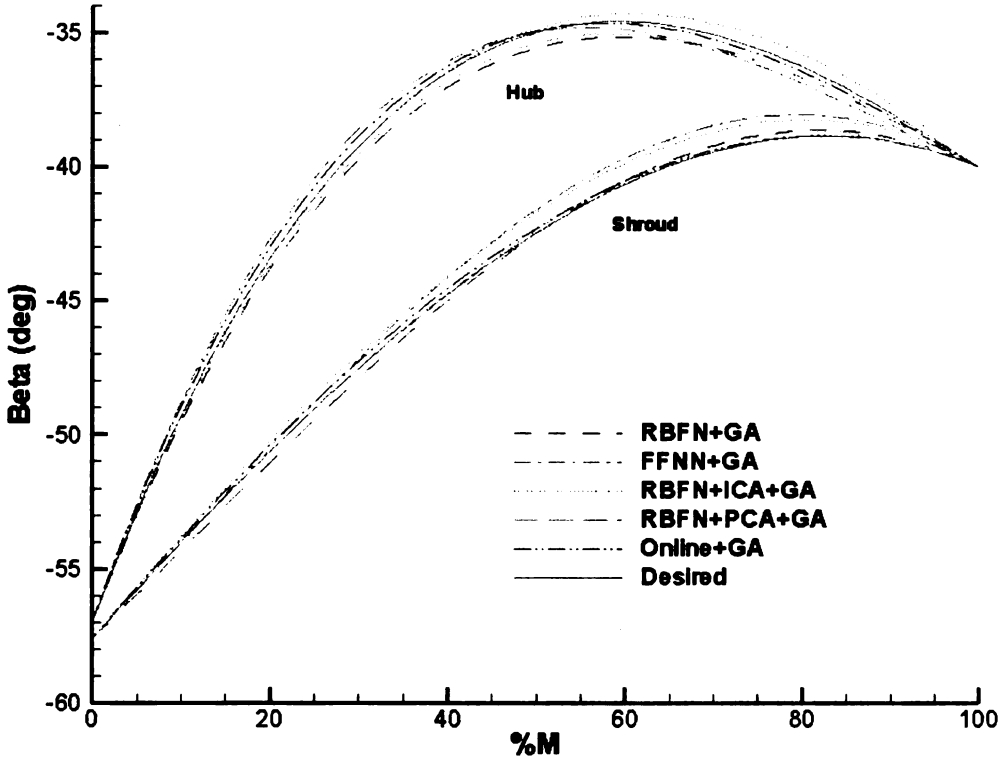

Figure 8-5 Comparison of optimal blade angle distributions

Results in Figure 8-3 show that optimal relative velocity distribution calculated by Online+GA is the closest to desired one. Besides, W distribution calculated by RBFN+GA and RBFN+PCA+GA are also closed to the desired ones. However, there are slightly differences between RBFN+GA and desired one at 60% to 90% normalized meridional distance and between RBFN+PCA+GA and desired one at 10% to 40%. There are significant differences between FFNN+GA, or RBFN+ICA+GA and desired ones at 30% to 80% or 40% -70% normalized meridional distance respectively.

As for the contour (Figure 8-4), optimal shroud are similar while RBFN+GA, RBFN+PCA+GA and Online+GA are slightly better than FFNN+GA and RBFN+ICA+GA; RBFN+PCA+GA calculates the closest optimal hub to the desired one while optimal hub profiles calculated from RBFN+GA and FFNN+GA are slightly closer to the desired one compared to RBFN+ICA+GA and Online+GA.

The comparisons of optimal blade angle distributions are shown in Figure 8-5. For the first half of blade angle distribution on hub, RBFN+ICA+GA is the closest while FFNN+GA is the furthest compared to the desired one. For the second half, Online+GA provides closest while RBFN+ICA+GA becomes the furthest. RBFN+PCA+GA provides the closet optimal blade angle distribution on shroud while FFNN+ICA and RBFN+ICA+GA has significant differences from desired one, which may be the reasons for slightly worse performance of optimization procedure.

8.3 Evaluation Using ANSYS CFX

ANSYS CFX is used to evaluate the optimal geometry eventually. The mesh of flow passage of one blade is shown in Figure 8-6. The mesh of flow passage is mainly determined based on mesh on shroud and hub. Therefore, the mesh on shroud and hub are shown in Figure 8-7 and Figure 8-8 respectively. The mesh statistics of shroud, hub and passage are as shown in Table 8-2.

Table 8-2 Mesh statistics

	Minimum face angle	Maximum face angle	Maximum aspect ratio
Mesh on shroud	37.0	142.175	48.5826
Mesh on hub	26.5801	160.337	58.3881
Mesh of passage	Number of Nodes	Number of Elements	Hexahedra
	27594	22680	22680
	Volume:	Max Edge Length Ratio	
	0.000184265 [m^3]	80.045	

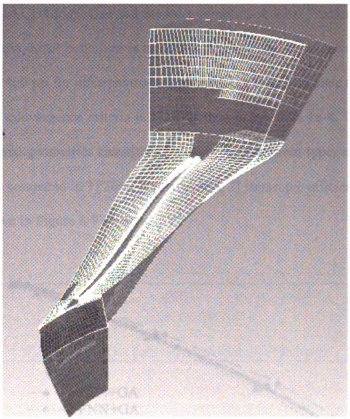

Figure 8-6 Meshing of one blade passage

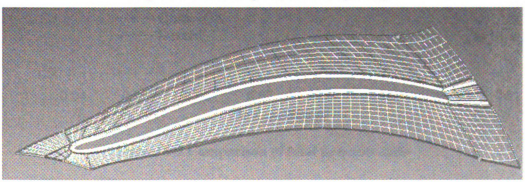

Figure 8-7 Meshing of shroud

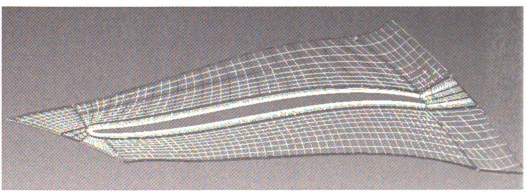

Figure 8-8 Comparison of hub

The fluid is used CH4 Ideal Gas and the inlet condition is Total Pressure and equal to 500 psi while the outlet condition is the static pressure, and equals to 615, 610, 600, 580, 540, 500, 460 psi for different mass flow rate. The fluid timescale control is Auto Timescale and convergence criteria is Max residual is less than 1e-4. The calculation results of optimal geometries calculated by using five different types of optimization procedures are compared in 1) Total pressure ratio, 2) isentropic efficiency 3) Head 4) Work and shown in Figure 8-9 - Figure 8-12.

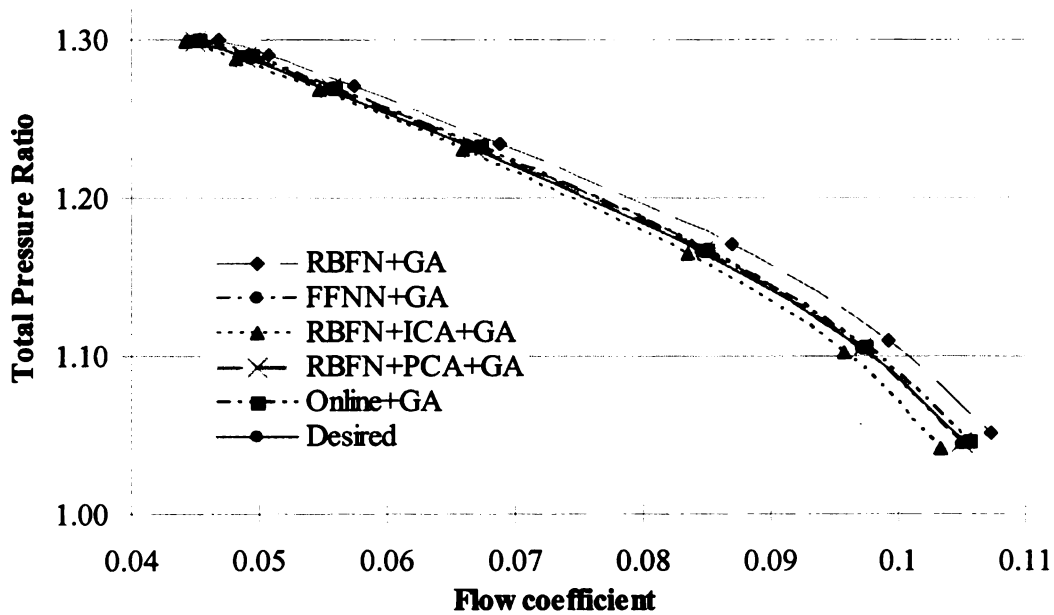

Figure 8-9 Comparison of total pressure ratio

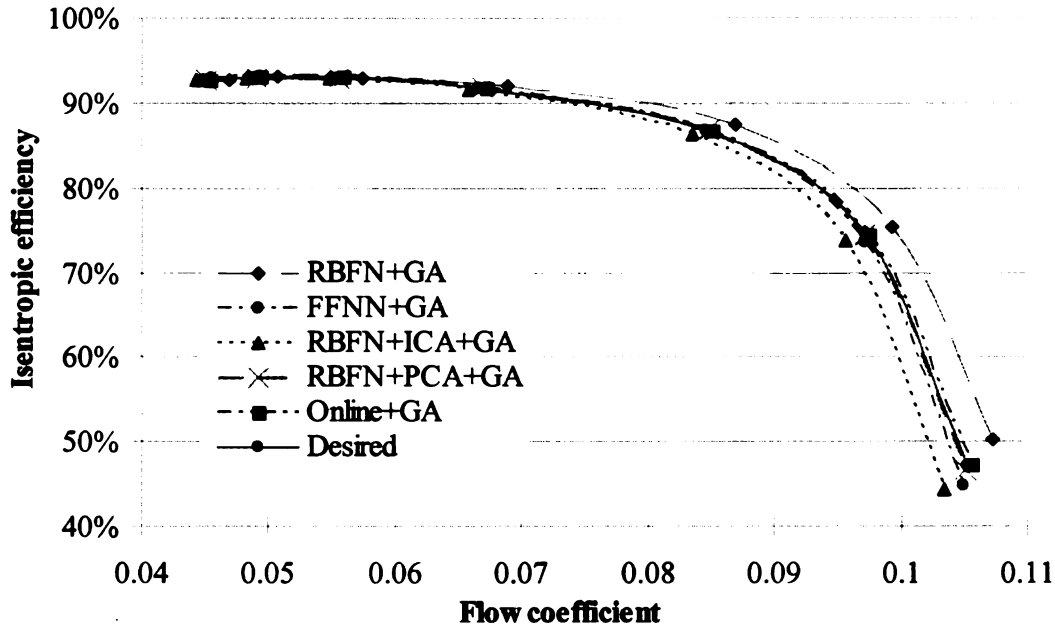

Figure 8-10 Comparison of isentropic efficiency

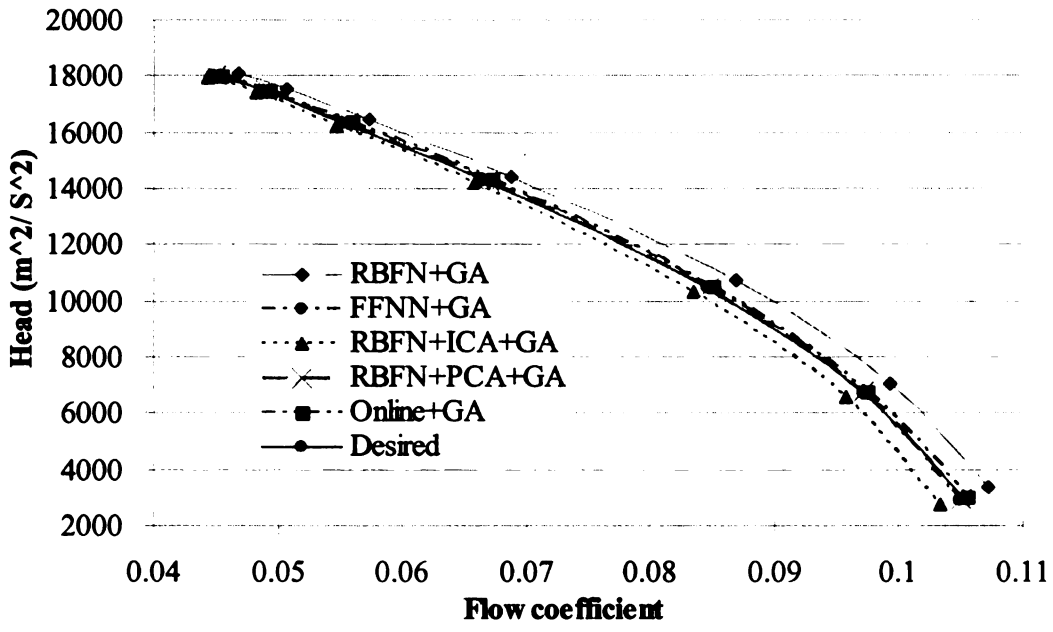

Figure 8-11 Comparison of head

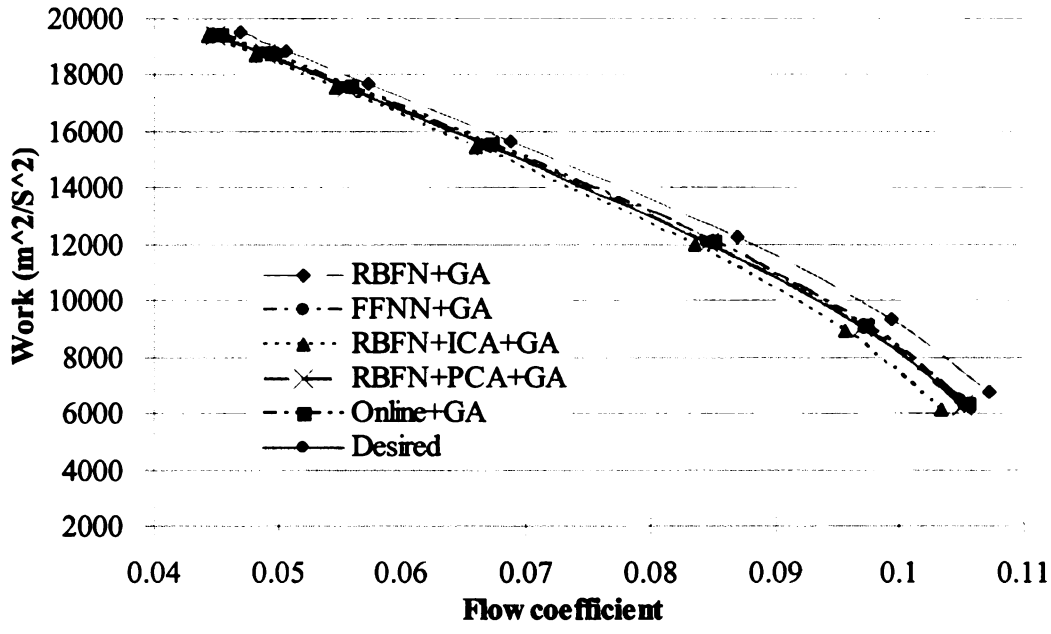

Figure 8-12 Comparison of work

8.4 Discussion and Conclusions

In this chapter, ANSYS CFX is used to evaluate the comprehensive performances of optimal impeller geometry found by five different types of optimization procedures: RBFN+GA, FFNN+GA, RBFN+ICA+GA, RBFN+PCA+GA, and Online+GA, which has been introduced in former chapters.

Total pressure ratio, isentropic efficiency, work, head are compared not only each other, but also with desired one. The results in Figure 8-9 - Figure 8-12 indicate that there are no significant differences between FFNN+GA, RBFN+PCA+GA or Online+GA and desired ones. It means that FFNN+GA, RBFN+PCA+GA and Online+GA provides the better performance and find optimal one closer to the global optimal compared to RBFN+GA and RBFN+ICA+GA. Furthermore, performances impellers found by FFNN+GA, RBFN+PCA+GA and Online+GA are not quite different from each other though their relative velocity distributions are different.

Although impeller found by RBFN+GA is not as close as desire one, it has better performance: higher isentropic efficiency, higher total pressure ratio. This suggests

that the given desired relative velocity is not correlated to the highest achieved efficiency. There is still possibility existed to reach the geometry correlated to the better performance, which is based on the numerical simulation.

CHAPTER 9

CONCLUSIONS

The background and purposes of developing a computer-aided optimization tool for centrifugal compressor impellers have been proposed. Its aim is to assist designer to reach a desired geometry within a more efficiency and effective way before impellers are manufactured and tested.

First of all, a geometry generation tool, which is called BladeCAD is developed in this study. In BladeCAD, centrifugal impellers as well as inlet casings and diffusers can be created and modified. NASA Quasi-3D dimensional codes MERIDL and TOSNIC are modified and linked to BladeCAD and calculate the compressor performance including velocity, pressure, flow angle distribution and etc. The reasons of developing this geometry generation tool are to allow the optimization finished in this tool and decrease the adesigning time.

Five different types of optimization procedures are developed as following:

1) In the first optimization procedures, Radial Basis Function Network is used to create the performance map, and Genetic algorithm is used as optimization method to search for the optimal geometry.
2) The second optimization procedure is very similar to the first one. However, Feed-forward Neural Network (FFNN) is used to create the performance map instead of Radial Basis Function Network.
3) In the third optimization procedure, Independent Component Analysis (ICA) is applied to transform the coordinate system into new one, in which the optimization procedure finished.
4) Principle Component Analysis (PCA) instead of ICA is used to transform the

original coordinate system in fourth optimization procedure. Although transformations used in third or fourth optimization procedure, the new coordinate systems are quite different. In ICA, the coordinates are independent from each other while maximum variances are projected on the coordinates in PCA.

5) The online flow solver is used in the fifth optimization procedure.

The calculation results of each optimization procedure are compared. Moreover, ANSYS CFX is applied to evaluate optimal geometries. The advantages and drawbacks of each method are discussed. During the comparison, Genetic Algorithm (GA) is used in all five types of optimization procedures and settings are same. The influences of GA operators and parameters on optimization procedures are also studied and presented.

BIBLIOGRAPHY

[1] S. L. Dixon, *Fluid Mechanics and Thermodynamics of Turbomachinery*: Butterworth-Heinemann, 1998.

[2] L.Sapiro, "Performance Formulas for Centrifugal Compressors," Solar Turbines, A Caterpillar Company, 1996.

[3] R. V. d. Braembussche, "Design and Optimization of Centrifugal Compressor," 1990.

[4] Y.Dai, "Impeller-Diffuser-Volute Modeling and Flow Analysis Together with Test Validation," vol. Ph.D., 2003.

[5] M. A. B. Yunus A. Çengel, *Thermodynamics: An Engineering Approach*, 1998.

[6] F. A. Lyman, "On the conservation of rothalpy in turbomachines," *Journal of Turbomachinery*, vol. 115, pp. 520-526, 1993.

[7] F. A. Lyman, "Effect of Blade Thickness Tapes on Axial Velocity Distribution at the Loading Edge of an Entrance Rotor Blade Row with Axial Inlet and the Influence of This Distribution on Alignment of the Rotor Blade for Zero Atack," 1953.

[8] D. Eckardt, "Detailed Flow Investigation within a High Speed Centrifugal Compressor," *American Society of Mechanical Engineers* vol. Vol.98 No.3, pp. 309-402, 1976.

[9] J. Earl Logan, *Turbomachinery, Basic Theory and Applications*, 1993.

[10]P.L.Miller, "Blade Geometry Description using B-splines and General Surfaces of Revolution," in *Mechanical Engineering*, vol. Ph.D. Ames: Iowa State University, 2001.

[11]J. N. F. F. Monies, W. Rubio, J.M. Redonnet,, "Five-axis NC Milling of Ruled Surfaces: Optimal Geometry of a Conial Tool," *International Journal of Production Research*, 2002.

[12]T. Katsanis and W. D. McNally, "Programs for computation of velocities and streamlines on blade-to-blade surface of turbomachine," 1969.

[13]T. Katsanis, "Programs for calculating quasi-three dimensional flow in a turbomachine blade row," *NASA Technical Memorandum*, pp. 21, 1984.

[14]T. Katsanis, "Quasi-three-dimensional calculation of velocities in turbomachine blade rows," *American Society of Mechanical Engineers (Paper)*, pp. 8, 1972.

[15]H. Y. Fan, Yam, R., and Dang C., "A preliminary study of the use of genetic algorithms in flow field numerical analysis," *IMEchE Part A J. Power and Energy*, vol. 215, pp. 203-212, 2001.

[16]A. Veress and R. Van Den Braembussche, "Inverse design and optimization of a return channel for a multistage centrifugal compressor," *Journal of Fluids Engineering, Transactions of the ASME*, vol. 126, pp. 799-806, 2004.

[17]D. Bonaiuti and M. Zangeneh, "On the coupling of inverse design and optimization techniques for turbomachinery blade design," presented at ASME Turbo Expo 2006, Barcelona, Spain, 2006.

[18]M. Casey, F. Bersbach, and C. Robinson, "An optimization technique for radial compressor impellers," Berlin, Germany, 2008.

[19]A. Demeulenaere, O. Leonard, and R. Van den Braembussche, "A two-dimensional Navier-Stokes inverse solver for compressor and turbine blade design," *Proceedings of the Institution of Mechanical Engineers, Part A: Journal of Power and Energy*, vol. 211, pp. 299-307, 1997.

[20]R. Bellman *Adaptive Control Processes: a Guided Tour.* Princeton, New Jersey: Princeton University Press, 1961.

[21]X. F. Wang, G. Xi, and Z. H. Wang, "Aerodynamic optimization design of centrifugal compressor's impeller with Kriging model," *Proceedings of the Institution of Mechanical Engineers, Part A: Journal of Power and Energy*, vol. 220, pp. 589-597, 2006.

[22]X. Q. Xing and M. Damodaran, "Application of simultaneous perturbation stochastic approximation method for aerodynamic shape design optimization," *AIAA Journal*, vol. 43, pp. 284-294, 2005.

[23]A. Huppertz, P. M. Flassig, R. J. Flassig, and M. Swoboda, "Knowledge-based 2D blade design using multi-objective aerodynamic optimization and a neural network," New York, NY 10016-5990, United States, 2007.

[24]D. Bonaiuti, Arnone, A., Ermini, M., and Baldassarre, L., "Analysis and optimization of transonic centrifugal compressor impellers using the design of experiments technique," *American Society of Mechanical Engineers*, 2002.

[25]T. Verstraete, Z. Alsalihi, and R. A. Van Den Braembussche, "Multidisciplinary optimization of a radial compressor for micro gas turbine applications," Montreal, Canda, 2007.

[26]D. Japikse, "Optimization of Industrial Centrifugal Compressors Part 6A:Studies in Component Performance--Eight Design Cases from 1972 to 1982," *American Society of Mechanical Engineers*, 1986.

[27]H. Y. Fan, "A neural network approach for centrifugal impeller inverse design," *Proceedings of the Institution of Mechanical Engineers, Part A: Journal of Power and Energy*, vol. 214, pp. 183-186, 2000.

[28]H. Y. Fan, "Inverse design method of diffuser blades by genetic algorithms," *Proceedings of the Institution of Mechanical Engineers, Part A: Journal of Power and Energy*, vol. 212, pp. 261-268, 1998.

[29]A. Oyama, M.-S. Liou, and S. Obayashi, "Transonic axial-flow blade optimization: Evolutionary algorithms/three- dimensional Navier-Stokes solver," *Journal of Propulsion and Power*, vol. 20, pp. 612-619, 2004.

[30]H. Y. Fan, "Neural network approach for centrifugal impeller inverse design," *Proceedings of the Institution of Mechanical Engineers, Part A: Journal of Power and Energy*, vol. 214, pp. 183-186, 2000.

[31]R. A. Van den Braembussche and R. H. Kul, "Inverse design of radial compressor impellers by numerical optimization," Washington, DC, USA, 1991.

[32]A. Oyama, "Transonic Axial-Flow Blade Shape Optimization Using Evolutionary Algorithm and Three-Dimensional Navier-Stokes Solver," presented at 9th AIAA/ISSMO Symposium on Multidisciplinary Analysis and Optimization, Atlanta, Georgia, 2002.

[33]J. Sun and R. L. Elder, "Numerical optimization of a stator vane setting in multistage axial-flow compressors," *Proceedings of the Institution of Mechanical Engineers, Part A: Journal of Power and Energy*, vol. 212, pp. 247-259, 1998.

[34]C. M. Jang and K. Y. Kim, "Optimization of a stator blade using response surface method in a single-stage transonic axial compressor," *Proceedings of the Institution of Mechanical Engineers, Part A: Journal of Power and Energy*, vol. 219, pp. 595-604, 2005.

[35]D. H. Brian, "Parallel Thermoelastic Optimization of 3-D Serpentine Cooling Passages in Turbine Blades," presented at Proceedings of Turbo Expo 2003, Atlanta, Georgia, 2003.

[36]F. Dallenbach, "Aerodynamic design and performance of centrifugal and mixed-flow compressors," New York, NY, United States, 1961.

[37]B. L. a. G. D. E. Miller, "Genetic Algorithms, Tournament Selection, and the Effects of Noise, Evolutionary Computation," *Evolutionary Computation*, vol. 4, pp. 193-212, 1996.

[38]J. E. Baker, "Reducing Bias and Inefficiency in the Selection Algorithm," presented at In second International Conference on Genetic Algorithms on Genetic algorithms and their application, Massachusetts Institute of Technology Cambridge, Massachusetts, United States, 1987.

[39]C. R. J. Houck, J.A., and Kay, M.G., "A Genetic Algorithm for Function Optimization: A Matlab Implementation," 1995.

[40]P. Moraal, and Kolmanovsky, I., "Turbocharger Modeling for Automotive Control Application," *SAE Transactions*, vol. 10, pp. pp. 1324-1338, 1999.

[41]T. Mengistu, W. Ghaly, and T. Mansour, "Aerodynamic shape optimization of turbine blades using a design-parameter-based shape representation," New York, NY 10016-5990, United States, 2007.

[42]K. Ghorbanian and M. Gholamrezaei, "Axial compressor performance map prediction using artificial neural network," New York, NY 10016-5990, United States, 2007.

[43]N. Papila, W. Shyy, L. Griffin, and D. J. Dorney, "Shape optimization of supersonic turbines using global approximation methods," *Journal of Propulsion and Power*, vol. 18, pp. 509-518, 2002.

[44]B. L. Miller and D. E. Goldberg, "Optimal sampling for genetic algorithms," Fairfield, NJ, USA, 1996.

[45]C.-C. Lo and W.-H. Chang, "Multiobjective hybrid genetic algorithm for the capacitated multipoint network design problem," *IEEE Transactions on Systems, Man, and Cybernetics, Part B: Cybernetics*, vol. 30, pp. 461-470, 2000.

[46]S. N. D. S. N. Sivanandam, *Introduction to Genetic Algorithms*: Springer, 2007.

[47]P. Venkataraman, *Applied Optimization with MATLAB Programming*: Wiley-IEEE, 2002.

[48]M. T. Barton, M. L. Mansour, J. S. Liu, and D. L. Palmer, "Numerical optimization of a vaned shroud design for increased operability margin in modern centrifugal compressors," *Journal of Turbomachinery*, vol. 128, pp. 627-631, 2006.

[49]W. T. Tiow, K. F. C. Yiu, and M. Zangeneh, "Application of simulated annealing to inverse design of transonic turbomachinery cascades," *Proceedings of the Institution of Mechanical Engineers, Part A: Journal of Power and Energy*, vol. 216, pp. 59-74, 2002.

[50]F.-Y. Shao, J.-G. Yang, Z.-D. Liu, and J. Hu, "Improved streamline curvature throughflow method and its application in a bypass compression system design," *Hangkong Dongli Xuebao/Journal of Aerospace Power*, vol. 23, pp. 1072-1076, 2008.

[51]M. V. Casey and P. Roth, "Streamline curvature throughflow method for radial turbocompressors," Bury St. Edmunds, Engl, 1984.